

RESISTIVE SWITCHING IN MIXED CONDUCTORS

Ag_2S as a model system

RESISTIVE SWITCHING IN MIXED CONDUCTORS

Ag₂S as a model system

Proefschrift

ter verkrijging van
de graad van Doctor aan de Universiteit Leiden,
op gezag van Rector Magnificus prof. mr. P. F. van der Heijden,
volgens besluit van het College voor Promoties
te verdedigen op donderdag 12 januari 2012
klokke 10:00 uur

door

MONICA MORALES MASIS

geboren te Cartago, Costa Rica
in 1982

Promotiecommissie

Promotor: Prof. dr. J. M. van Ruitenbeek
Overige leden: Prof. dr. E. R. Eliel
Prof. dr. H. D. Wiemhöfer Universität Münster
Prof. dr. ir. H.J.W. Zandvliet Universiteit Twente
Prof. dr. J. Aarts
Dr. ir. S. J. van der Molen
Dr. A. I. Yanson

ISBN: 978-90-8593-115-7

Casimir PhD series, Delft-Leiden 2012-2



This work is part of the research program of the Foundation for Fundamental Research on Matter (FOM), which is part of the Netherlands Organization for Scientific Research (NWO).

Cover: design by Monica Morales Masis

A mis padres

Contents

1	Introduction	1
1.1	Introduction and Motivation	2
1.2	Resistance Switching in Chalcogenides	3
1.3	Ag ₂ S as the model system to study conductance switching effects	12
1.4	Concepts and phenomenological transport equations of mixed conductors	16
1.5	Conclusion	19
2	Ag₂S: Fabrication and Characterization Techniques	21
2.1	Introduction	22
2.2	Sulfurization of Silver Thin Films	23
2.3	Reactive Sputtering of Ag ₂ S thin films	30
2.4	Fabrication of in-plane electrodes and Ag ₂ S deposition issues . . .	32
2.5	Conclusions	35
3	Conductance switching in Ag₂S devices fabricated by sulphurization	37
3.1	Introduction	38
3.2	Measurement setup	38
3.3	Electrical conductivity	39
3.4	Electrical Switching	40
3.5	Conclusion	47
4	Towards a Quantitative Description of Solid Electrolyte Conductance Switches	49
4.1	Introduction	50
4.2	Measurement setup	51
4.3	Results	51
4.4	Theory	53

Contents

4.5	Discussion	59
4.6	Conclusion	64
4.7	Appendix	65
5	Bulk and Surface Nucleation Processes in Ag₂S Conductance Switches	67
5.1	Introduction	68
5.2	Experimental procedure	68
5.3	Conditions for vacuum tunneling on Ag ₂ S	69
5.4	Nucleation and Conductance Switching	70
5.5	Topography scans	76
5.6	Discussion	78
5.7	Conclusion	83
6	Observing “Quantized” Conductance Steps in Silver Sulfide: Two Parallel Resistive Switching Mechanisms	85
6.1	Introduction	86
6.2	Experimental details	86
6.3	Results	87
6.4	Discussion	93
6.5	Conclusion	96
7	Discussion and Outlook	97
7.1	Introduction	98
7.2	Ag ₂ S as a model material to study conductance switching	98
7.3	Ag ₂ S as a material for resistive memories	99
7.4	Challenges for the future of conductive bridge memories	99
7.5	Conclusion	101
	Appendix A	103
	Bibliography	105
	Summary	111
	Samenvatting voor de leek	115
	Acknowledgments	121
	Curriculum vitae	123

1

Introduction

In this first chapter, the motivation for this thesis is given. Historical background and the basic concepts of resistance switching in solid state memories are also presented. The second part of the chapter is dedicated to the introduction of our model material, Silver Sulfide. In the final section, general concepts of mixed conductors are also presented.

1.1 Introduction and Motivation

Since the invention of the transistor in 1947, the semiconductor industry has been looking for small, fast, high density storage and low power consumption memory devices. The ultimate memory device will be miniaturized down to few nanometers, requiring an ultimate downscaling of the active components to atomic scales.

Nonvolatile memories (NVM) are computer memories in which information is stored even when the power is off. One of the most commonly used type of NVM is Flash memory, which is found in solid state hard disks and memory cards used for digital cameras and cell phones. Although flash memory chips have reached downscaling sizes up to several tens of nanometers, they are now reaching the physical scaling limit, that is miniaturization of devices beyond 20nm [1].

To overcome this problem, in the past 10 years, new concepts have been introduced for the development of new NVM [1]. One of these new concepts is Resistance Switching, also known as Resistance Random Access Memories (RRAM). The concept is based on electrically switching the resistance of a material from high resistance (insulating behavior) to low resistance (metallic behavior) state, forming the 0s and 1s of stored digital data bits [2].

The concept of electrically switching the resistance of a material has been widely explored in the last few years. And with it a long list of materials that present resistance switching have been reported in literature [3]. The materials are in the family of insulators or semiconductors and the typical configuration of the system is a two terminal device of the form $M_1/X/M_2$, with X a resistive material sandwiched between the two metal electrodes M_1 and M_2 .

To switch the conductance of the resistive material in the two-terminal device $M_1/X/M_2$, a voltage above a certain threshold needs to be applied between the two metal electrodes. The switching in resistance is electrically induced in all cases, however, the physical process that causes the resistance switching is different depending on the resistive material 'X' used. These physical processes can be thermal, electronic, magnetic and ionic effects [1, 4]. In most of the cases the electrode material and asymmetry of the electrode configuration also play an important role.

Although resistance switching devices have been categorized according to the physical mechanism involved [4], many unsolved questions about the microscopic mechanisms, metallic nature of the on state, atomic arrangements at every switching cycle, switching reproducibility and many other detailed physical processes have not yet been elucidated.

Our contribution to this field, is to build a better understanding of the physical properties and processes involved before, during and after resistance switching in one specific case: when resistance switching is due to ion transport, and the ‘on’ and ‘off’ states are defined by the voltage induced reversible formation of a conductive path between the metal electrodes. Regarding this, our interest also lies in investigating the possibilities for reversible atomic wire formation.

All the different experiments performed in order to build this understanding are described in detail in this thesis. In this first chapter I will describe the basic principle of resistance switching in chalcogenide materials and the physical properties of our model material: Silver Sulfide (Ag_2S). In Chapter 2 I will present the fabrication techniques used to grow the Ag_2S thin films and deposition of electrodes, as well as the characterization techniques. Chapter 3 deals with the reversible conductance switching properties measured in Ag_2S films fabricated by sulfurization, and placed between Pt electrodes. Next, in Chapter 4 a quantitative analysis of transport in Ag_2S devices under steady state is presented. The Ag_2S films fabricated by reactive sputtering and placed between a Ag and a Pt electrode. In Chapter 5, STM measurements and conductance switching with the presence of a tunnel gap are presented. Chapter 6 demonstrates the presence of two conductance switching mechanisms in silver sulfide, from a study of conductance breaking traces. To conclude, Chapter 7 provides a summary and conclusive remarks from the presented chapters, and a discussion about the prospects of these “proof-of-concept” memories.

1.2 Resistance Switching in Chalcogenides

As mentioned in the introduction, several physical processes can be involved, individually or combined, in the process of resistance switching. I will focus on switching due to thermal and ionic effects, which typically occur in chalcogenide materials. Later in this thesis I will focus only on the switching due to ionic transport.

1.2.1 Chalcogenides

Chalcogenide materials are amorphous semiconductors composed of a chalcogen element from the group VIA of the periodic table: sulfur (S), selenium (Se) or tellurium (Te), excluding oxygen (O), and one or more electropositive elements: Au, Ag, Cu, Ge, Sb, Si among others. There are binary (Ge-Se, As-S, Ge-Te, Cu-S, Ag-S, Ag-Se), ternary (Ag-Ge-Se, Ge-Sb-Te, Ag-Sb-Te) and alloy chalcogenide compounds, and they exist in a wide range of atomic ratios and therefore present also a rich variety of electronic properties [4]. Another special property of solid chalcogenides is how the material properties can be easily modified by small changes in temperature, pressure, or other external parameters, like the application of a voltage [4, 5]. These unique properties make solid chalcogenides extremely interesting materials for electronic devices, in the fabrication of e.g. solar cells, fuel cells, batteries and memory devices.

Chalcogenide compounds with high ion mobility are also called solid electrolytes, examples of which are Cu and Ag chalcogenides (Ag_2S , AgGeSe , Cu_2S). Silver is especially appropriate for mass transport applications due to its ease of both reduction and oxidation and high mobility at room temperature [5]. The ionic mobility makes solid electrolytes interesting materials for the study of the effect of conductance switching as it will be further described in this chapter.

1.2.2 Resistance Switching

The concept of resistance switching in amorphous materials was first reported in the 1960's by Ovshinsky [6]. This report started a significant interest in materials that present a phase transition from amorphous to a crystalline phase. The phase transition causes a pronounced change of electrical and optical properties. This, together with reversibility of the process, are properties that have been widely studied for memory applications, e.g. NVM and optical rewritable media. Optical storage media have reached the level of commercialized products like compact disk (CD), digital versatile disk (DVD) and blu-ray disk (BD) [7].

Another resistance switching mechanism that was much later explored for possible application in non-volatile memories, is the reversible formation of conductive filaments across the solid electrolyte. This switching behavior was first reported in 1976 by Hirose and Hirose [8]. Using Ag-doped As_2S_3 as the resistive material, Hirose reported on the formation and annihilation of Ag dendrite as the

cause of resistance switching. The interest of this resistance switching concept, was later triggered in the 90's by Kozicki et al.[9]

These two concepts, phase change and conducting bridge memories, together with the valence exchange switching in transition oxide materials are the three main resistance-change memory concepts [10]. A brief description of these resistance switching processes is given below.

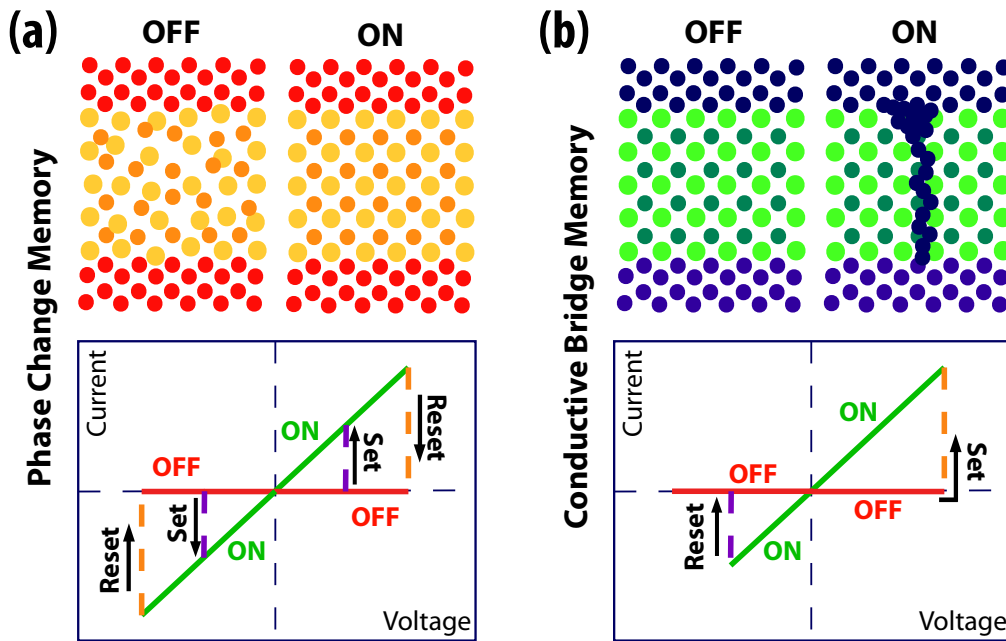


Figure 1.1: Schematic diagram of two switching processes. Current voltage characteristic of the switching and indication of the polarity dependence of the set and reset voltages.

Phase Change - based Resistance Switching

In phase change materials, the change from a disordered amorphous state to an ordered crystalline state causes a pronounced change in the resistance. The amorphous state has high resistance. When a voltage pulse is applied (a voltage above a threshold for switching), it locally heats the amorphous region causing recrystallization. The crystalline phase has low resistance. The application of a higher voltage pulse leads to local melting and the amorphous phase is formed again on rapid quenching. The system is then back to the high resistance state.

A representation of the transition from crystalline to amorphous is presented in Fig.1.1a. This switching mechanism presents unipolar switching, i.e. the set and reset voltages depend only on the amplitude of the voltage but not on the polarity. This is represented in the current-voltage characteristics of Fig.1.1a. Materials that show phase change switching are for example $\text{Ge}_2\text{Sb}_2\text{Te}_2$, Sb_2Te_3 , GeTe [11, 12].

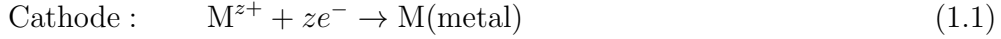
Phase Change materials are already being used in rewritable optical storage media and are probably the best candidates for future non-volatile memories. However, its use as non-volatile memories at low power operation and with high endurance, combined with scalability down to a few nanometers still present challenges [7, 10]. An extended review on this topic can be found in [7, 12, 13].

Conductive Bridge - based Resistance Switching

Also called electrochemical metalization cell (ECM), conductive bridge random access memories (CB-RAM) or programmable metalization cell (PMC) in the literature, as its name suggest, this memory concept is based on the reversible formation of metallic filaments inside a solid electrolyte lattice (Fig.1.1b) [14]. This is the type of memory that we have studied in this thesis.

The key ingredients in this type of memories are the mobile metal ions, a solid electrolyte as the ion conducting layer, an active electrode (A.E) working as the reservoir of the metal ions (e.g. Ag, Cu) and an inactive electrode (I.E) made of an inert metal (e.g. Pt, W). This switching mechanism presents bipolar switching, i.e. the set and reset voltages depend on the amplitude and polarity of the voltage applied. This is schematically represented in the current-voltage characteristics of Fig.1.1b.

The reversible switching process is commonly described as follows: initially the solid electrolyte has a large resistance, defined as the off state. When a sufficiently large voltage is applied between the electrodes, and when the negative polarity is applied at the inert electrode, the metal ions (M^{z+}) migrate towards the cathode and are reduced to metal atoms,



On the anode side (the active electrode) the metal atoms are oxidized to metal ions that dissolve into the electrolyte, maintaining the ion concentration in the electrolyte constant,



As long as the voltage is applied, ion migration in the electrolyte and further reduction of the ions, leads to the formation of a metallic filament that grows towards the anode. The first deposited metal enhances the electric field at its tip and this leads to the formation of a filament instead of a uniform deposition at the cathode. The metallic filament forms a conducting bridge between the electrodes, switching the device to the low resistance state ('on' state). When the voltage polarity is reversed, the metal atoms forming the filament will be dissolved back into the solid electrolyte and be deposited at the active electrode [2].

Figure 1.2 presents a typical current voltage characteristic of the switching and the corresponding diagram for each switching step.

There is a long list of materials that have shown this filamentary resistance switching concept [3]. The main requirement for the electrolyte is good cation conductivity, and one active electrode containing the cation (Ag, Cu). The solid electrolyte can contain the mobile metal ion in its composition (e.g. Ag_2S , Ag_2Se , Cu_2S) or host the foreign metal ions that are transported through the electrolyte from the active electrode to the cathode. In this case the electrolyte is a compound with high solubility of the active cation (e.g. Ag in GeSe) [2].

Oxide materials have also been used as the resistive layer in this type of memories. In this case two mechanisms can be distinguished according to the nature of the oxide layer and the contact material. The first mechanism is the same as the cation migration and reduction, forming and breaking a metallic filament inside the resistive layer. In this case the system consists of one active electrode (Ag, Cu), an oxide semiconductor that can work as the ion conducting lattice and an inert electrode (Pt, W). Some examples of these systems are Ag/ZnO:Mn/Pt

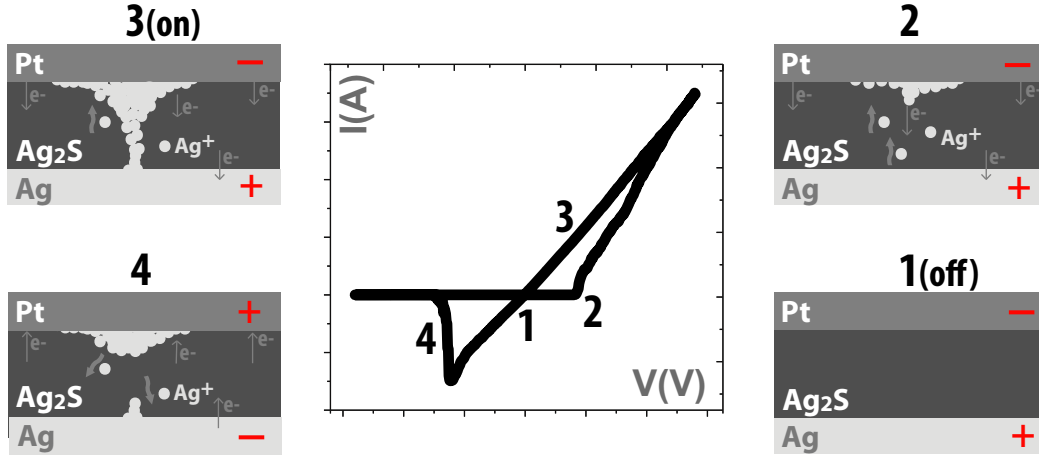
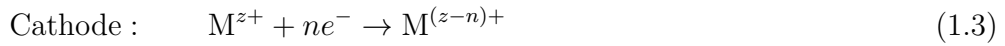


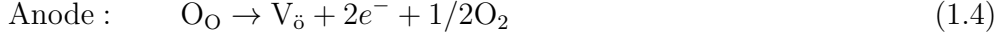
Figure 1.2: Current voltage characteristic of resistance switching caused by redox processes at the solid electrolyte-electrode interface [2]. The numbers from 1 to 4 indicate the order of the events.

[15] and Ag/Al₂O₃/Pt [16].

The second process has been defined as a valence change mechanism (VCM) by Waser et al.[4] and occurs in transition metal oxides or perovskites with at least one transition metal ion, when the oxygen vacancies have a higher mobility than the metal cations. The switching process is similar to the one described for the cation reduction, with the main difference that the mobile ions are oxygen vacancies. When a voltage is applied to the electrodes, the oxygen vacancies drift towards the cathode, and accumulate at the interface with the electrode. At the region where the oxygen vacancies accumulate, the valence of the transition metal is modified by the reduction reaction,



For example if the oxide is Ti₂O then $Ti^{4+} + ne^{-} \rightarrow Ti^{(4-n)+}$ [14]. The valence rich region grows towards the anode and forms a conducting path between the electrodes. The system is then in the on state. At the anode side, it is proposed that to compensate the cathodic reaction, the injection of vacancies into the electrolyte, written according to the Kröger-Vink notation, is given by



with O_O the oxygen ion in a regular site in the lattice, $\text{V}_\ddot{\text{O}}$ the oxygen vacancies (double positive charge) and O_2 oxygen gas produced due to the oxidation reaction [14].

To switch the device to the low conductance state, the bias voltage is reversed and the vacancy rich filament is dissolved back and the system is back to the off state. The filamentary nature of the vacancy rich region at the on state has been demonstrated for the systems $\text{Pt}/\text{SrTiO}_3/\text{Pt}$ [17] and $\text{Pt}/\text{Ti}_2\text{O}/\text{Pt}$ [18].

The VCM process described is just one of many other switching processes observed in oxide materials, which are not covered in this thesis.

Fig.1.3 presents a classification of the proposed conducting bridge resistance switches, that work within the concept of redox reactions at the electrode interfaces.

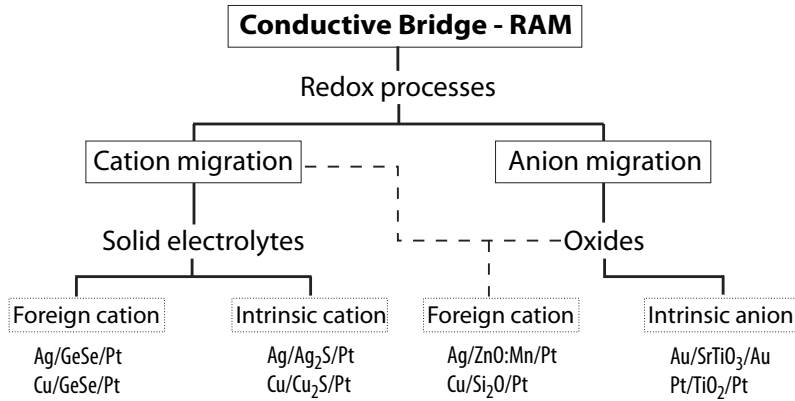


Figure 1.3: Classification of conducting bridge memories according to the type of mobile ions, electrode and resistive material. The examples of electrodes and resistive materials are written in the notation: active electrode/resistive material/inert electrode.

The resistance switching pictures explained above give just a rough description of the main physical processes widely accepted in the literature on resistance switching driven by redox reactions. However, there is a broad range of open questions about the electrochemical reactions on the electrodes, the ions involved in the process, the occurrence of more than one physical mechanism, the nature of the metallic state and many other that need to be solved before the conducting bridge concept can be implemented as solid state memories.

Atomic switches

The ultimate conductive bridge RAM, will be that in which the ‘on’ and ‘off’ states are defined by the addition and removal of a single atom, i.e. an atomic switch. When this is feasible, scaling of the switching devices down to few nanometers, low power consumption and ultra high speed operation would be possible.

Atomic-scale metallic point contacts have been broadly studied previously, and their technological prospects for their use, for example in transistors, is a motivation for the intense investigation. Metallic wires with a cross section area of few atoms lead to the appearance of quantum mechanical effects, and with it, quantization of the conductance in units of $1G_0 = 2e^2/h = 77\mu S$. For gold and silver, the conductance of a single atom is $1G_0$ [19].

Atomic switches have been fabricated in several ways. For example, three terminal gate-controlled atomic quantum switches, that can operate at room temperature, have been successfully developed by Xie et al.[20, 21] and Martin et al.[22] using different approaches. The first approach is the electrochemical deposition in liquid of Ag atoms between two large gold electrodes[20]. The number of Ag atoms in the quantum point contact were controlled with the potential of the gate electrode, allowing the reproducible switching of the contact between a quantized on state ($G = nG_0$, $n=0,1,2,3...5$) and insulating off state. The second approach consisted of a gated mechanically controllable break junction [22]. More specifically, a gold bridge with an atomic constriction suspended on top of a gate electrode. The electrostatic attraction between the source and drain electrodes leads to the reversible switching between a single atom contact ($G = 1G_0$) and tunneling regime.

In spite of these exciting results, indicating the possibility of individual atom manipulation for future atomic transistors, these switches still require special conditions to work (high vacuum), large setups (e.g. mechanical controllable break junctions) or liquid electrolytes that are difficult to implement in integrated circuits.

In 2005 Terabe *et al.* reported the reversible formation of Ag atomic contacts in the tunneling gap between the surface of a silver sulfide (Ag_2S) thin film and a Pt electrode. This was the first atomic switch proposed under the concept of conductive bridge random access memories (CB-RAM)[23]. The switching from low conductance (tunneling) to high conductance was induced by the applied bias between the Pt electrode and a Ag bottom electrode. The metallic Ag was formed by the reduction of Ag at the Pt electrode (negatively biased). To break the contact the polarity of the voltage is reversed and the Ag filament dissolves back into the Ag_2S layer. The ‘on’ and ‘off’ states of conductance were stable, and the authors presented the possibility to prepare the switch in well-defined quantized states of conductance, with $G = 0, 1G_0, 2G_0$ and $3G_0$, suggesting the possibility to realize a multilevel memory switch.

The interpretation presented, concerning the creation of an atomic switch, suggested that the metallic filament was formed on the surface of the Ag_2S , and that a tunneling gap is necessary to achieve a clear change in conductance from ‘on’ to ‘off’ states. However, we will argue that this interpretation cannot be valid, and we believe that the Ag metal filament formation takes place **inside** the Ag_2S layer, and that a tunnel gap is not necessary as the intrinsic conductance of silver sulfide is already very low.

The indications for the possible formation of atomic wires in an environment that will provide both mechanical stability and chemical protection, all under ambient conditions, is what motivated part of the work that is presented in this thesis. This also formed the trigger of many fundamental questions about the processes occurring in Ag_2S switches.

1.3 Ag_2S as the model system to study conduction switching effects

The material used for all the experiments described in this thesis is Silver Sulfide (Ag_2S). This dark gray colored material, which tarnishes silverware or silver objects over time, has called the attention of solid state scientists since the times of Faraday.

Silver Sulfide is a mixed conductor material, with a total conductivity due to the transport of, both, Ag^+ -ions and electrons. Silver sulfide presents good chemical stability and it exists in three stable phases, α , β and γ in order of increasing temperature [24]. Ag_2S corresponds to the family of the silver chalcogenides, which includes Ag_2Se and Ag_2Te . The structure of these materials is usually a rigid body-centered cubic (bcc) lattice, formed by covalently bonded chalcogen atoms. The Ag^+ -ions are distributed in octahedral and tetrahedral positions in the lattice. The number of octahedral and tetrahedral sites available is much larger than the number of Ag^+ -ions, and therefore there are always positions in the lattice available for the ions to move into. This results in a high ion mobility observed in all silver chalcogenides [5].

The physical properties of Ag_2S , i.e. electronic and ionic conductivity, crystal structure and distribution of defects, are strongly modified with temperature and composition (Ag/S ratio). Figure 1.4 presents the phase diagram of Ag_2S , indicating the stable range for each of the three phases as a function of temperature and stoichiometry parameter δ . The stoichiometry parameter δ indicates the excess ($\delta > 0$) or deficit ($\delta < 0$) of Ag in $\text{Ag}_{2+\delta}\text{S}$.

The low temperature phase ($\alpha\text{-Ag}_{2+\delta}\text{S}$), also called acanthite, is only stable within the narrowest range of non-stoichiometry (Fig.1.4b) with a composition range, δ_{max}^α , in the order of 10^{-6} [24, 25]. At 177°C , Ag_2S transforms to $\beta\text{-Ag}_{2+\delta}\text{S}$, the high temperature phase, also called argentite. The range of non-stoichiometry of the β -phase is much broader than the α phase (Fig.1.4a), with δ_{max}^β in the order of 10^{-3} [24, 26].

The formulation of the basic rules of solid state electrochemistry and its application to Ag_2S , were first given by Carl Wagner in the 1930's [27]. Since then, the most studied phase has been $\beta\text{-Ag}_{2+\delta}\text{S}$, due to its superionic properties. For

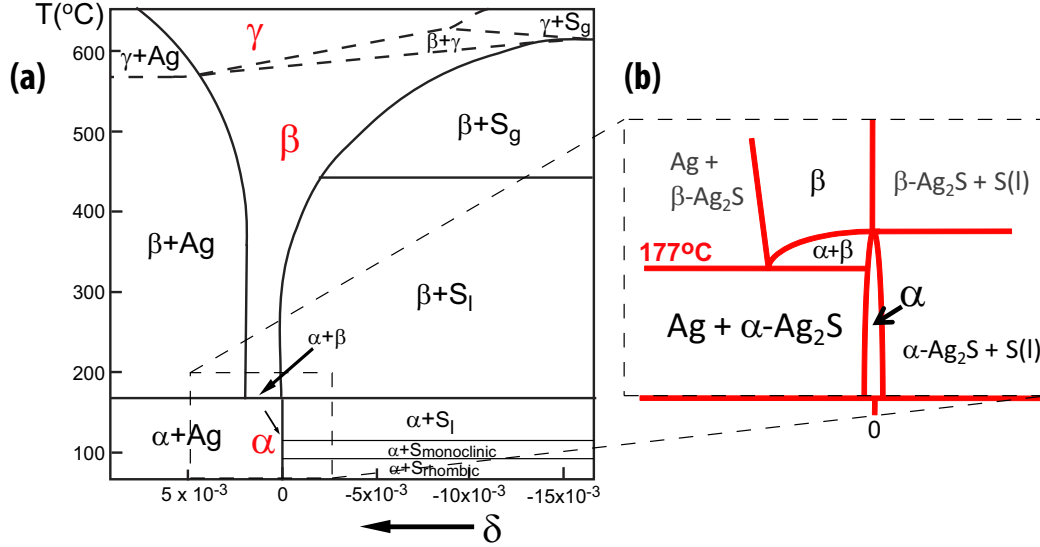


Figure 1.4: Phase diagram of the Ag-S binary system. a) The three phases of $\text{Ag}_{2+\delta}\text{S}$ are presented. Starting with $\alpha\text{-Ag}_{2+\delta}\text{S}$, the low temperature phase is stable from 0 to 177°C . At 177°C it transforms to $\beta\text{-Ag}_{2+\delta}\text{S}$ which is stable from 177°C up to around 590°C (depending on non-stoichiometry). Above 600°C , $\gamma\text{-Ag}_{2+\delta}\text{S}$ is the stable phase. Finally at above 840°C (not presented in the diagram) $\text{Ag}_{2+\delta}\text{S}$ is liquid. b) Zoom-in of the phase diagram at the α - β transition region. Data obtained from Ref.[24].

our purpose, the α phase is of special interest because it is the stable phase at room temperature. In the following section I will present the physical properties of the α and β phases, as reported in literature.

1.3.1 Crystal Structure

The crystal structure of the low temperature phase $\alpha\text{-Ag}_{2+\delta}\text{S}$ is monoclinic, space group $\text{P}2_1/c$, with $a = 4.231 \text{ \AA}$, $b = 6.930 \text{ \AA}$, $c = 9.526 \text{ \AA}$ and $\beta = 125.48^\circ$ [28]. This superstructure is composed of a slightly distorted body-centered cubic (bcc) lattice of sulfur atoms. The silver atoms are equally distributed in positions close to the tetrahedral and octahedral sites of the sulfur bcc array [29, 28]. Figure 1.5 presents the monoclinic structure of $\alpha\text{-Ag}_{2+\delta}\text{S}$.

At the high temperature phase, $\beta\text{-Ag}_{2+\delta}\text{S}$, the sulfur atoms form an ordered

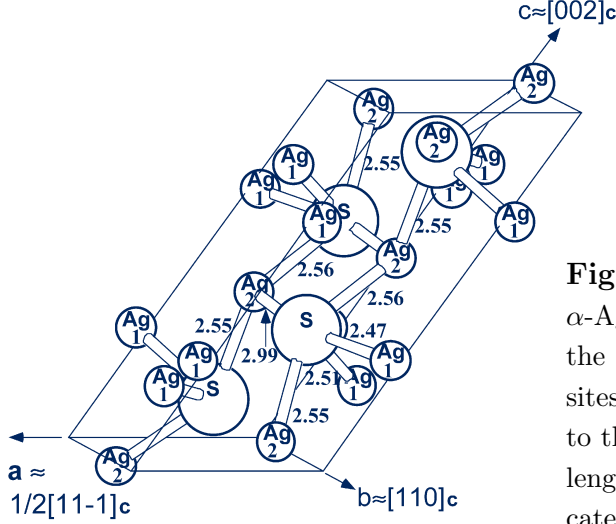


Figure 1.5: Crystal structure of α - $\text{Ag}_{2+\delta}\text{S}$. In the figure, Ag(1) are the atoms close to the octahedral sites and Ag(2) are the atoms close to the tetrahedral sites. The bond length to the S atoms is also indicated. Reproduced from Ref.[29].

bcc lattice. The Ag atoms occupy the tetrahedral and octahedral sites in the lattice, with a higher occupancy of tetrahedral sites. Cava et al.[28] determined an occupancy ratio of 3:1 at the α - β phase transition, and an increase of the ratio with temperature up to 260°C when all the occupied sites are tetrahedral. The space group of β - $\text{Ag}_{2+\delta}\text{S}$ is the $\text{Im}\bar{3}\text{m}$, with $a = 4.860 \text{ \AA}$ [24].

In summary, for both phases, $\text{Ag}_{2+\delta}\text{S}$ consist of a rigid immobile sulfur sub-lattice and a mobile Ag sub-lattice. The large mobility of the Ag^+ -ions in the lattice is due to the excess of octahedral and tetrahedral sites in the sulfur lattice as compared to the amount of silver in $\text{Ag}_{2+\delta}\text{S}$.

1.3.2 Electronic and Ionic Conductivity

As mentioned before, the total conductivity σ_t of Ag_2S is due to the simultaneous motion of both, Ag^+ -ions and electrons. Then, $\sigma_t = \sigma_e + \sigma_{\text{Ag}^+}$.

The temperature dependence of the total conductivity is presented in Fig.1.6. In the low temperature phase, α - $\text{Ag}_{2+\delta}\text{S}$, the total conductivity increases exponentially with temperature, presenting semiconductor behavior. At the α to β phase transition, the ionic conductivity increases nearly two orders of magnitude, and the electronic conductivity nearly three orders of magnitude [29]. The conductivity in the β phase only varies slightly with temperature, presenting metallic

1.3. Ag_2S AS THE MODEL SYSTEM TO STUDY CONDUCTANCE SWITCHING EFFECTS

behavior. In both α and β phases, the total conductivity is strongly dependent on stoichiometry.

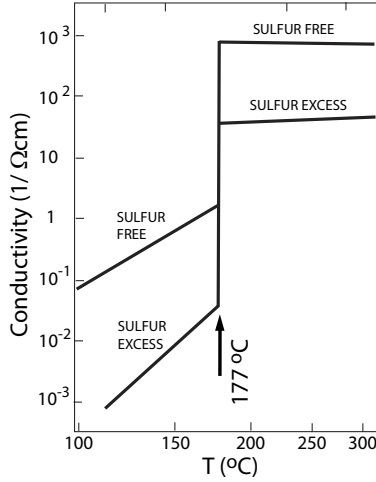


Figure 1.6: Electrical Conductivity ($\sigma_e + \sigma_{\text{Ag}^+}$) as a function of temperature. The pronounced change in the conductivity with the composition and phase transformation is clearly observed in the plot. The composition range presented shows the limits of silver sulfide in equilibrium with silver (sulfur free), and silver sulfide in equilibrium with sulfur (sulfur excess). Reproduced from Ref.[30].

Further research on the α phase demonstrated that $\alpha\text{-Ag}_{2+\delta}\text{S}$ is an n-type semiconductor, with a band gap ranging between 0.6 and 1.2 eV [26, 29, 31, 32].

In spite of the large number of reports on Ag_2S [29, 30, 33, 35], data on the electrical properties at room temperature are rare in literature. Bonnecaze et al.[25] published one of the few reports on the electrical properties of Ag_2S at temperatures ranging from room temperature up to 177°C , the phase transition. At room temperature, $\sigma_e \approx 7.8 \times 10^{-2} \Omega^{-1}\text{m}^{-1}$ and $\sigma_{\text{Ag}^+} \approx 3.4 \times 10^{-3} \Omega^{-1}\text{m}^{-1}$, which represents a contribution of 96% (σ_e) and 4% (σ_{Ag^+}) to the total conductivity (σ_t). The contribution of the electronic conductivity to the total conductivity is, in the low and high temperature phases, higher than the ionic contribution. However, at the high temperature phase, the ionic conductivity values are as high as those measured in purely ionic conductors (e.g. AgI) [24]. This is why $\beta\text{-Ag}_2\text{S}$ receives the name of superionic conductor.

The ionic conductivity is independent of composition or non-stoichiometry δ . This is explained to be due to the considerable freedom of the Ag^+ ions to move within several positions in the crystal lattice [30, 34]. Contrary to the ionic conductivity, the electronic conductivity is strongly dependent on non-stoichiometry (δ). Additional silver in silver sulfide acts as an n-type donor increasing the elec-

tronic conductivity. Then, as observed in the conductivity vs temperature plot (Fig.1.6), the increase of the total conductivity with additional silver is all due to the increase in the electronic conductivity.

The finding that the ionic conductivity is independent of the change on stoichiometry, led to the conclusion that α -Ag₂S has a majority of intrinsic thermal ionic defects, with these defects being of Frenkel-type [25].

1.4 Concepts and phenomenological transport equations of mixed conductors

In this section a brief background of defects and electrical transport in mixed conductors, as well as the phenomenological transport equations are presented.

1.4.1 Charge Carriers in Solids

The understanding of mixed charge transport and compositional variation in solids is possible using point defect chemistry, concepts that were developed in the 30's by Frenkel [37], Schottky and Wagner. Point defects are atomic size defects, and consist of vacant lattice sites, extra atoms in not regular lattice positions (also called interstitial positions) and chemical impurities. Higher dimension defects, like dislocations, grain boundaries, and voids are conglomerations of these point defects. Thus, ionic and electronic conductivity as well as diffusion processes, all depend on local deviations from the perfect crystal lattice, i.e. on the presence of point defects [36, 38]. The possible combinations of point defects in a crystal, following the principle of electric neutrality are presented in Fig1.7.

The most accepted notation for point defects is the so-called Kröger-Vink notation [38]. In a mixed conductor MX with cation Frenkel disorder, this notation indicates the elements of the structure as follows,

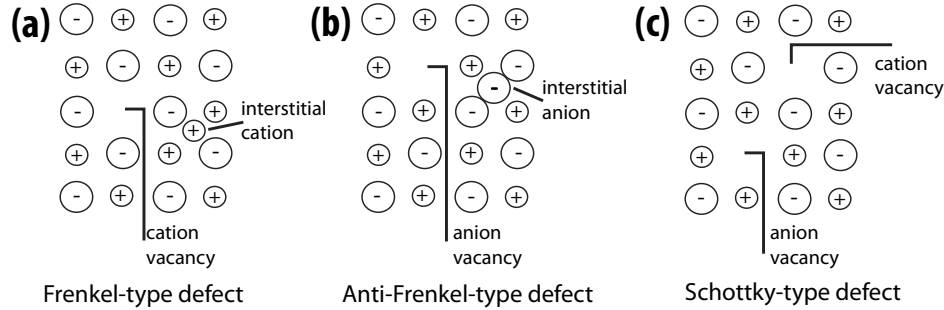


Figure 1.7: Types of point defects in a crystal. a) and b) Frenkel defect: combination of a vacancy and an interstitial ion. c) Schottky defect: a cation and an anion vacancy. Reproduced from [36].

- M_M Cation, M^+ , located on a regular site of the lattice (position represented with the subscript M).
- V_i Vacant interstitial site, a normal component of the ideal lattice.
- M_i^\bullet Cation on interstitial site (subscript i) with a relative charge +1 (superscript \bullet)
- V_M' Vacancy at cation site with a relative charge -1.
- e', h^\bullet Electron, hole and their respective charge.

The relative charge is the difference in charge at the defect site relative to the charge at the site of the perfect crystal (A dot for each extra positive charge or a slash for each extra negative charge) [38]. The Kröger-Vink notation is important in the definition of equilibrium reactions and deviations from stoichiometric compositions. This will be shown in Chapter 4.

1.4.2 Transport equations

The transport of charge carriers in mixed conductors is correctly described by the theory of irreversible thermodynamics. The theory relates the occurrence of fluxes (J_j) to perturbing forces (X_j) in a system. In an irreversible process, the rate of entropy production ($\dot{s} > 0$) is related with the flux and perturbing force as,

$$\dot{s} = \frac{1}{T} \sum_{j=1}^n J_j \cdot X_j \quad (1.5)$$

with T the temperature.

The theory as developed by Onsager [39] states that as long as a force-flux relation can be expressed as in equation 1.5, the forces and their fluxes are linearly related. The linear relation is given by the Onsager theorem [39],

$$J_j = \sum_k L_{jk} X_k \quad (1.6)$$

with the coefficient L_{jk} independent of X_k . According to the Onsager theorem [39], in systems near equilibrium $L_{jk} = L_{kj}$.

The importance of these relations in the description of transport in mixed conductors, is that the linear macroscopic laws of transport (e.g. Ohm's law for conduction) are generalized, so they include cross-terms. These cross-terms represent all fluxes and forces, for example in case of more than one mobile species, it counts the interaction between the fluxes of the distinct species in the solid.

As an example, let's consider again the mixed conductor MX with mobile cations and electrons. In this case, there are two types of fluxes, the electron flux j_e and ion flux j_i . When these fluxes are induced by potential gradients, the forces can be written as,

$$X_e = \nabla \tilde{\mu}_e = \nabla \mu_e - e \nabla \phi \quad (1.7)$$

$$X_i = -\nabla \tilde{\mu}_i = -\nabla \mu_i + e \nabla \phi \quad (1.8)$$

and from equation 1.6,

$$j_e = \frac{\sigma_e}{e} \nabla \tilde{\mu}_e - \frac{\sigma_{ei}}{e} \nabla \tilde{\mu}_i \quad (1.9)$$

$$j_i = -\frac{\sigma_i}{e} \nabla \tilde{\mu}_i + \frac{\sigma_{ie}}{e} \nabla \tilde{\mu}_e \quad (1.10)$$

where j_e and j_i are the electronic and ionic current densities, and σ_e and σ_i are the conductivities. The conductivity is given by $\sigma = eZN\mu$, where N the concentration (cm^{-3}) and μ the mobility (cm^2/Vs). For some mixed conductors, the Onsager cross coefficients (σ_{ei} and σ_{ie}) are negligibly small compared with σ_e and σ_i [40, 41]. Therefore the cross-coefficients will usually be omitted in the treatment of silver chalcogenides with cation Frenkel disorder.

1.5 Conclusion

In this chapter we presented a new concept for memory devices, with the prospect to overcome the scalability limit of few nanometers of traditional, transistor based memories. This concept is based on Resistance Switching. Silver and Copper chalcogenides with high ionic mobility, are candidate materials investigated for the development of this type of memory devices. Silver Sulfide is one of these chalcogenides, and presents interesting properties as mixed conductivity, semiconducting properties and high ion mobility. These properties made Ag_2S attractive as our model system to investigate the fundamentals of switching in mixed conductor materials.

1. INTRODUCTION

2

Ag₂S: Fabrication and Characterization Techniques

This chapter describes two fabrication methods used for the growth of Ag₂S thin films. The specific growth parameters are presented for each method as well as the subsequent characterization of the thin films. The advantages and disadvantages of each method will also be presented in the chapter.

2.1 Introduction

In the previous chapter we have shown that the conductivity of Ag₂S is strongly dependent on the stoichiometry. Hence, to study the conductance and switching properties of Ag₂S thin films we need a sample preparation technique, which is reproducible and that results in thin films with the desired stoichiometry.

Thin films of α -Ag₂S have been prepared by different methods in several research groups, which include the use of silver sulfide pellets for the very first investigations on Ag₂S [35, 42], to newer methods as chemical vapor deposition (CVD) [43], chemical bath deposition (CBD) [44, 45] and thermal evaporation [32, 46]. For the growth of our Ag₂S devices we investigated two different methods. One is the sulfurization of a Ag thin film in vacuum, and the second is Ag sputtering in a Ar/H₂S atmosphere.

Silver sulfurization is the conversion of a Ag thin film to Ag₂S by reaction with sulfur vapor,



It is a relatively simple method and it can be performed in UHV [46], HV [47, 48] and even at atmospheric pressure [49], and at temperatures ranging from room temperature up to approximately 700 K, depending on the pressure and setup. Because of the single oxidation state of Ag, the sulfurization of a Ag film usually results in a single phase material (for example acanthite, the room temperature phase). Sulfurization of other transition metals, can result in multiple phases due to the several possible oxidation states. This is the case, for example, of copper sulfide. Copper sulfide has at least five phases at room temperature, defined by various stoichiometries and valence states, and therefore several phases can coexist in a single sulfurized Cu film [50, 51].

In the first section of this chapter, the specific sulfurization parameters used to grow our samples and the subsequent characterization of the thin films will be presented.

The second method is radiofrequency (RF) sputter deposition. The RF sputter deposition method is a slightly more complex technique. It consist of a vacuum

chamber, with a Ag target and a Si substrate mounted on a sample holder in front of the target. An Ar plasma is ignited between the target and the grounded sample holder. The Ar⁺-ions knock Ag atoms from the target, which deposit on the substrate, forming a Ag thin film. In addition to this, for the deposition of Ag₂S, we introduce H₂S into the chamber, which then reacts with Ag forming Ag₂S,



In this process, also called reactive sputtering, the partial pressure of the reactive gas in the chamber is a very important parameter to achieve the correct sample stoichiometry. RF sputter deposition is a widely used deposition method for industrial applications. It also allows deposition of metals and insulating materials, therefore it is a very appropriate method for the growth of chalcogenide thin films as demonstrated in [52, 53].

In the second section of this chapter, the specific sputter parameters used to grow our samples and the subsequent characterization will be presented.

2.2 Sulfurization of Silver Thin Films

The Ag₂S devices are grown on clean Si (100) substrates with a native oxide layer. The fabrication steps are presented in Fig.2.1. First, a layer of Pt (100nm thickness and 10x10 mm² surface area) is sputtered onto the substrate, followed by a layer of Ag (200nm thickness and 5x5 mm² surface area) which is sputtered using a shadow mask. After sputtering follows the synthesis of Ag₂S by sulfurization of the Ag film. Sulfur powder (reagent grade powder purified by sublimation) is loaded into a quartz tube (18mm internal diameter) and the sample is held at 10 cm vertical distance facing the sulfur powder. Once the sulfur and the sample are loaded, the tube is evacuated to a pressure of 1 x 10⁻⁶ mbar. The temperature in the tube is then increased to 523 K (± 3K) using a vertical furnace with a programmable temperature control. The tube is kept under static vacuum to create a sulfur atmosphere, while the temperature remains constant at 523 K (± 3K) for one hour. After one hour, the tube is evacuated but kept at 523 K (± 3K) to anneal the samples during one more hour. Finally, the sample is slowly cooled down to room temperature at a rate of 1 K/min.

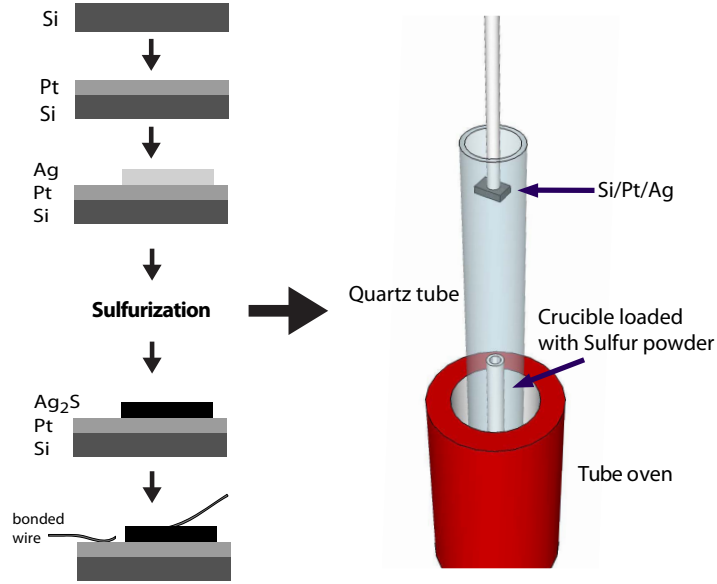


Figure 2.1: Schematic diagram of the fabrication steps of the Ag₂S devices and drawing of the oven set up used to sulfurize the Ag thin films.

Sulfurization starts with a direct reaction of Ag atoms on or near the surface of the film, with the S vapor forming a Ag₂S layer. During the sulfurization, the sample is held at a temperature above the phase transition temperature of 451 K, therefore, the initially formed Ag₂S is in the β -phase. This phase is characterized by a very large Ag ion mobility. This large mobility together with the high temperature, allows a continuous reaction of the sulfur vapor with the diffusing Ag atoms on the growing surface. When cooling down, a phase transition should occur from β to α -Ag₂S. We cooled down the samples after annealing at a slow rate (1K/min) to avoid frozen-in argentite β -Ag₂S crystals within the acanthite α -Ag₂S films [45, 46].

Powder X-ray diffraction (XRD) patterns were taken at room temperature using a Phillips X'Pert Pro diffractometer. The spectra indicate the formation of acanthite Ag₂S (Fig.2.2a). The highest intensity peaks of the spectra correspond to the (012) and (013) peaks of acanthite Ag₂S. In addition, the (-112), (-103), (103) and (014) peaks of α -Ag₂S are also present in the spectra.

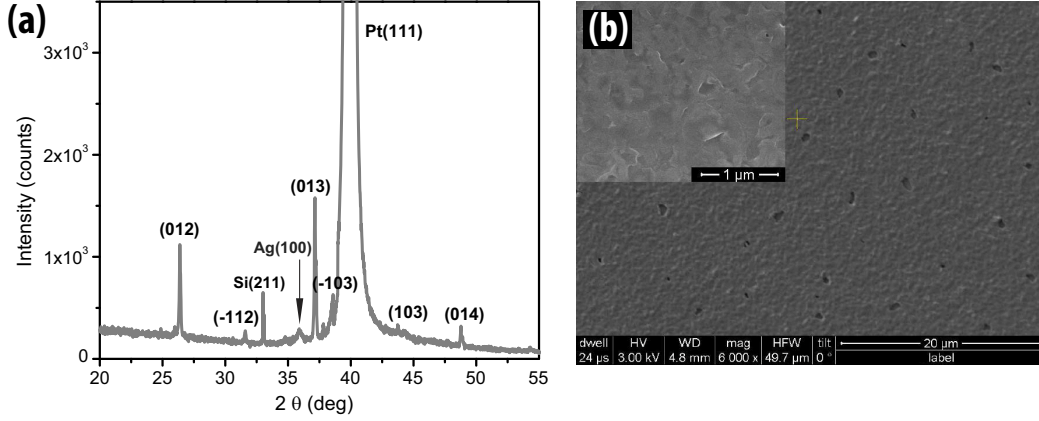


Figure 2.2: a) XRD spectra of the Ag_2S thin films deposited on top of a Pt layer. The observed peaks in the spectra correspond to Ag_2S . Additional peaks indicated in the spectra as Si(211), Ag(100) and Pt(111) correspond to the Si substrate, the Pt electrode at the bottom of the film and the Ag inclusions in the film. Rutherford backscattering spectroscopy (RBS) data of the Ag_2S devices confirmed that the observed Ag peak is not a remaining Ag layer between the Pt and the Ag_2S . b) SEM top view of the surface morphology for a typical Ag_2S sample scanned with an electron beam energy of 3kV. A fairly smooth surface is observed with holes at some locations, as more clearly seen in a close-up view of the surface morphology as presented in the inset.

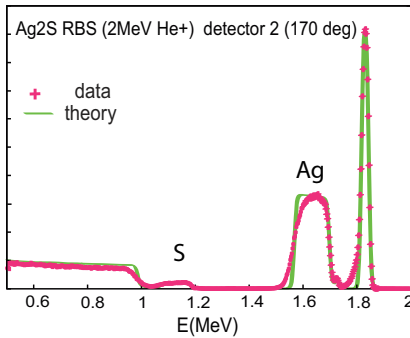


Figure 2.3: Rutherford backscattering spectroscopy (RBS) data of the Ag_2S devices. A comparison with the theoretical spectra of Ag_2S is used to indicate the formation of stoichiometric samples. The observed divergence from the theoretical data is due to the film roughness.

We expect from literature (JCPDS file 14-0072) that the strongest diffraction peaks are the (-103) and (-112). We find the strongest intensity at the (013) and (012) peaks. The difference in the intensity of the diffraction peaks can be explained by a preferential orientation that the crystal domains acquire during the growth process. In spite of the difference in intensity between the recorded spectra and the expected values, all peaks are found at the correct θ value. This

latter observation confirms that the material probed by XRD is indeed acanthite Ag₂S. Additional peaks are also observed in the spectra. The narrow peak at $\theta = 33.01^\circ$ corresponds to the (211) peak of crystalline Si (JCPDS file 14-0072) and is coming from the substrate. At $\theta = 35.9^\circ$ a broad peak is observed, indicating the presence of disordered metallic Ag (JCPDS file 87-0598). This may indicate small inclusions of the initial Ag film that did not react during sulfurization. Finally, a strong Pt peak is observed at $\theta = 39.9^\circ$, due to the exposed area of the Pt film on the sample. The stoichiometric ratio of Ag:S = 2:1 was confirmed by Rutherford Back Scattering (RBS). Figure 2.3 shows the spectrum obtained from one of our samples compared to the theoretical spectrum for stoichiometric Ag₂S. In addition to the Ag and S signals, in the measured sample we observed the signal from the Si substrate and a top Au thin layer.

The surface morphology of the as-grown films was examined by scanning electron microscopy (SEM) at low electron beam energies (3-5 kV). In Fig.2.2c we present the typical surface morphology of the Ag₂S films. In this image a fairly smooth surface is observed. The appearance of holes at some locations of the film is probably caused by the cooling down process, where a phase transition from β to α phase occurs. This phase transition corresponds to a volume contraction and an increased lattice disorder [54]. Apart from the phase transition, another cause could be a difference in the thermal expansion between the Ag₂S and the Pt bottom electrode, however, to our knowledge this has not been reported in literature.

At high electron beam energies, from 10 to 15 kV, the precipitation of Ag protrusions on the surface towards the electron beam is clearly observed. Figure 2.4a-h presents frames of a movie (in chronological order from a to h) recorded while imaging the Ag₂S surface. The white spots on the surface are the Ag protrusions that grow spontaneously as a result of the exposure to the electron beam. The zoomed in image (Fig.2.4d) shows the size of the Ag protrusions of approximately 100 nm diameter. The zoomed out images (Fig.2.4e-h) shows the modification caused on the exposed region of the film as well as the precipitation of more Ag filaments in the newly exposed area.

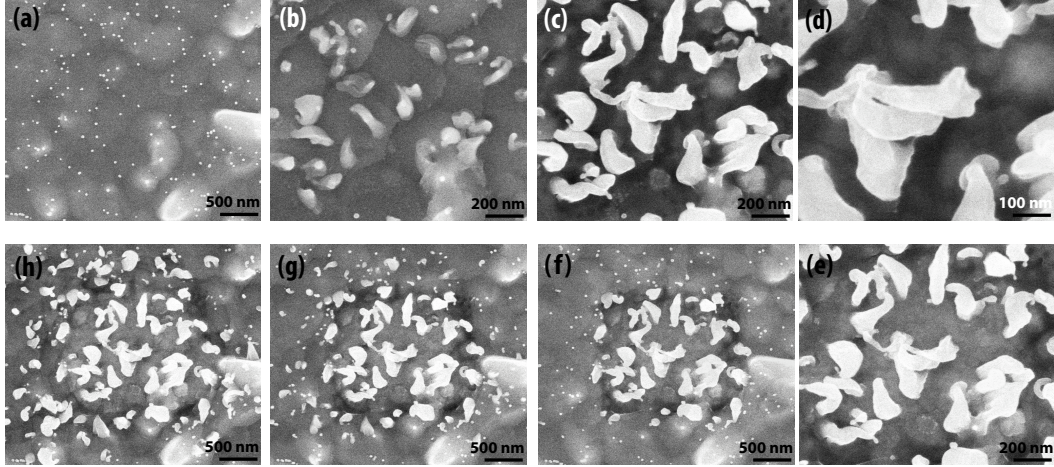


Figure 2.4: Precipitation of Ag protrusions at the surface of the Ag_2S film observed by scanning electron microscope (SEM). The figures from (a) to (h) are frames (in chronological order) of a movie recorded while zooming in and out on the surface.

2.2.1 Ag_2S Single Crystal Whiskers

An interesting effect observed when tuning the parameters for the sulfurization of Ag films, is the formation of Ag_2S single crystal whiskers that grow from the sample surface. These whiskers grow to sizes of several micrometers in length and approximately $1 \mu\text{m}$ wide, presenting well defined facets on the lateral surfaces. Figure 2.5 presents SEM images of several whiskers found on different sulfurized Ag films. The bottom left image of Fig.2.5 presents the growing of Ag protrusions on one whisker induced by the electron beam.

The formation of Ag_2S whiskers has been previously observed on Ag_2S samples prepared by sulfurization [55, 56], and its formation mechanism has been explained to be analogous to the Vapor-Liquid-Solid (VLS) mechanism [57]. The process consist of the formation of a Ag_2S droplet, which acts as the nucleation site for the whisker growth. Under a constant S vapor pressure, the Ag_2S whisker will then grow along the energetically favorable crystal orientation. According to the authors [55] the presence of a catalyst particle at the end of the whisker was not always observed, which was explained by the non-stability of the droplet at specific thermodynamic conditions. In our whiskers we did not observe the presence of a catalyst particle at the end of the whiskers.

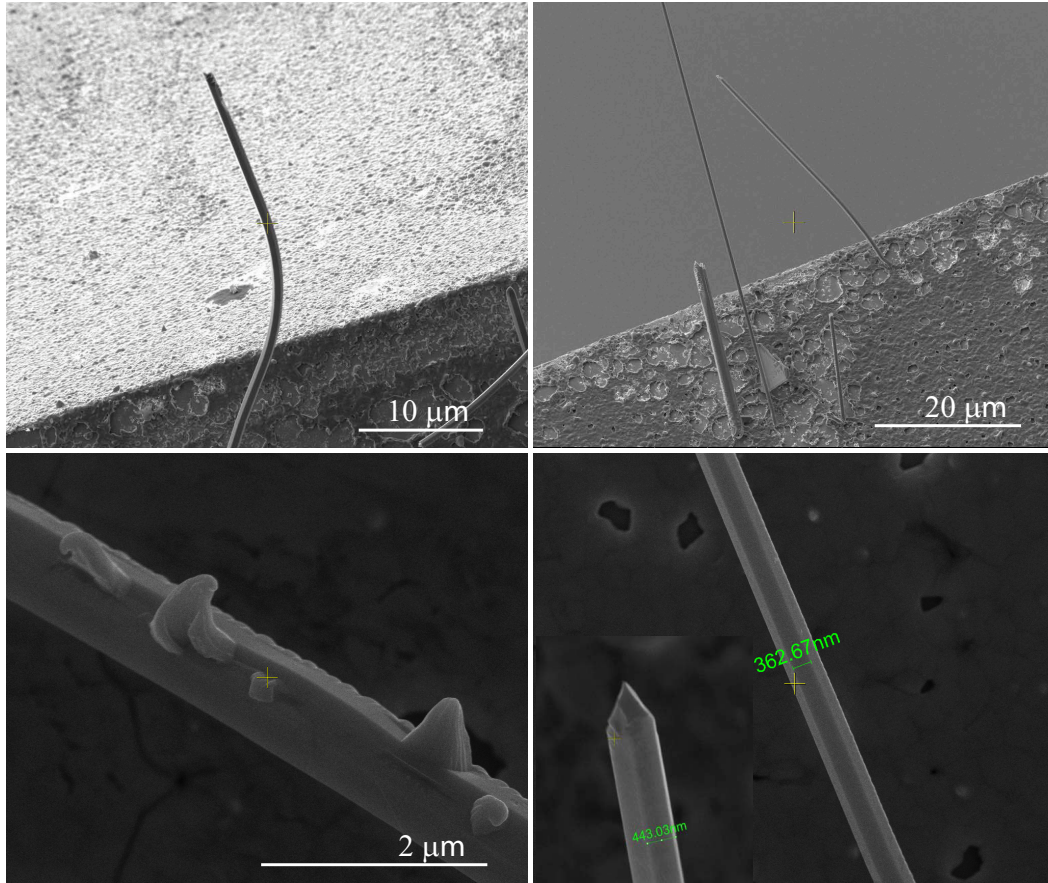


Figure 2.5: Scanning electron micrograph of several whiskers formed on sulfurized Ag₂S thin films. The bottom left picture shows Ag protrusions growing from the whisker activated by the electron beam.

With our Ag sulfurization method, the main parameter that differentiates from obtaining either a smooth sulfurized film, or a film with whiskers growing on the surface is the sulfurization time (the whiskers grow at sulfurization times longer than the typical 2 hours used for the films). A low S vapor pressure in the tube is another parameter that possibly influences the whisker growth, although this was not confirmed. We analyzed the composition of the whiskers by energy dispersive spectroscopy (EDS) and the result is presented in Fig.2.6a. The EDS spectra confirm that the whiskers are composed of only Ag and S atoms, and with an atomic percentage of 67.1% Ag and 32.9% S ($\pm 0.1\%$).

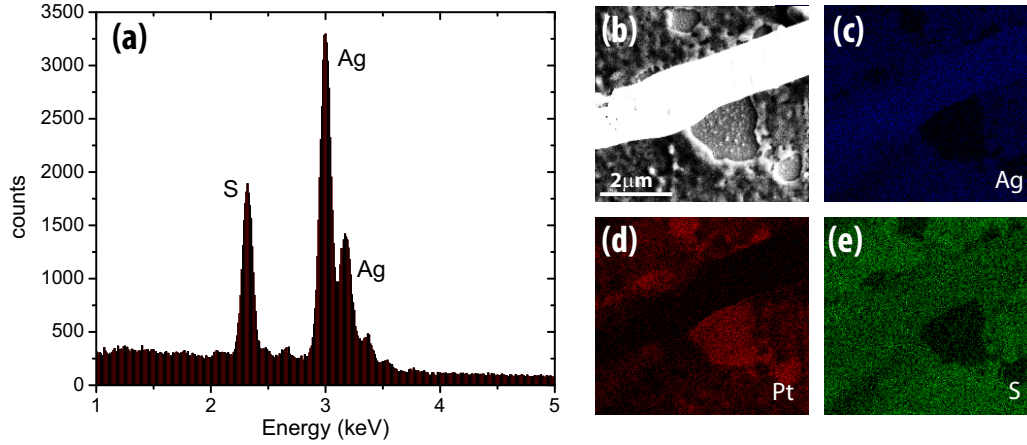


Figure 2.6: a) EDS spectrum acquired on the whisker presented in (b). The spectrum indicates Ag content of 67.1% and S content of 32.9% in atomic percentage. Elemental mapping showing the distribution of c) Ag and d) S content on the whisker and the sample surface. e) Pt content map indicating its presence only on the surface of the sample.

2.2.2 Summary

The characterization of the samples fabricated by Ag sulfurization, indicate that this is a reliable method to obtain acanthite (α -) Ag_2S films. This method presents the advantage that is simple and can be easily implemented in the fabrication of layered devices of the form $\text{Si}/\text{Pt}/\text{Ag}_2\text{S}$. On the other hand, we have learned that parameters as temperature, sulfurization time and cooling down rate strongly influence the formation of holes in the film or grow of whiskers. Another disadvantage is the controllability of the Ag_2S layer thickness and therefore the formation of a well defined $\text{Ag}/\text{Ag}_2\text{S}$ interface. This is important in the fabrication of devices with the layers $\text{Si}/\text{Ag}/\text{Ag}_2\text{S}$. The advantage of having a Ag bottom electrode instead of Pt is the fact that Ag fixes the chemical potential at the $\text{Ag}/\text{Ag}_2\text{S}$ interface, and therefore, the stoichiometry is also fixed at the maximum in equilibrium with Ag. The sulfurization method as we performed it, did not reproducibly allow the control of the Ag film thickness to be sulfurized, to keep one clean (no sulfurized) Ag bottom electrode. To achieve this, we used the second method that is reactive sputtering.

2.3 Reactive Sputtering of Ag₂S thin films

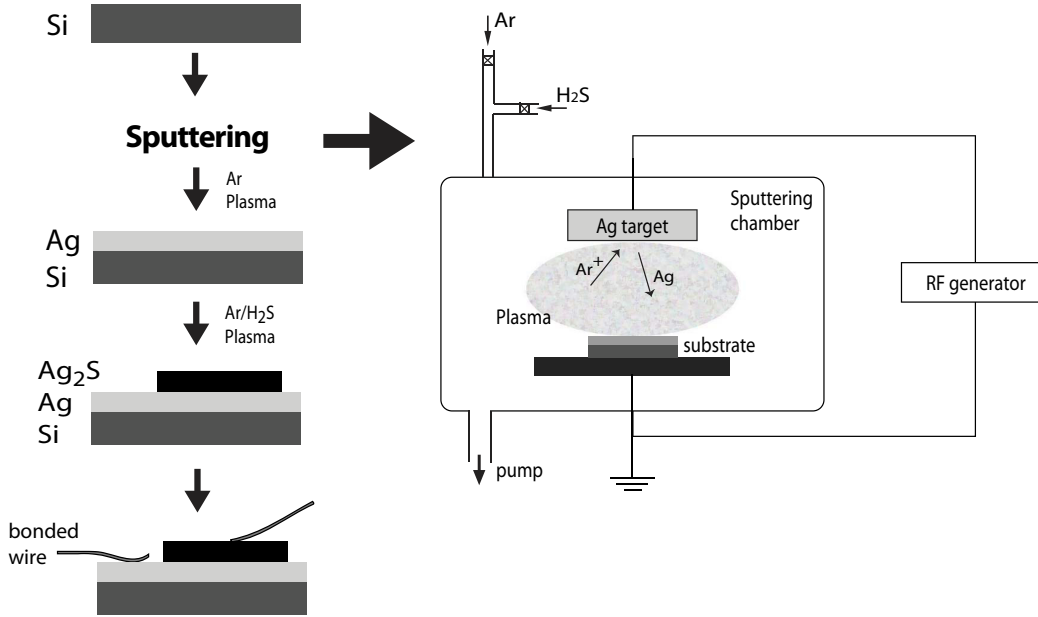


Figure 2.7: Schematic diagram of the fabrication steps of the Ag₂S devices and drawing of the sputtering system used to grow the samples.

For the fabrication of Ag₂S devices by reactive ion sputtering we used a specialized Leybold Z-400 RF diode sputtering system equipped with one silver target and 2-channel gas blending for Ar and H₂S. The fabrication steps are presented in Fig.2.7. A layer of Ag (100nm thickness and 10 x 10 mm² surface area) is sputtered onto a clean Si(100) substrate covered with a native oxide layer. On top of the Ag layer, the Ag₂S layer (200nm thickness and 5 x 5 mm² surface area) is grown by sputtering of Ag in a Ar/H₂S plasma, with the use of a shadow mask. For the preparation of stoichiometric Ag₂S by RF-sputtering, the most important parameter is the partial pressure of H₂S in the sputtering atmosphere. To estimate the partial pressure of H₂S in the sputtering chamber, we measure the total pressure ($P_{\text{total}} = P_{\text{H}_2\text{S}} + P_{\text{Ar}}$) with a Compact Capacitance Gauge (CMR 264, Pfeiffer Vacuum). First the Ar partial pressure is set to establish the sputtering discharge (pre-sputtering), and only then, H₂S is introduced in the chamber. To achieve a stoichiometric composition, the partial pressure of H₂S used is $\approx 6 \times 10^{-4}$ mbar. Once the plasma, pressure and gas flow are stable, the sputtering

deposition is performed. The deposition process is all at room temperature and no post-deposition treatment was carried out on the samples.

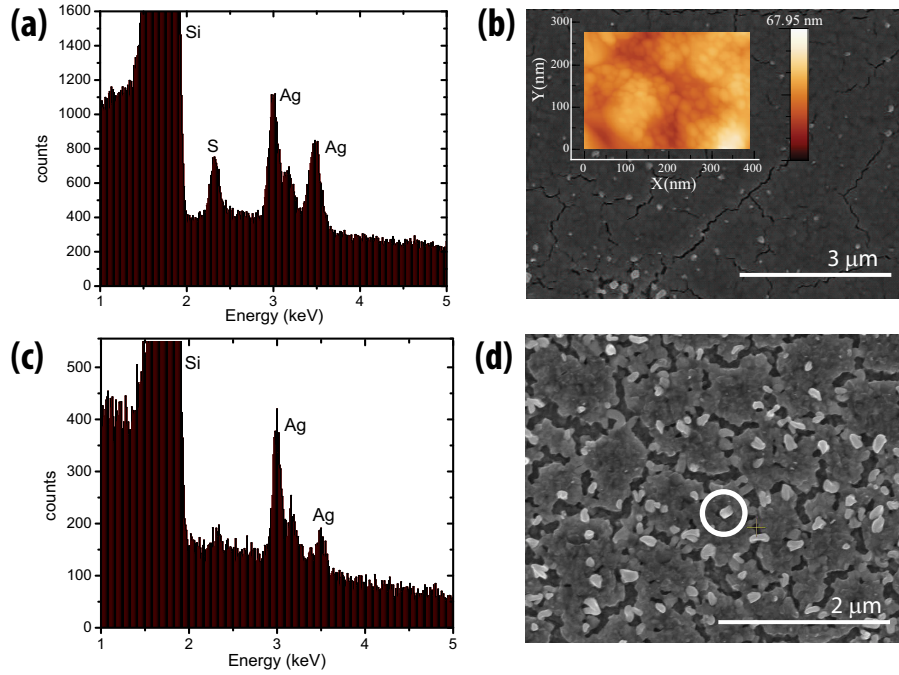


Figure 2.8: a) EDS spectrum of a sputtered Ag_2S film deposited on a Si substrate on top of a previously sputtered Ag layer. The observed peaks indicate the Ag and S content on the film, as well as a Si peak of the substrate. b) Surface morphology of a typical sputtered Ag_2S film examined by SEM and AFM (inset). The cracks on the surface are caused by the exposure of the film to the electron beam, and therefore the formation of Ag protrusions (white spots on the surface). These cracks become larger at longer exposure times. c) EDS spectrum of one of the Ag filaments growing on the surface of the film (the encircled filament in the SEM scan presented in (d)). The observed peaks indicate the presence of Ag but negligible S content on the protrusion.

The composition of the samples was analyzed by x-ray diffraction (XRD) and energy dispersive x-ray spectroscopy (EDS). The XRD spectra did not show as clear Ag_2S peaks as for the sulfurized samples, suggesting the formation of an amorphous or nanocrystalline film. The chemical composition was therefore checked by EDS. We used a FEI XL30 SEM equipped with an EDS system from the FOM Amsterdam nanocenter facilities. The spectra (Fig.2.8a) were taken at 10 kV electron beam energy and show the presence of the elements Si, Ag and S.

The dominant Ag peaks correspond to the characteristic x-ray lines of the L series 2.985, 3.151 and 3.511 keV. The S peak corresponds to the characteristic x-ray line 2.308 keV of the K Series. Discarding the Si content, the spectra indicate atomic percentages of 66.7% Ag and 33.3% S ($\pm 0.1\%$). The presence of the Ag bottom electrode was confirmed by testing the resistance of the bottom layer and by XRD. The formation of semiconducting Ag₂S and the sample stoichiometry was confirmed with electrical transport measurements. This will be presented in Chapters 4 and 5.

The surface morphology of the sputtered samples was examined by Scanning Electron Microscopy (SEM) and Atomic Force Microscopy (AFM). Figure 2.8b shows a SEM micrograph of the surface morphology of a sputtered Ag₂S film. The inset shows an AFM topography image of the surface. We observe a rough surface with grain sizes of approximately 20 to 40 nm diameter. Figure 2.8d shows a closer view of the sample surface with Ag protrusions activated by the electron beam. An EDS spectrum was taken at the Ag protrusion (white circle in the figure) showing only the elemental Ag peaks (Figure 2.8c) and a vanishing of the S peak. No Ag₂S whiskers were formed on samples prepared using the sputtering method.

2.3.1 Summary

Sputtering deposition allows the fabrication of devices with Ag or Pt bottom electrodes. This method presents the advantage of Ag and Ag₂S layer thickness deposition control and a continuous film without holes, in contrast to the sulfurization method. The absence of whiskers is also an advantage of this technique. Growth of the films at room temperature leads to the formation of amorphous or nanocrystalline Ag₂S films.

2.4 Fabrication of in-plane electrodes and Ag₂S deposition issues

In section 2.2 and 2.3 it was shown that either sulfurization of a Ag thin film, or reactive sputtering, are appropriate methods for the fabrication of so called out-of-plane devices, layered devices of the form Si/X/ α -Ag₂S/Pt(nano- top contact), with X = Pt or Ag. For these devices the electrical measurements are performed

perpendicularly across the Ag_2S layer. A large part of our investigations was performed with these devices using different top electrodes, as will be presented in Chapters 3, 4, 5 and 6. Although it is important to study the electrical switching properties, for these devices the direct visualization of Ag nanowire formation in Ag_2S is not possible. To achieve this we fabricated so called in-plane devices, where the electrical measurements are performed parallel to the surface of the Ag_2S thin films. We combined electron beam lithography techniques to pattern the electrode structure, conventional deposition techniques to deposit the Pt electrodes, and the sulfurization or the sputtering method to deposit the Ag_2S layer. The results and challenges found in the fabrication of these devices are presented below.

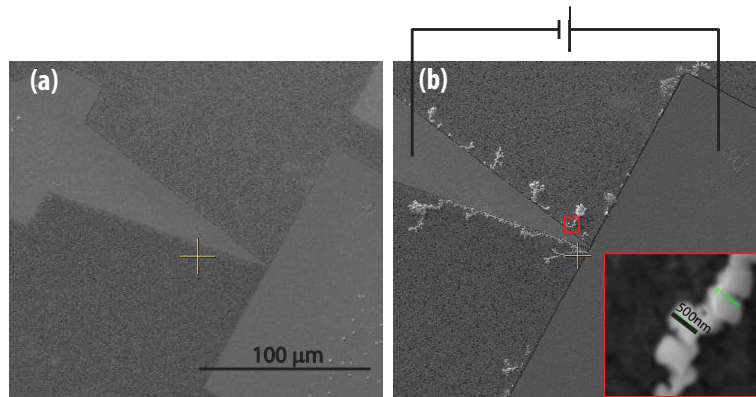


Figure 2.9: Scanning electron micrograph of a two terminal in-plane device. The gap between the electrodes is approximately $1\mu\text{m}$. a) Pt electrodes with the Ag_2S layer deposited on top before the activation of the device. b) When a voltage difference is applied between the electrodes, Ag filaments formed at the regions close to the negatively biased pointed electrode.

Using e-beam lithography (EBL), Pt electrodes were patterned on a Si wafer with a native oxide layer. Each pair of electrodes formed a gap of few micrometers or few tens of nanometers. Ag_2S was deposited on top of the electrode structure centered at the gap between the electrodes. The Ag_2S layer therefore contacts the two electrodes forming a two terminal device of the form Pt/ Ag_2S /Pt. The first in-plane devices were fabricated with the geometry presented in Fig.2.9. The Pt electrodes are separated by a gap of approximately $1\mu\text{m}$. The Ag_2S layer on top of the electrodes was deposited by reactive sputtering as described in section

1.3. In-situ electrical measurements performed in the SEM showed that, when a voltage was applied between the electrodes, the growth of small Ag filaments was induced, as presented in Fig.2.9b.

Aiming for the formation of a Ag bridge between the electrodes with atomic scale sizes, we proceeded with the fabrication of much smaller devices, i.e., devices with nanogaps between the electrodes. The nanoscale devices were fabricated partly in the Nanolab Groningen facilities (fabrication of the Pt electrodes), and in our laboratory in Leiden (the deposition of the Ag₂S layer). At these dimensions the Ag₂S deposition methods, both sputtering and sulfurization, did not result in good Ag₂S films. Figure 2.10b-c present the result of the Ag₂S deposition by sulfurization of a Ag film on the nanoscale electrodes presented in Fig.2.10a. The SEM images indicate that the Ag shrinks into clusters of Ag or Ag₂S. It is important to mention that for the sulfurization of the Ag nanosquare areas, the sulfurization parameters were adjusted to a sulfurization temperature of 420 K and a sulfurization time of only 30 min without further annealing. Figure 2.11b-d presents the result of the Ag₂S deposition by reactive sputtering on the electrodes given in Fig.2.11a. The SEM images show the formation of non-continuous films and the disappearance of a previously deposited Ag electrode. The sputtering parameters were the same as those presented in Section 2.3.

A possible explanation as to why the deposition of Ag₂S in such small areas was not successful, may be the lack of an adhesion layer on the Si (for example Cr or Ti) before the evaporation of Ag or sputtering of Ag₂S. Another explanation could be that the deposited film thickness was not enough to form a continuous layer. The last problem is related to the compromise between the resist layer thickness and the thickness of the deposited layer to achieve a good lift-off process. Fine-tuning of the sputtering parameters (the partial pressure of H₂S on the chamber and slower deposition rate) or fine tuning of the sulfurization parameters (much lower temperatures and shorter sulfurization times) will be required for the successful fabrication of lithographically patterned nano-Ag₂S. Direct evaporation of Ag₂S powder could be a good alternative to the presented methods.

Because of research priorities and estimated time needed for the optimization of EBL fabrication parameters, we did not proceed with this type of samples.

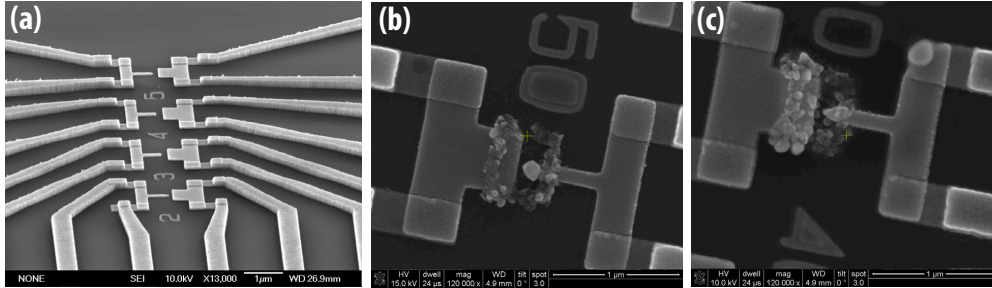


Figure 2.10: a) Scanning electron micrograph of two terminal devices, each pair of electrodes separated by 20, 30, 40 and 50 nm gaps. b) and c) Result after deposition of Ag and sulfurization at 420 K.

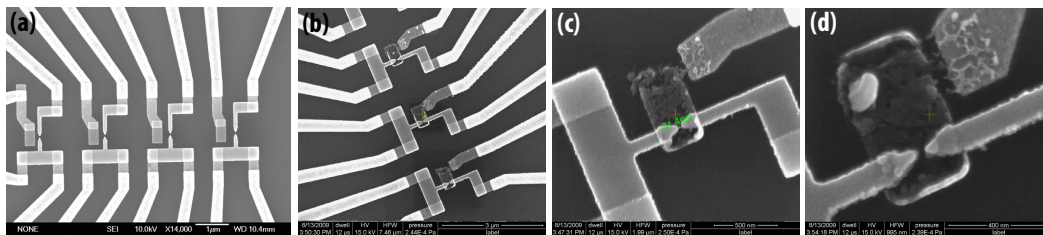


Figure 2.11: a) Scanning electron micrograph of three terminal devices, formed by Pt electrodes separated by nanogaps of 30 nm and a Ag third electrode. b, c, d) Result after reactive sputtered deposition of Ag_2S in the nanoscale area between the electrodes.

2.5 Conclusions

Two fabrication methods were presented in this chapter. Both sulfurization and reactive sputtering are suitable for the growth of semiconducting Ag_2S thin films. The silver sulfide samples prepared by sulfurization of a Ag thin film are polycrystalline. A side effect of the high temperature and sulfur vapor pressure used in this method, is the formation of micrometer long whiskers. Silver sulfide samples prepared by reactive sputtering are possibly amorphous or nanocrystalline (no clear X-ray peaks observed), the films are continuous and the samples do not present evidence for the formation of whiskers. For a good control of the growth parameters and a well defined Ag/ Ag_2S interface, the reactive sputtering method is the most suitable fabrication process. Both types of Ag_2S fabrication processes need to be further tuned for application in EBL fabricated devices.

2. Ag₂S: FABRICATION AND CHARACTERIZATION TECHNIQUES

3

Conductance switching in Ag_2S devices fabricated by sulphurization

The electrical characterization and switching properties of the $\alpha\text{-Ag}_2\text{S}$ thin films fabricated by sulfurization are presented in this chapter. The $\alpha\text{-Ag}_2\text{S}$ thin films show semiconductor behavior at low bias voltages, whereas they exhibit reproducible bipolar resistance switching at higher bias voltages. The transition between both types of behavior is observed by hysteresis in the IV curves, indicating decomposition of the Ag_2S and formation of a conductive path between the electrodes.

This chapter is partly based on M. Morales-Masis, S. J. van der Molen, W. T. Fu, M. B. Hesselberth and J.M. van Ruitenbeek, *Nanotechnology* **20** 095710 (2009)

3.1 Introduction

Silver Sulfide is a mixed conductor material, with the total conductivity (σ_t) determined by that of the Ag^+ -ions (σ_{Ag^+}) and electrons (σ_e), i.e. $\sigma_t = \sigma_e + \sigma_{\text{Ag}^+}$. In the low temperature phase, $\alpha\text{-Ag}_2\text{S}$, the total conductivity increases with temperature representing semiconductor behavior.

Silver sulfide also presents conductance switching characteristics when a thin film of this material is placed between metal electrodes, and a sufficiently large voltage is applied. Previous studies [14] indicated that the conductance switching is of filamentary nature, meaning that switching occurs due to the reversible formation of a conductive path across the Ag_2S layer. The conductive path connects the electrodes causing the switching in conductance, and the persistence of the conductive path after the removal of the bias can be exploited for memory applications. As mentioned in Chapter 1, the requirements for this type of memories are the mobile metal ions (the Ag^+ -ions in the case of Ag_2S) and an asymmetry of the electrodes, defined either by the type of metal or by the geometry of the electrodes [5].

This chapter presents our study of the electrical properties of Ag_2S devices prepared by the sulfurization method (described in Chapter 2 Section 2.2). The chapter starts with the description of the measurement hardware and software. Next, conductivity measurements as a function of temperature are presented, serving for the electrical characterization of the sulfurized Ag_2S films. The last part of the chapter is dedicated to the conductance switching properties measured on devices of the form $\text{Pt}/\text{Ag}_2\text{S}/\text{Pt}$ (micro-contact). In these devices, the asymmetry of the electrodes is imposed by the geometry, a large Pt bottom contact and a small Pt micro contact on top, and this asymmetry defines the voltage polarity at which the device switches ‘on’ or ‘off’. Bipolar switching (setting of the ‘on’ state at one voltage polarity and setting of the ‘off’ state at the reverse polarity) is studied for a range of bias voltages.

3.2 Measurement setup

To measure the electrical properties of the Ag_2S devices we used a simple electronic circuit, presented in Fig.3.1. It consists of a dc voltage source, for which we use an analog output of a National Instruments Data Acquisition Card (NI

USB-6251, M Series DAQ). The current through the sample due to the dc voltage applied is converted into a voltage using a FEMTO current amplifier (DLPCA-200 variable gain transimpedance [V/A] amplifier), and the output of the current amplifier is read by an analog input channel of the NI USB-6251 DAQ.

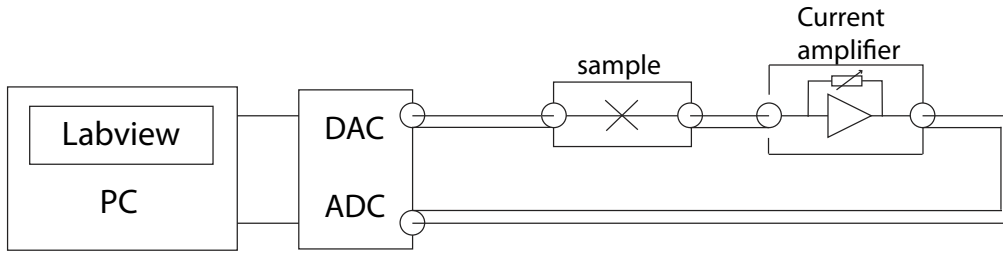


Figure 3.1: Schematic diagram of the measurement circuit.

The NI DAQ is programmed with the LABVIEW development package of National Instruments. The LABVIEW programs allow the simultaneous control of the bias voltage and the monitoring of the current input. For each experiment, a specialized LABVIEW program was developed according to the requirements for each of the measurements (e.g. waveform of the output voltage, frequency, sampling rate).

3.3 Electrical conductivity

Conductivity measurements as a function of temperature were performed for electrical characterization of the sulfurized Ag_2S films. For these experiments the samples were prepared with a specific electrode configuration, using two parallel electrodes (Pt and Ag stripes, 0.5mm width and 0.5mm separation) crossing the Ag_2S film (150nm thickness), as shown in the inset on Fig.3.2. The electrodes and Ag_2S were deposited on a mica substrate. Measurements were performed by applying an alternating voltage (± 50 mV square wave, 1 Hz) to the parallel electrodes, and by increasing the temperature in steps of 5 K starting at room temperature. In Fig.3.2 we present an Arrhenius plot for one of our samples. In the plot two slopes are observed: one in the temperature range from 299 K to 417 K and a second one for $T > 417$ K, where a steep rise in conductivity is observed. From the first slope (in the temperature range $299 \text{ K} < T < 417 \text{ K}$), the calculated activation energy for electrical conductance is 0.64 ± 0.03 eV, which

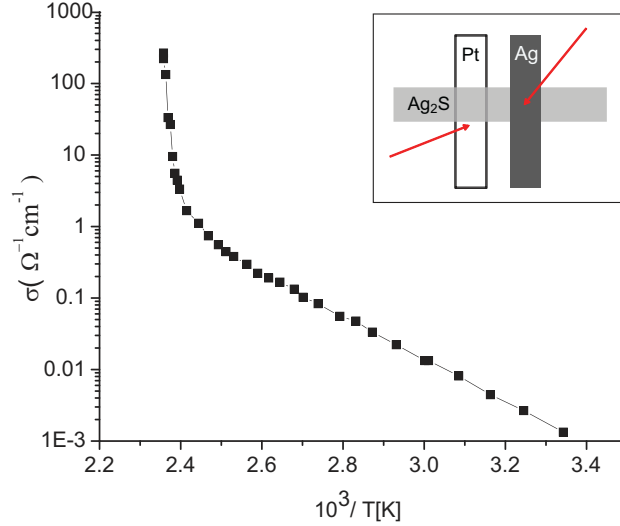


Figure 3.2: Arrhenius plot of the electrical conductivity of a Ag_2S film. The inset shows the electrode configuration used for the two-probe measurements. The arrows indicate the position of the contacts to the Pt and Ag electrodes.

is in close agreement with reported values in literature [58, 59]. This is known to be due to an electronic activated behavior associated with the semiconductor bandgap. We suspect that the steep rise in the conductivity for $T > 417$ K is a direct consequence of measuring in a temperature range close to the phase transition temperature ($T_{\alpha\beta} = 451$ K). This transition is the so-called order-disorder transition when the electronic and ionic conductivity increase by several orders of magnitude [26]. The measured conductivities agree with conductivity values reported in literature by Bonnacaze et al. [25] and Miyatani [58], confirming the semiconductor properties of the fabricated α - Ag_2S thin films.

3.4 Electrical Switching

Electrical measurements of switching were performed perpendicularly across the Ag_2S layer, using a two-probe configuration. A Pt film is used as the bottom electrode and a micrometer-scale probe contact (a Pt or Ag wire, 0.1mm diameter) as the top electrode, applied with a small mechanical load. A diagram of the electrode configuration is shown in Fig. 3.3. A bias voltage V_b is applied to the Pt bottom electrode and the current is measured between the top electrode

on the Ag₂S film and ground. All experiments were done at room temperature and under atmospheric pressure.

3.4.1 I-V characteristics

Current- voltage (IV) curves were obtained by continuously sweeping the voltage from $0 \rightarrow V_{max} \rightarrow 0 \rightarrow -V_{max} \rightarrow 0$, where V_{max} is the maximum applied bias voltage. We present a summary of the measurements in Fig. 3.3, which features six values of V_{max} (200, 250, 350, 450, 550 and 700 mV, respectively). At low bias voltages, $V_{max} = 200\text{mV}$ (Fig. 3.3a), the device presents a rectifying characteristic. We define this behavior as the pre-switching state: Ag₂S presents semiconductor properties and no hysteresis is observed in the IV curves. The shape of this IV curve and the steady state behavior (pre-switching) will be described in detail in Chapter 4.

At $V_b > 200$ mV (Fig. 3.3b, c and d), the asymmetry of the IV curves remains, but in addition we observe hysteresis, starting at positive bias voltages. Upon increasing the bias voltage range, this hysteresis evolves into full bipolar switching (see Fig. 3.3e and f). In this case, the ‘on’ and ‘off’ states of the device are clearly observed. Following the arrows in the IV curve (Fig. 3.3f), a clear jump in the current is observed when a positive voltage is applied to the Pt bottom electrode (curve section ‘1’). The current increases, reaching values in the mA range at V_{max} , which represents the ‘on’ state. Sweeping back the voltage (curve section ‘2’), the ‘on’ state persists even at moderate negative voltages. When a sufficiently high negative voltage is reached, we observe a sudden decrease in the absolute value of the current. We define this as the switching of the device to the ‘off’ state (curve section ‘3’). The device remains in the ‘off’ state until a positive voltage switches the device back to the ‘on’ state. The polarity for switching is imposed by the geometry of the electrodes, a micro-scale top contact and a large bottom electrode, as shown in the diagram at the top of Fig. 3.3.

Upon calculating the resistance in the ‘on’ state of Fig. 3.3f, we find values from 90 to 125 Ω . This high metallic conductance property of Ag₂S films after switching has been reported in the literature [14, 23, 60]. In these reports the linear IV curves are interpreted as being due to the formation of a metallic filament which grows due to ionic transport and the subsequent reduction of the Ag⁺-ions at the negative electrode. A metallic Ag filament will then form connecting the

3. CONDUCTANCE SWITCHING IN Ag_2S DEVICES FABRICATED BY SULFURIZATION

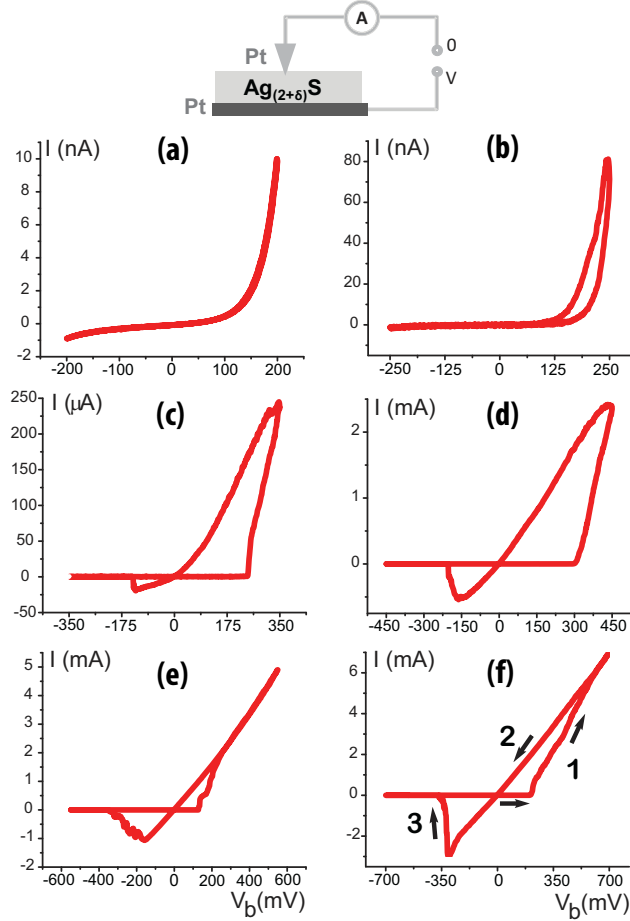


Figure 3.3: Top: Electrode configuration for electrical measurements of switching behaviour. The top electrode is a Ag wire. (a-f) Current- voltage characteristics of the device for different bias voltage ranges ($V_{max} = 200, 250, 350, 450, 550$ and 700 mV, respectively).

electrodes and turning the switch ‘on’. Switching ‘off’ is achieved by changing the polarity of the bias voltage, causing the metal atoms to oxidize and dissolve, annihilating the filament. Although the picture of redox processes at the electrodes is widely accepted, in the case of Ag_2S , the interpretation of the switching mechanism is not consistent in the reported literature. In many cases, the high conductance is attributed to a Ag metallic wire which bridges a tunneling gap between the surface of the Ag_2S and a Pt electrode, claiming that Ag_2S is an electrode with resistance of $\approx 100 \Omega$ [23, 49, 61]. In other articles, the same group attributed the high conductance to a Ag metallic filament growing inside

the Ag_2S film [46, 60, 62]. Because Ag_2S is a high resistive material, we believe that the metallic filament should grow inside the film (even in the presence of a tunneling gap (See Chapter 5)) to reach resistance values of 90Ω .

Following the idea of the formation of a conductive filament, we can interpret our IV measurements as follows. Initially, and as long as the Ag_2S is not decomposed, only the semiconductor behavior is observed. When the applied electrical potential is higher than a threshold voltage, the Ag_2S decomposes and elemental silver starts forming at the cathode (the micro-electrode) [63]. The metallic Ag starts accumulating at the boundary and grows towards the anode (the large bottom electrode). The filamentary growth of the deposited Ag can be explained as the result of the field pattern formed between the electrodes (Fig. 3.4). Furthermore, irregularities on the deposited metal enhanced the electric field and thus the flux of Ag ions is onto their tips. Consequently, the distance between the growth front and the anode is reduced enhancing the field even more, and causing the tip to move faster than the surrounding metal front. Finally this tip connects the bottom electrode shorting the device. The hysteresis in Fig. 3.3b is a result of the relatively low bias applied. Hence, the effective switching time is much longer than the inverse frequency of the IV measurement ($f = 1\text{Hz}$). At higher biases, the driving force on the ions will be larger, so that switching will be faster. We will elaborate on this below.

When sweeping the voltage over multiple cycles, we also observed a change in the IV curves from the first to the following runs, i.e. a memory effect in the sample. In Fig. 3.5 the first IV curve (orange curve) presents a higher switching voltage and lower conductance than all later curves, while the last curves present the lowest switching voltage and higher conductance. In the framework of the model discussed above, we propose the following interpretation. When the device is switched ‘on’ from its virgin state, it is possible that a lattice modification occurs, accompanying the filament growth. When the device is switched back ‘off’, the lattice does not return to its initial state, and the accumulation of ions at the negative electrode will not be completely undone. This supports the assumption that permanent changes occur in the sample when mass transport of ions initiates. In Chapter 6 this topic will be further discussed.

To investigate the changes in conductance as a function of V_b as well as its time dependence, an additional experiment has been performed. Starting with

3. CONDUCTANCE SWITCHING IN Ag_2S DEVICES FABRICATED BY SULFURIZATION

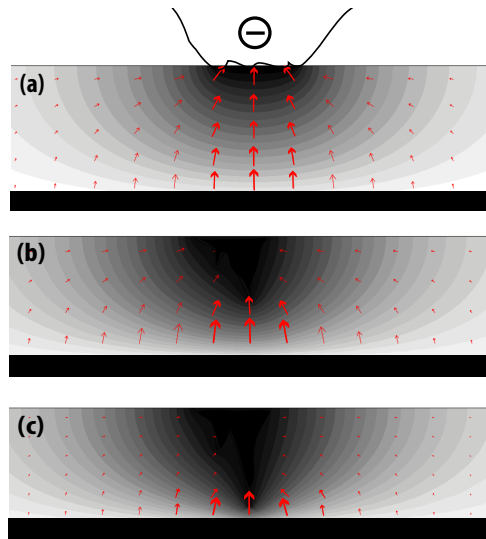


Figure 3.4: Simulation of the electric field lines (represented with the arrows) and the electrical potential (contour plot) across the Ag_2S layer when a voltage is applied between the two metals electrodes. The black bottom layer represents the large Pt electrode, and the Pt or Ag top contact wire is sketched at the top of (a). The metallic filament is also presented in black growing from the cathode towards the anode. In (b) and (c) the asymmetry of the Ag filament results from the possible irregularities in the metal deposited.

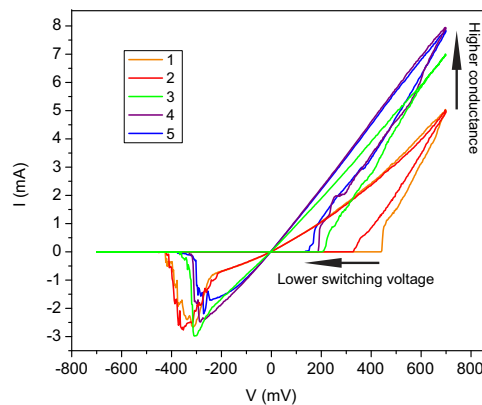


Figure 3.5: Multiple sweeping in voltage shows the changes (indicated by the black arrows) in the IV curves from the first curves with higher switching voltage and lower conductance (curves 1 and 2) to the last curves with lower switching voltage and higher conductance (curves 3, 4 and 5).

the device in the ‘off’ state, a positive voltage bias is applied to the bottom electrode by a step function (from 0V to V_b), and is kept constant until the device reaches its maximum value in conductance. We present the results in Fig. 3.6.

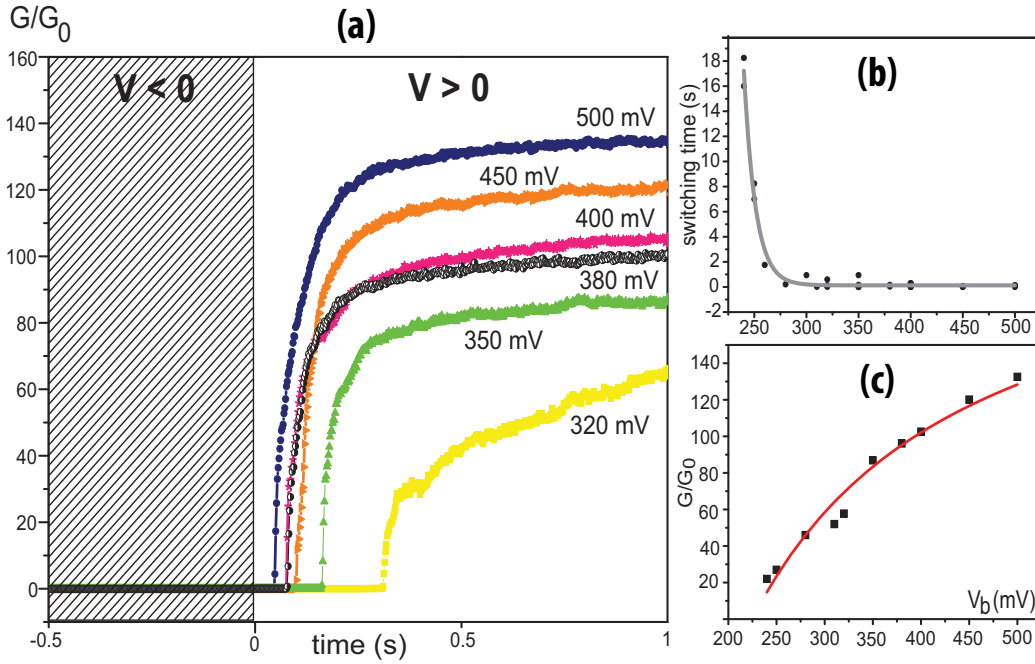


Figure 3.6: a) Increase in the conductance when a step function is applied to the device and keeping the voltage constant at its maximum amplitude, V_b (at $V < 320$ mV switching occurs at $t > 1$ s). b) Switching time as a function of the applied step voltage amplitude (V_b). c) Total conductance reached by the device as a function of V_b . The data points are in good agreement with a simple model, incorporating a series conductance $G_{series} = (233 \pm 10)G_0$ and a threshold voltage $V_{th} = 225 \pm 5$ mV (red curve).

Figure 3.6a presents the increase in conductance as a function of time. The switching time is defined here as the time at which the conductivity rises above $1G_0$, where $G_0 = 2e^2/h$. The time required to switch the device from the ‘off’ to the ‘on’ state depends strongly on the amplitude of the step in the voltage. At voltages from 200 to 275mV, it takes several seconds until the sudden rise in conductance is observed. This is consistent with the observation of hysteresis, i.e. incomplete switching, in the IV measurements of Fig. 3.3b, taken at $f = 1$ Hz.

3. CONDUCTANCE SWITCHING IN Ag₂S DEVICES FABRICATED BY SULFURIZATION

However, at $V_b > 275\text{mV}$, the switching occurs in less than a second. The dependence of the switching time with the applied voltage is presented in Fig. 3.6b.

When keeping the voltage constant, we observe after several seconds that the total conductance, G_{total} , reaches a maximum value and remains in this state until the applied voltage is changed. The measured saturation value of total conductance (expressed in multiples of the conductance quantum) increases with the applied voltage, as shown in Fig. 3.6c.

To understand this, we apply a model as follows. The conductance increases as a result of a combination of factors. In the interior of the Ag₂S film a conducting path is formed that consists of a metal filament and a modification of the local lattice of the material. The first of these two processes will continue as long as the applied voltage over the sample V_b is higher than a threshold voltage V_{th} . Assuming a fixed conductance for the external circuit, G_{series} , the voltage drop across the sample decreases as the sample conductance increases. As soon as this voltage drop is lower than V_{th} , the growth of the filament stops. Thus, for higher applied voltage, V_{th} will be reached at a higher conductance value, with a larger total cross section of the filaments formed.

We fit the experimental data in Fig. 3.6c with the equation for a voltage divider,

$$G_{total} = \left(1 - \frac{V_{th}}{V_b}\right) G_{series} \quad (3.1)$$

where $1/G_{total} = 1/G_{sample} + 1/G_{series}$ and V_{th} and G_{series} the fittings constants. As observed in Fig. 3.6c, the resulting curve (red curve in the plot) fits the experimental data very well. The value obtained for V_{th} is $(225 \pm 5)\text{mV}$ and for G_{series} is $(233 \pm 10) G_0$, which corresponds to a series resistance of $\approx 55 \Omega$. This series resistance can be largely attributed to the input impedance of the current amplifier. The value found for V_{th} is consistent with what we found from the IV characteristics of Fig. 3.3.

The calculated values of the sample conductance are within the range $24G_0 < G_{sample} < 307G_0$. This indicates that the final sample conductances, especially those corresponding to the higher applied voltages (450mV and 500mV), are already limited by the series conductance. Hence, in principle, by choosing a

proper V_b and G_{series} , the final sample conductance can be tuned and with it the filament formation in the device. The switching time, can also be regulated by the same parameters i.e. to obtain a lower switching time with the same G_{sample} , a higher V_b with lower G_{series} should be chosen. This principle was tested and is presented in Fig. 3.7. The Figure shows the measured conductance of the device, excluding the added series conductance. The measurements are performed after adding a series resistor of $4.3k\Omega$, and applying a step voltage from 0 (at $t=0s$) to 500, 700 and 800 mV. As expected, at voltages of 700 and 800 mV the device is switched on almost immediately, with times shorter than 10^{-5} s, where the measured time is limited by the sampling rate used. The sample conductances (G_{sample}) are only few units of G_0 and close to the values predicted using Eq.3.1, conductances much lower as compared with the conductances shown in Fig. 3.6a at $t = 0.5s$.

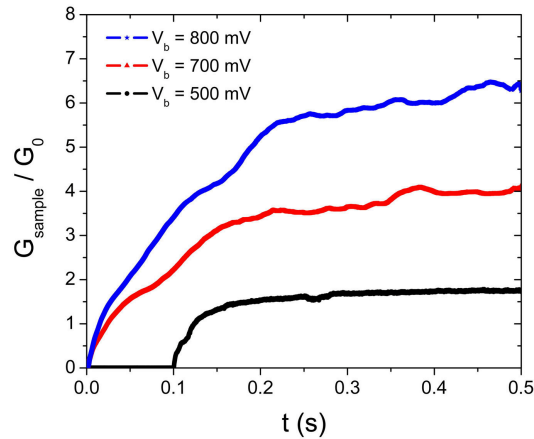


Figure 3.7: Increase in the conductance when a step function is applied to the device with voltage bias amplitudes of 500, 700 and 800mV. A series resistance of $4.3k\Omega$ is added to the measurement circuit. The sample conductance is calculated from the measured total conductance (G_{total}) and using $1/G_{sample} = 1/G_{total} - 1/G_{series}$

3.5 Conclusion

We have presented the electrical switching properties of Ag_2S thin films fabricated by sulfurization, and sandwiched between two asymmetric Pt electrodes. The electrical (IV) measurements enable the identification of an initial semicon-

3. CONDUCTANCE SWITCHING IN Ag_2S DEVICES FABRICATED BY SULFURIZATION

ductor behavior, followed by bipolar switching at higher bias voltages, when Ag_2S decomposes and a conductive path is formed. Bipolar resistance switching is observed during multiple cycles in all samples, provided that the applied voltage is higher than a threshold voltage V_{th} . The observed threshold voltage depends on the choice of electrode metals, and on the stoichiometry of Ag_2S . We will see in Chapter 4 that this value is significantly lower for a Ag bottom electrode, which provides a reservoir of Ag and fixes the chemical potential of Ag in Ag_2S . We show that the switching time and the final ‘on’-state conductance can be adjusted by choosing the series resistance and bias voltage properly. Understanding of the microscopic mechanism of switching is of great importance in order to optimize these systems for possible applications, e.g as ‘memristive’ devices [64].

4

Towards a Quantitative Description of Solid Electrolyte Conductance Switches

We present a quantitative analysis of the steady state electronic transport in a resistive switching device. The device is a thin film of Ag_2S contacted by a Pt nano-contact acting as ion-blocking electrode, and a large area Ag reference electrode. When applying a bias voltage both ionic and electronic transport occurs, and depending on the polarity it causes an accumulation of ions around the nano-contact. At small applied voltages (pre-switching) we observed this as a strongly nonlinear current-voltage curve, which has been modeled using the Hebb-Wagner treatment for polarization of a mixed conductor. This model correctly describes the transport of the electrons within the polarized solid electrolyte in the steady state up until the resistance switching, covering the entire range of non-stoichiometries, and including the supersaturation range just before the deposition of elemental silver. In this way, this forms a step towards a quantitative understanding of the processes that lead to resistance switching.

This chapter has been published as M. Morales-Masis, H. D. Wiemhöfer and J. M. van Ruitenbeek, *Nanoscale* **2** 2275 (2010)

4.1 Introduction

Understanding the physical mechanisms driving the resistance switching in metal/chalcogenide/ metal systems is of great importance, as the interest on their implementation in memory devices is increasing. Various models have been proposed to explain the switching mechanism; many of these models are based upon the concept of the formation of a conductive filament and its annihilation at opposite bias, inside the insulator material [14, 65, 66]. Nevertheless, a deep understanding of the microscopic mechanisms responsible for filament formation is still lacking.

In this paper we demonstrate the use of the Hebb-Wagner formalism [30, 67] for the analysis of the steady state I-V characteristics of memory resistors based upon mixed ion and electron conductors. We apply this formalism to fit our experimental I-V characteristics, and describe the ionic and electronic transport within the electrolyte before the full resistance switching is observed.

The mixed conductor used for the present study is Ag_2S . However, this description should also be valid for other mixed electronic and ionic conductors, e.g. Cu_2S and AgGeSe . In general, one needs to take into account that the formation of a space charge layer occurs for many solid electrolytes. In the case of Ag_2S , effects due to depletion or space charge at the Pt contact are negligible. The device we consider consists of a Ag_2S thin film contacted by a Ag thin film at the bottom (which helps to achieve a reference state with constant silver concentration at that contact), and a nano-scale Pt contact on the top realized by means of a conductive AFM tip.

Our measurements and simulations at low bias voltages (steady state) confirm the predictions of the theory: the increase in the electronic current at forward bias (negative polarity at the Pt contact) is due to the initial accumulation of Ag^+ -ions towards the nano-scale contact. This causes a Ag concentration gradient, i.e. local deviations from the ideal stoichiometry in the region close to the nano-contact. We note that this occurs before any switching is observed.

The Hebb-Wagner concepts have originally been formulated for bulk materials, and until today, to our knowledge, have not been applied to nano-scale contacts or thin film devices. We demonstrate that the theory still holds for nano-scale devices.

4.2 Measurement setup

The electrical measurements were performed with the use of a conductive atomic force microscope (C-AFM) (Veeco Multimode AFM/SPM system). In the setup, the Ag layer is the bottom contact to the Ag_2S layer and the top contact is a Pt-coated AFM tip. See the diagram in Figure 4.1. The measurement circuit is as described in Chapter 3 Section 3.2, and is independent of the AFM controller.

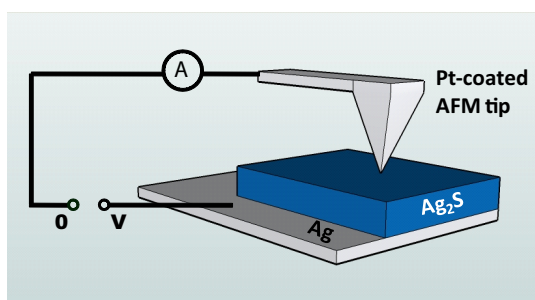


Figure 4.1: Schematic diagram of the electrode configuration for the measurements with the Conductive Atomic Force Microscope (CAFM)

The current-voltage characteristics of the samples were obtained by continuously ramping the voltage linearly from 0 to V_{max} down to $-V_{max}$ and back to 0, at a frequency of 0.25 Hz. Voltages are given throughout with respect to the potential of the Pt tip (taken as 0V). For the steady state analysis, the value of V_{max} was kept below the potential at which we observed hysteresis in the I-V characteristics [47], meaning that no significant changes are induced in the solid electrolyte by decomposition of the Ag_2S [63]. All the experiments were performed at ambient conditions.

Platinum is a chemically inert metal, and as an electrode in the system it blocks the ionic current. By using a nano-scale Pt electrode and a reference (Ag) electrode at the bottom with a large surface area, the changes in electrical conductivity will be concentrated in the vicinity of the nano-contact. The Ag_2S thin film has been fabricated by reactive sputtering, described in Chapter 2 Section 2.7.

4.3 Results

The current-voltage characteristics show an exponential behavior that is fully reversible on the time scale of the experiment. The curve is asymmetric, with an

increase in the current at the positive bias. We refer to this as the ‘pre-switching’ steady state behavior and, in the Ag/Ag_{2+δ}S/Pt junctions, it is observed for voltages below about 75mV (Figure 4.2a). When increasing the bias voltage beyond 75 mV, the I-V curves present hysteresis, which evolves into full bipolar switching for still larger voltages (Figure 4.2b). In the full bipolar switching case, the ‘on’ and ‘off’ states of the device are clearly observed, with a resistance ratio ($R_{\text{off}}/R_{\text{on}}$) of approximately 10^5 . The switching from ‘on’ to ‘off’ state is explained by the formation of conducting paths that are formed and dissolved within the solid electrolyte, connecting and disconnecting the electrodes (diagrams in Figure 4.2b) [14].

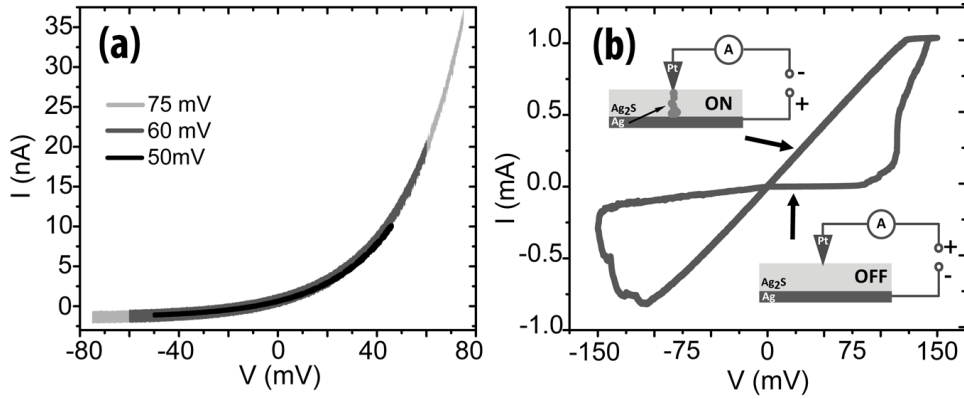


Figure 4.2: a) Steady State and b) full bipolar switching current-voltage characteristics of the Ag/Ag_{2+δ}S/Pt(nano-contact) system. In the full bipolar switching case the transition from ‘off’ to ‘on’ states and back is explained by the formation and dissolution of a conductive path.

We focus on the exponential, or steady-state, I-V curves (Figure 4.2a). The shape of the curve is reminiscent of curves measured for metal-semiconductor junctions, and it is known that Ag_{2+δ}S is a n-type semiconductor [29]. However, the obtained curves have the inverse curvature as compared to that expected for a Pt/n-type semiconductor junction (i.e. Schottky contact). In the case of solid electrolyte semiconductors, this must be attributed to a combination of ionic and electronic conduction in the electrolyte. The main observation is the fact that the shape of the IV-curves depends strongly on the type of electrode used: material, size and symmetry of the electrodes [68].

In our experiment, with the use of a nano-scale contact and a much larger bottom contact, we have introduced an asymmetry in the potential distribution across the mixed conductor. When a potential difference is applied to the system Ag/Ag_{2+δ}S/Pt, where Pt is the nano-contact, the strength of the electric field is concentrated in the vicinity of the nano-contact. If the potential is small, such as to avoid decomposition of Ag_{2+δ}S, a steady state composition gradient is induced in the Ag_{2+δ}S film, as a result of the mobility of Ag⁺-ions [30].

For a mixed electronic and ionic conductor such as Ag_{2+δ}S, the electronic conductivity is a function of the deviations from the stoichiometric composition (δ). When the negative polarity is at the Pt tip (nano-contact), the Ag⁺-ions move towards the tip, acting as n-type donors. The local enhancement of the Ag ion concentration results in an increase of the electronic conductivity in the small region close to the tip. We will elaborate on this below.

4.4 Theory

A model for the current-voltage behavior of mixed ionic conductors under steady state conditions goes back to Hebb and Wagner [30, 67].

Silver sulfide is a mixed conductor as both silver ions and electrons are mobile. Applying a voltage V to a silver sulfide sample between two electrodes, sets up a difference of the Fermi levels, ε_F'' and ε_F' , between both contacts.

If we can neglect the interface resistances, the applied electrical potential difference V imposes a difference of the local electrochemical potentials of electrons in the ionic conductor between the two electrode interfaces on the mixed conductor

$$-e V = \varepsilon_F'' - \varepsilon_F' = \tilde{\mu}_e'' - \tilde{\mu}_e' \quad (4.1)$$

where $-e$ is the electron charge. The values at the boundaries are denoted as double prime for the Ag bottom contact and prime for the Pt nanocontact.

According to Eq.(4.1), applying a voltage generates a gradient of the electrochemical potential $\tilde{\mu}_e$ within the mixed conducting silver compound and, thus,

an electronic current density j_e given by

$$\vec{j}_e = \frac{\sigma_e}{e} \vec{\nabla} \tilde{\mu}_e \quad (4.2)$$

with σ_e as the conductivity of electrons.

A gradient of the electrochemical potential of electrons is accompanied by a gradient of the electrochemical potential of silver ions, and vice versa. The corresponding silver ion current density is given by a complementary expression to Eq.(4.2) according to

$$\vec{j}_{\text{Ag}^+} = -\frac{\sigma_{\text{Ag}^+}}{e} \vec{\nabla} \tilde{\mu}_{\text{Ag}^+} \quad (4.3)$$

with σ_{Ag^+} as the conductivity of silver ions. The general equations for the partial current densities of ions and electrons are given according to transport theory of irreversible thermodynamics (Chapter 1. Section 1.4).

Furthermore, the currents of electrons and silver ions will be coupled by the equilibrium of electrons and ions according to



The assumption of local thermodynamic equilibrium between silver ions and electrons is valid, if the electrochemical potential gradient in Eq.(4.2) is not too high [27]. This approach is well accepted for mixed conducting silver chalcogenides [69]. Then, the condition of thermodynamic equilibrium holds for Eq.(4.4) at all positions in the sample. With μ_{Ag} denoting the chemical potential of neutral silver, it follows

$$\mu_{\text{Ag}} = \tilde{\mu}_{\text{Ag}^+} + \tilde{\mu}_e \quad (4.5)$$

According to the local equilibrium condition (4.5), the boundary condition Eq.(4.1), imposed by the voltage applied between the ion blocking Pt nano-contact and the silver back contact leads also to the following alternative expression for the applied voltage

$$-eV = \left(\mu''_{\text{Ag}} - \mu'_{\text{Ag}} \right) - \left(\tilde{\mu}''_{\text{Ag}^+} - \tilde{\mu}'_{\text{Ag}^+} \right) \quad (4.6)$$

Let us consider two simple limiting cases which lead to simplified equations for the voltage. The first concerns a sample with a homogeneous composition initially. At $t = 0$, just after a sudden jump of the voltage from $V = 0$ to $V > 0$, the chemical potential of neutral silver has a constant value throughout the whole sample. Under this condition, the difference of the chemical potentials of silver in Eq.(4.6) vanishes and accordingly, the remaining difference of the electrochemical potentials of silver ions in Eq.(4.6) will be identical to the difference of the electrochemical potentials of electrons in magnitude but opposite in sign.

$$t = 0 : \quad -eV = \tilde{\mu}''_e - \tilde{\mu}'_e = - \left(\tilde{\mu}''_{\text{Ag}^+} - \tilde{\mu}'_{\text{Ag}^+} \right) \quad (4.7)$$

For increasing times $t > 0$, the initial silver ion current builds up a concentration gradient in the sample. This leads to an increasing value of the chemical potential difference $(\mu''_{\text{Ag}} - \mu'_{\text{Ag}})$ and a decreasing electrochemical potential difference of silver ions which finally reaches zero. Accordingly, the electrochemical potential difference of silver ions, and hence the ionic current, will vanish for long enough times $t \gg 0$ giving

$$t \gg 0 : \quad -eV = \tilde{\mu}''_e - \tilde{\mu}'_e = \mu''_{\text{Ag}} - \mu'_{\text{Ag}} \quad (4.8)$$

The metallic silver bottom electrode fixes the chemical potential at the interface Ag/Ag₂S at μ_{Ag}° . Because of this, the chemical potential of silver (and accordingly the non-stoichiometry δ) at the ion-blocking electrode, is the only variable in the system which is linearly dependent on the applied voltage. Therefore, under steady state conditions, Eq.(4.8) simplifies to

$$-eV = \mu_{\text{Ag}}^{\circ} - \mu'_{\text{Ag}} \quad (4.9)$$

Note in this case that for $V = 0$, the chemical potential of silver at the ion-blocking contact is equivalent to that of metallic silver. Therefore, if no supersaturation occurs, any positive voltage should lead to the formation of metallic silver deposits. However, this is not observed for positive voltages up to 75 mV meaning that around the ion-blocking contact, a supersaturated composition occurs

4. TOWARDS A QUANTITATIVE DESCRIPTION OF SOLID ELECTROLYTE SWITCHES

with $\delta > \delta^\circ$ where δ° corresponds to the non-stoichiometry in thermodynamic equilibrium with silver metal.

Hence, in the steady state, the gradient of the electrochemical potential of silver ions and the ionic current density vanish. Then, the gradient of the electrochemical potential of electrons is equivalent to the gradient of the chemical potential of silver, and the total electric current density j_{total} is carried by the electrons only. This is summarized in the following,

$$t \gg 0 : \quad \nabla \tilde{\mu}_{\text{Ag}^+} = 0, \quad j_{\text{Ag}^+} = 0 \quad (4.10)$$

$$\nabla \tilde{\mu}_e = \nabla \mu_{\text{Ag}}, \quad j_{\text{total}} = j_e \quad (4.11)$$

Therefore, in the steady state, the electronic current can be expressed by the gradient of the chemical potential of neutral silver according to

$$t \gg 0 : \quad j_e = j_{\text{total}} = \frac{\sigma_e}{e} \nabla \mu_{\text{Ag}} \quad (4.12)$$

The typical time to reach the steady state as assumed for Eqs.(4.9) to (4.12) is estimated as $\tau = L_{\text{diff}}^2/2 D_{\text{Ag}}$, with τ denoting the relaxation time for building up a steady-state silver concentration gradient in the sample, L_{diff} the diffusion length through the sample (for a linear geometry the distance between the two electrodes), and D_{Ag} the chemical diffusion coefficient of silver that is given by [70]

$$D_{\text{Ag}} = \frac{\sigma_e \sigma_{\text{Ag}^+}}{\sigma_e + \sigma_{\text{Ag}^+}} \cdot \frac{1}{e^2} \cdot \frac{d\mu_{\text{Ag}}}{dc_{\text{Ag}}} \quad (4.13)$$

with c_{Ag} denoting the local concentration of Ag atoms in $\text{Ag}_{2+\delta}\text{S}$.

The chemical diffusion coefficient in the low temperature phase of $\text{Ag}_{2+\delta}\text{S}$ is very high, at 80°C the value is of the order of $10^{-2} \text{ cm}^2/\text{s}$. At ambient conditions, it is still around $10^{-5} \text{ cm}^2/\text{s}$. Therefore, decay of concentration gradients in $\text{Ag}_{2+\delta}\text{S}$ occurs much faster than in many other mixed conducting solids. The reason is that the thermodynamic factor $\frac{d\mu_{\text{Ag}}}{dc_{\text{Ag}}}$ in Eq.(4.13) has an extremely large value due to the small range of non-stoichiometry [25].

It has to be remarked that the relations discussed above are only valid as long as no deposition of metallic silver occurs. If silver metal is formed near and at the ion-blocking contact, the ion-blocking boundary condition is no more valid and a continuous silver ion current will flow. The total current then is a sum of electronic and ionic currents and will not reach a steady state. At a nano-contact, the current will usually increase, because the formation of metallic silver will increase the contact area of the nano-contact. Finally, one expects a short-circuiting of the electrodes by the grown silver filaments.

When the steady-state conditions with no silver deposition are fulfilled, Eq.(4.12) can be applied and a well defined, unambiguous relation exists between the electronic conductivity and the chemical potential of silver. Following a concept by C. Wagner [67], one can calculate the electronic conductivity from the slope of the steady state I-V curve. First, the chemical potential and the space variable are separated according to

$$e \vec{j}_{\text{total}}(\vec{r}) \cdot d\vec{r} = \sigma_e d\mu_{\text{Ag}} \quad (4.14)$$

The relation is given for a general case where the current density may vary along the coordinates \vec{r} . Integrating Eq.(4.14), with integration limits set by the boundary conditions at the two electrode contacts, we have

$$e \int_{r''}^{r'} \vec{j}_{\text{total}}(\vec{r}) \cdot d\vec{r} = \int_{\mu_{\text{Ag}}^0}^{\mu_{\text{Ag}}'} \sigma_e d\mu_{\text{Ag}} \quad (4.15)$$

The left-hand side of Eq.(4.15) depends on the geometry of the contacts. We will simplify the integrals by assuming the chemical potential drops only along one coordinate, say r . The integral becomes simple for a sharp point contact (radius a) and a hemispherical reference electrode at $r'' \rightarrow \infty$. In this case we have,

$$e \int_{r''}^{r'} j_{\text{total}}(r) dr = -\frac{e}{2\pi a} I \quad (4.16)$$

More generally we obtain an expression with the total electrical current I and a constant K that depends on the distribution of the current density through the sample:

$$e \int_{r''}^{r'} \vec{j}_{\text{total}}(\vec{r}) \cdot d\vec{r} = -\frac{e}{K} I \quad (4.17)$$

with $K = A/L$ for a specimen in the shape of a pellet with area A and thickness L , $K = 2\pi a$ for a hemispherical contact of radius a , and $K = 4a$ for a disk shaped contact to a semi-infinite sample.

With this result for the left hand side of Eq.(4.15), following C. Wagner [27] one can differentiate both sides with respect to the upper integration boundary μ'_{Ag} . This yields

$$-\frac{e}{K} \cdot \frac{dI}{d\mu'_{\text{Ag}}} = \frac{d}{d\mu'_{\text{Ag}}} \left(\int_{\mu_{\text{Ag}}^0}^{\mu'_{\text{Ag}}} \sigma_e d\mu_{\text{Ag}} \right) = \sigma_e(\mu'_{\text{Ag}}) \quad (4.18)$$

From Eq.(4.9) we have $\mu'_{\text{Ag}} = \mu_{\text{Ag}}^0 + eV$, accordingly $d\mu'_{\text{Ag}} = e dV$ and

$$\left(\frac{dI}{dV} \right)_{\text{steady state}} = -K\sigma_e(\mu'_{\text{Ag}}) \quad (4.19)$$

Now that we have eliminated the unknown chemical potential we can integrate again over the electrical potential to obtain the final current-voltage relation in the steady state

$$I(V) = - \int_V^0 K \cdot \sigma_e(V) dV \quad (4.20)$$

In our case, we are working in the range of stoichiometry $\delta > 0$, i.e. the n-type range. Under this assumption the electronic conductivity is given by $\sigma_e = \sigma_0 e^{(eV/kT)}$ [71]. The voltage dependence arises from the relation between the local Ag^+ -ion concentration (doping) and the local electrical potential.

Thus, we obtain

$$I(V) = K\sigma_0 \frac{k_B T}{e} (e^{(eV/k_B T)} - 1) \quad (4.21)$$

where k_B is Boltzmann's constant and K is a constant representing the geometrical factor mentioned in Eq.(4.17). In the limit near zero bias, i.e. $eV \ll kT$,

Eq.(5.8) reduces to $I = K\sigma_0V$.

As indicated in Eq.(4.9), the relation above applies only in the cases when one of the electrodes maintains a constant chemical potential for Ag, and all changes occur at the small electrode. In other experiments [47], by using two Pt electrodes with the same asymmetry in the geometry, we observed a slight deviation from the theory due to additional chemical potential changes at the Pt bottom contact. From a thermodynamic point of view, in principle I-V relations could also be calculated, if one knows the initial non-stoichiometry δ of the sample. But as they depend on the initial δ , it is not easy to achieve well defined experimental conditions.

In order to approach the limit of the semi-infinite sample (no changes at the bottom electrode) we need to make use of a very small contact. This allow us also to test the theory for nanometer size limit.

4.5 Discussion

Figure 4.3 shows two sets of data for a 200nm thick Ag₂S film on top of a Ag bottom reference electrode (black curves). The curve in Fig.4.3a is taken with a Pt coated AFM tip at very small load in order to minimize the contact size. The curve in Fig.4.3b is taken with a Pt wire contact for a larger macroscopic contact.

Using $\sigma_0 = 7.8 \times 10^{-2} \Omega^{-1}m^{-1}$ [25] and $T = 298$ K, we can compare the experimental data of the steady state I-V curves with Eq.(5.8). The result of the fitting is shown in figure 4.3 (red curves).

The geometry of the electrodes and sample enters through the constant K in Eq.(5.8), which is the only adjustable parameter. Assuming that the end of the AFM tip has approximately hemispherical shape, $K = 2\pi a$, we obtain an estimate for the tip contact radius, a ,

$$a = K/(2\pi) = 12\text{nm}$$

which agrees well with the AFM tip radius observed by electron microscopy of approximately 20 nm. Using finite element simulations, we have modeled the

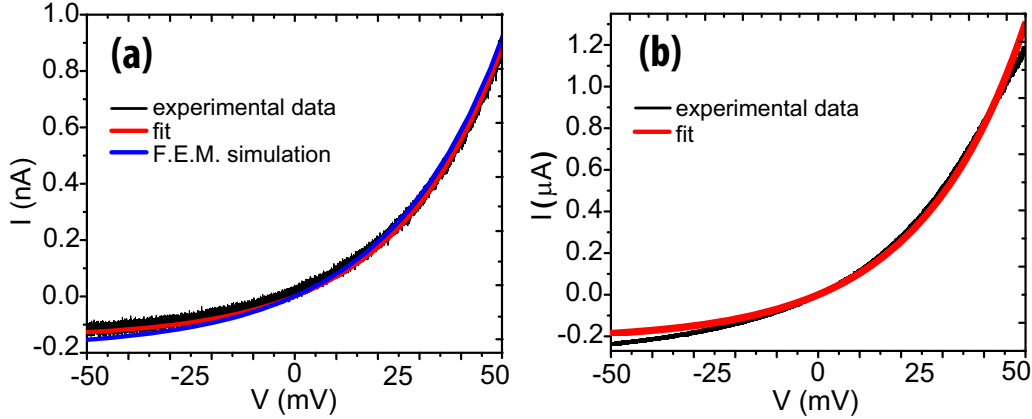


Figure 4.3: Steady state current-voltage characteristics of the Ag/Ag_{2+ δ} S/Pt system, measured with (a) a Pt-coated AFM tip and (b) a Pt wire. Fit with Eq.(5.8) are shown as the red curves.

sample and electrodes geometry (Figure 4.5). The resulting total current as a function of the applied voltage (same as used for the measured IV's) results in a IV curve reproducing those obtained from the experiment and fitting.

For comparison to the measurements with the AFM tip, we have also used a macroscopic Pt wire of 0.1 mm diameter as the top contact. The steady state IV-curve as well as the corresponding fitting with Eq.(5.8) is shown in the right side of Figure 4.3. The quality of the fit is much less good than in the case of the nano-contact. This, is because the assumption of a semi-infinite sample is not longer valid. In our case, fitting with Eq.(5.8) led to a calculated effective contact radius of 17 μ m. However, assuming a perfect contact, the total current must be much higher than observed in Figure 4.3. In our experiment, the Pt wire will not be a perfect contact, but rather the total area in contact with the Ag₂S surface is reduced to only few contact points distributed in an effective radial area of \approx 17 μ m.

Systematic measurements of AFM tip load with contact size were also performed to further verify the relation presented in Eq.(5.8). The measurements start when the tip is just in contact with the Ag₂S surface, followed by an increase of the tip-sample interaction. For each point (tip load), an IV curve is measured and fitted with Eq.(5.8). From the fitting the contact radius is calculated (using

$K = 2\pi a$) and plotted as a function of the load tip force (Fig.4.4). In the plot we observed, as expected, a systematic increase of the contact radius with the tip load. Additionally, more than 80% of the measurement range presents a linear relation, probably related to the AFM tip shape.

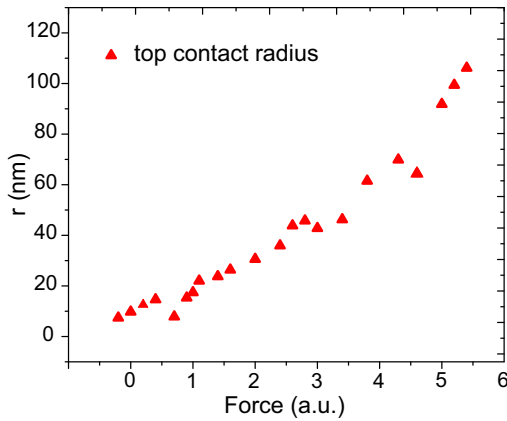


Figure 4.4: Contact radius calculated from a set of experimental I-V curves using Eq.5.8, at different load AFM tip forces. The measurements start when the tip is just in contact with the surface of the Ag_2S (smallest contact radius) followed by an increase of the tip-sample interaction.

This measurement, confirms the consistency of Eq.5.8 to calculate the tip contact radius from experimental steady state IV curves. Additionally, this type of measurement serve as a calibration of the AFM tip load for minimizing the tip contact size, as was performed for the measurement presented in Fig.4.3.

For visualization of the top electrode size effect, we have simulated the voltage drop and local conductivity across the thickness of the Ag_2S sample. The model geometry is the same as used for the measurements: a Ag large bottom electrode, a 200nm thickness Ag_2S layer and a 20nm radius Pt top electrode with a nearly planar geometry. For the simulation we used axial symmetry around the nano-contact.

Figure 4.5 (top panel) shows the solution of the finite element simulation at a voltage of 52 mV (voltage polarity as defined for the experiment). The figure clearly shows that the conductivity changes are concentrated in the region close to the top electrode. Also, we observed that the conductivity increases when the negative polarity is at the top electrode, indicating a local increase of Ag^+ -ion concentration (n-type donors). In the opposite polarity, the conductivity will decrease, due to the local depletion of Ag^+ -ions, leading to a lower conductivity. The

color bars at the right side of the simulation indicate the conductivity values (σ_e).

The bottom panel of Figure 4.5 is a plot of the variation in stoichiometry obtained from the simulation results (in this case at a voltage of 75 mV). It is plotted as a function of the vertical distance (d) from the center of the nanocontact to the Ag substrate. The deviation from stoichiometry is given by, [25, 33]

$$\delta = n - p = 2 K_i^{1/2} \sinh \left(\frac{e(V_0 - V(d))}{kT} \right) \quad (4.22)$$

where n and p are the electron and hole concentration and $K_i^{1/2} = n = p$ at the stoichiometric composition. In the calculation we have taken $K_i^{1/2} = 2 \times 10^{20} \text{ m}^{-3}$ and $V_0 = 105 \text{ mV}$ as reported by Bonneau *et al.* [25]. The equation above accounts for both p and n-type $\text{Ag}_{2+\delta}\text{S}$.

The range of homogeneity of the low temperature phase $\alpha\text{-Ag}_2\text{S}$ is extremely narrow, with $|\delta^\circ|$ in the order of 10^{-6} [24, 33]. For $\delta > 0$, Ag_2S has excess Ag (n-type regime), and for $\delta < 0$, there is a deficit of Ag (p-type regime). We define δ° as the non-stoichiometry limit in thermodynamic equilibrium with Ag (at the n-type regime). In our experiment this is the case where the Ag_2S is in contact with the Ag substrate.

In Figure 4.5 we observe that $\delta = \delta^\circ$ at the boundary Ag/ Ag_2S ($d = 200\text{nm}$) as expected, and $\delta > \delta^\circ$ over the whole range of the curve. This would mean that Ag should precipitate from the Ag_2S already over the full range. However, a certain level of supersaturation is needed before Ag starts precipitating. When a certain supersaturation level is reached, precipitation of metallic Ag will begin. In our geometry we will therefore observe precipitation of metallic Ag to start in the region near the nano-contact (Pt tip). This precipitation process is, in a later stage, responsible for the nucleation and further formation of Ag filaments. The formation of these filaments, which can grow to make a metallic contact between the Ag and Pt electrode, is the proposed mechanism that leads to full bipolar conductance switching.

The nucleation process is related to an overpotential threshold, at which nucleation will increase exponentially [2, 72]. The precipitation of metallic silver during our measurements from an oversaturated state can be understood from

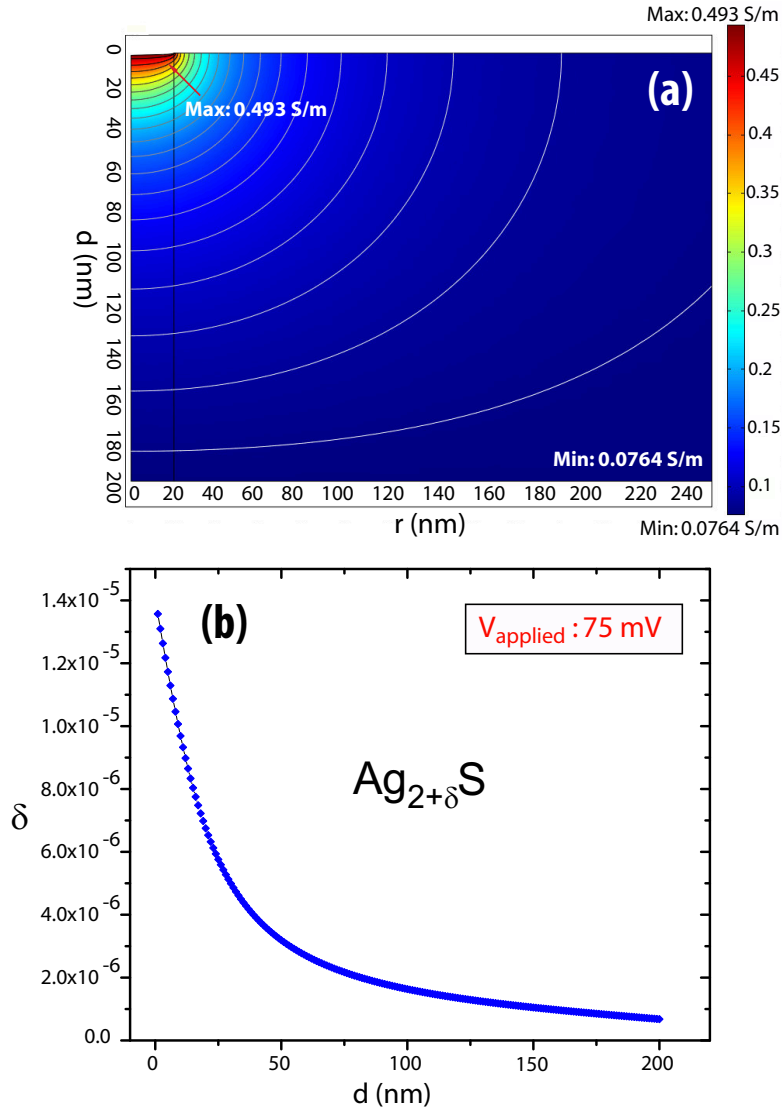


Figure 4.5: a) Finite element simulation of potential (contour plot) and conductivity (surface plot) at $V = 52\text{mV}$, across the 200 nm thick $\text{Ag}_{2+\delta}\text{S}$. Contact radius is 20nm, with a nearly planar geometry. b) Plot of the non-stoichiometry δ as a function of the vertical distance from the center of the nano-contact to the Ag substrate (d). The values of δ indicate a strong increase in Ag^+ -ion concentration at the region neighboring the nano-contact reaching the values of high supersaturation of Ag in $\text{Ag}_{2+\delta}\text{S}$.

the IV curves, i.e. the presence of hysteresis in the IV curves and further full conductance switching as described in Chapter 3. We observed metal deposition and switching to high conduction at a bias voltage beyond 75 mV, a value in agreement with earlier results [73]. As indicated above, the experimental data verify that there is a nucleation barrier for the formation of the metallic silver, that can be related with e.g. lattice deformation and surface free energy. However, further studies are needed to clarify the background for the observed threshold voltage for deposition of Ag and the complete description for the system beyond the critical supersaturation.

4.6 Conclusion

We present above a quantitative analysis of the steady state ionic and electronic transport in a solid electrolyte device that leads to resistance switching. The model presented here describes the electronic transport within the solid electrolyte in the steady state, covering the range of non-stoichiometries due to additional Ag in Ag_2S , up to the supersaturation range just before the deposition of elemental silver. The model is then a base for a complete description of solid electrolyte conductance switches, and it can be extended to other semiconductor materials with mobile donors or acceptors.

4.7 Appendix

4.7.1 Non-stoichiometry in Silver Sulfide

The non-stoichiometry (δ) in $\text{Ag}_{2+\delta}\text{S}$ indicates an excess or deficit of Ag. Using the Kröger-Vink notation (Chapter 1 Section 1.4), the non-stoichiometry per unit volume is the difference:

$$\delta = [\text{Ag}_i] + [\text{Ag}_i^\bullet] - [\text{V}_{\text{Ag}}] - [\text{V}'_{\text{Ag}}] \quad (4.23)$$

with $[\text{Ag}_i]$ and $[\text{Ag}_i^\bullet]$ the concentrations of neutral Ag and Ag^+ -ions in interstitial positions respectively, and $[\text{V}_{\text{Ag}}]$ and $[\text{V}'_{\text{Ag}}]$ the concentration of neutral and negative Ag vacancies.

In Ag_2S , additional silver is completely dissociated into Ag^+ -ions and electrons, i.e. addition of a silver atom to Ag_2S causes the production of a free electron, or the annihilation of an electron defect. With this, $[\text{Ag}_i]$ and $[\text{V}_{\text{Ag}}]$ are negligible [33, 40]. From this condition and the electro-neutrality equation,

$$p + [\text{Ag}_i^\bullet] = n + [\text{V}'_{\text{Ag}}] \quad (4.24)$$

with $n = [e']$ and $p = [h^\bullet]$ the concentration of electrons and holes, the non-stoichiometry δ (Eq.4.23) is reduced to,

$$\delta = n - p \quad (4.25)$$

with $n = K_i^{1/2} e^{eV/kT}$, $p = K_i^{1/2} e^{-eV/kT}$ and $K_i = np$ the concentration of electrons and holes at the stoichiometric point ($\delta = 0$) where $n = p$.

4. TOWARDS A QUANTITATIVE DESCRIPTION OF SOLID ELECTROLYTE SWITCHES

5

Bulk and Surface Nucleation Processes in Ag₂S Conductance Switches

We studied metallic Ag formation inside and on the surface of Ag₂S thin films, induced by the electric field created with a scanning tunnel microscope (STM) tip. Two clear regimes were observed: cluster formation on the surface at low bias voltages, and full conductance switching at higher bias voltages ($V > 70$ mV). The bias voltage at which this transition is observed is in agreement with the known threshold voltage for conductance switching at room temperature. We propose a model for the cluster formation at low bias voltage. Scaling of the measured data with the proposed model indicates that the process takes place near steady state, but depends on the STM tip geometry. The growth of the clusters is confirmed by tip retraction measurements and topography scans. This study provides improved understanding of the physical mechanisms that drive conductance switching in solid electrolyte memristive devices.

This chapter has been published as M. Morales-Masis, S. J. van der Molen, T. Hasegawa and J. M. van Ruitenbeek, *Phys. Rev. B* **84** 115310 (2011)

5.1 Introduction

In the previous chapter, we found that for Ag nucleation inside the Ag₂S film giving full conductance switching, a critical supersaturation of Ag ions inside the Ag₂S film is needed. This phenomenon only occurs at bias voltages above 70mV*, which is defined as the threshold voltage for switching at room temperature. In this chapter we confirm experimentally this threshold voltage for nucleation inside the film. We furthermore show that when starting from a tunneling gap between the top electrode and the sample, Ag clusters can be grown between the tip and the Ag₂S surface at voltages significantly lower than the observed threshold voltage for switching. At voltages above the threshold, a rapid nucleation inside the Ag₂S thin film is observed and the sample then exhibits full conductance switching.

5.2 Experimental procedure

The samples consist of Ag(200nm)/Ag₂S(200nm) layers, which are prepared as described in Chapter 2 Section 2.7. As the top electrode, we use an STM tip which is manually cut from either a Pt or PtIr wire. The measurements are performed at room temperature in a JEOL UHV STM/AFM system with a base pressure of 1×10^{-9} mbar. In this STM setup, the tunneling voltage is applied to the sample while the tip is connected to ground.

For the measurements we have connected an external data acquisition card (DAQ) from National Instruments to the JEOL STM controller. Our measurement software allows the simultaneous control of two outputs (bias voltage, piezo voltage) and the monitoring and recording of two inputs (current and Z piezo voltage). Hence, the measurements are fully controlled through LABVIEW independent of the STM controller.

*This value depends on the non-stoichiometry of Ag_{2+ δ} S. The value of 70 mV applies for a sample for which the Ag cation concentration is fixed by an intimate contact to a Ag metal reservoir.

5.3 Conditions for vacuum tunneling on Ag₂S

When performing STM measurements on Ag₂S, two important points must be considered: (1) Ag₂S is an n-type semiconductor, with a band gap ranging between 0.6 and 1.2 eV [29, 31]. (2) Ag₂S has both ionic and electronic mobile charges. The ionic mobile charges (Ag⁺-ions) act as n-type dopants within the Ag₂S film. Therefore, a local accumulation of ions in the sample causes changes in the local conductivity and band gap of the film. In our experiments, we apply a voltage between the STM tip (top contact) and the Ag layer (bottom contact), creating a strongly localized electric field near the tip. If a positive sample bias is applied, the mobile Ag⁺-ions in the Ag₂S will move towards the region closest to the tip, increasing the local conductivity and lowering the band gap. Due to the points mentioned above, the apparent sample resistance can vary depending on the values of the tunneling gaps and applied voltages.

We measured IV curves to characterize our sample and confirm the characteristics of the band gap and the effect of the mobile ions. A typical IV curve, measured at the tunneling gap of 10 GΩ, is shown in Fig.5.1a. The IV curve is asymmetric, with a flat region between approximately -600mV and +400mV. This flat region is the result of the band gap of the sample. At the negative bias the rapid increase in conductance below -600mV is associated with the valence band edge. At the positive bias side above +400mV the rise of the curve is related to the position of the conduction band edge. The position of the conduction band edge can be influenced by the n-type doping due to the accumulation of Ag⁺-ions.

The effects of n-type doping become more important when the tunneling gap is reduced. When working at tunneling gaps with a resistance in the range of several MΩ, a large part of the voltage drops across the sample (the sample resistance for a Pt atomic point contact with the Ag₂S sample is > 3 GΩ for voltages below the band edge), and therefore the activation of ions to move towards the tip is higher than for large tunneling gaps. Figure 5.1b presents an IV curve measured at a tunneling gap of 25 MΩ, set at a bias of -1V. The IV curve shows an exponential increase in the current at the positive bias side, at a voltage much lower than the band gap edge. This IV curve resembles our previous measurements [74] and confirms the prediction by Hebb [30] and Wagner [35], of an accumulation of Ag⁺-ions resulting in an enhanced electronic conductivity and an asymmetric IV curve with an exponential increase in the current at positive sample bias. Addi-

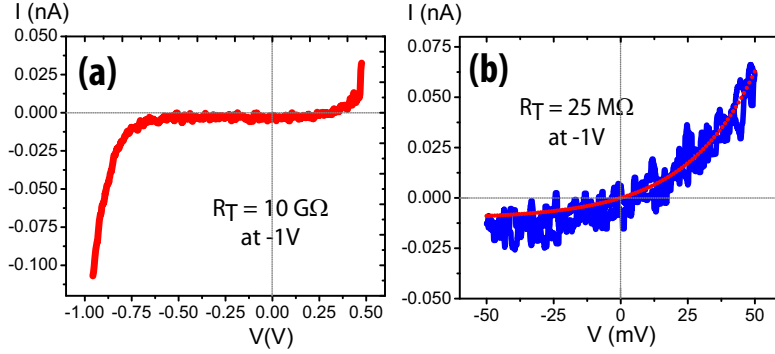


Figure 5.1: Current-Voltage characteristics of the Ag_2S thin film at two different tunneling gaps. a) At $10 \text{ G}\Omega$ (tunneling gap defined at -1V), the IV curve indicates the presence of the band gap in the Ag_2S sample. b) At $25 \text{ M}\Omega$ (tunneling gap defined at -1V), the IV curve shows an exponential increase in the current at positive bias, due to the accumulation of Ag close to the tip for close proximity of the tip to the sample. The red curve is a fit of the IV curve from which we calculate the effective top contact radius as 0.8nm .

tionally, fitting the exponential IV curve with the Hebb-Wagner formalism (red curve in Fig. 5.1b), allow us to calculate the top contact radius. We obtained an effective contact radius of 0.8 nm , indicating the close proximity, or touching, of the tip to the sample.

In order to assure that the tip is not in contact with the Ag_2S film, we choose to work with tunneling resistance between $10 \text{ G}\Omega$ and $1 \text{ G}\Omega$, which is set at a bias below the band edge at a voltage of -1V . We use positive sample bias to activate the ion mobility and Ag growth.

5.4 Nucleation and Conductance Switching

Our initial goal was to measure the growth rate of the Ag cluster (or filament), by following its growth with the STM tip, where the tip-sample (or tip-cluster) distance was kept constant by using the proper feedback parameters. Figure 5.2 is an example of such a measurement. For this specific trace, a tunneling gap is first defined at -1V sample bias and 0.3 nA tunneling current. Two seconds

after starting the measurement, the bias voltage is stepped from -1V to $+20\text{mV}$ (change in sign of the current in Fig.5.2). Almost immediately, an increase in the voltage output of the Z piezo is measured, which continues until the bias voltage is switched back to -1V . The increase of the Z piezo voltage indicates the total displacement of the tip away from the sample. In 10s we measure a total displacement of 36 nm. The tip displacement, therefore indicates the growth of a protrusion on the surface of the sample. We expect this protrusion to be composed of Ag atoms, due to the reduction of Ag^+ -ions at the surface of the Ag_2S film [75, 48].

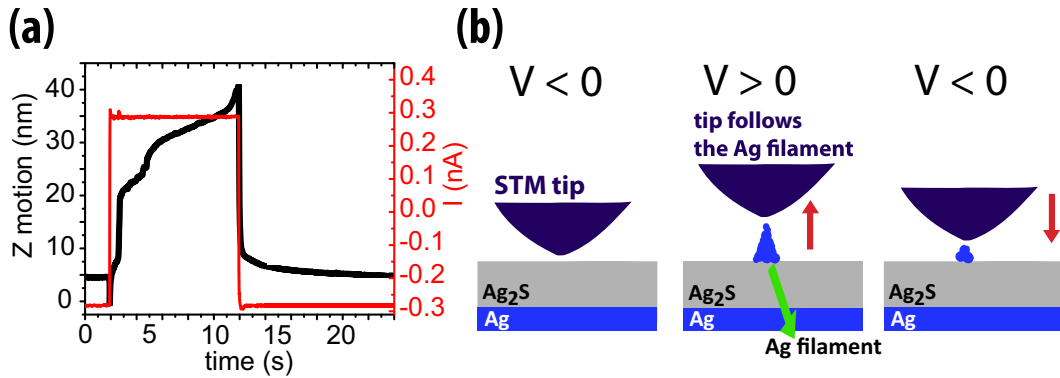


Figure 5.2: a) Z piezo displacement (black curve) and tunneling current (red curve) as a function of time. The growth of the Ag cluster was activated with $+20\text{mV}$ bias. Keeping the feedback on allow us to follow the growth of the cluster in the Z direction. b) Schematic of the filament growth on the surface of the Ag_2S sample.

Although qualitatively successful, this type of measurements has the disadvantage that tip contact with the sample cannot be avoided when the voltage is stepped from -1V (tunneling voltage) to the positive voltage to induced the filament growth. Because of the large resistance of the sample at low voltages, initially the voltage drops over the sample, not over the tunnel gap. The feedback responds to the resulting drop in the current by pushing the tip into contact with the sample (note the sharp spike to a lower Z position at the start in Fig.5.2a). At the same time a filament starts growing. In many occasions the cluster grows much faster than the feedback speed of our STM, causing large oscillations in the Z position and tunneling current. Because of this, the results show large variations in the growth rate, and it is not possible to accurately determine the dependence of the growth rate on the bias voltage.

As a different approach we decided to allow contact of the cluster with the tip, by switching off the feedback of the STM and measuring the evolution of the current with time (instead of the Z piezo displacement). At the start of the measurements, the tunneling gap is fixed at -1V sample bias and 1nA tunneling current. With a tunneling gap thus defined, the feedback is switched off and a positive bias voltage is applied to the sample. The positive bias voltage is kept constant while the current is being recorded as a function of time.

Figure 5.3a presents a typical measurement. The measurement is performed as follows: at $t=0$, the feedback is switched off, and we wait 2 seconds to confirm that the tip-sample distance remains constant. At $t=2s$ the bias voltage V is switched from -1V to +50mV. Immediately we observe a drop in the current, as expected from the high resistance of the sample at low bias voltages. A certain time elapses (induction time) before the current starts increasing (see inset in Fig.5.3a). The current increases until the bias voltage is switch back to -1V.

The same measurement was performed for bias voltages, V , ranging from +20mV to +90mV (Figure 5.3b). In this set of data, for the traces taken with +20mV up to +60mV we observe the same behavior as described for Fig.5.3a, with a systematic increase in the growth rate as a function of the applied bias voltage.

At +70mV a particular curve is observed: during the first 100 seconds it resembles the previous traces. However, this behavior is interrupted by a sudden increase of the current growth rate. The current increase is such that it quickly saturates the current amplifier. A similar behavior is observed at +80mV, with the main difference that the strong increase in current is observed at an earlier time. At +90mV, the increase of the current occurs almost immediately after the positive voltage is applied.

The measurements presented in Fig.5.3b, suggest the presence of two distinct physical processes. Figure 5.4 presents further measurements performed in order to distinguish the two processes. Figure 5.4a presents a set of traces of conductance (G) as a function of time, obtained by applying bias voltages of +70mV and higher. Each run the sample conductance increases sharply, reaching values larger than $1G_0$, where $G_0 = 2e^2/h = 77\mu S$ is the conductance quantum. We

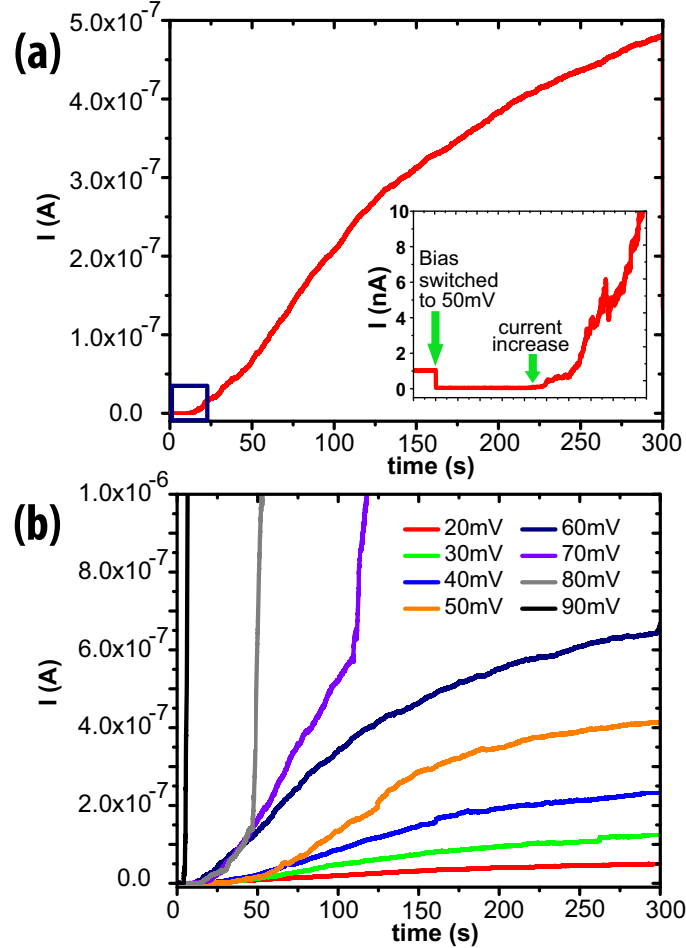


Figure 5.3: a) Current evolution observed when a step in the voltage from -1 V to $+50$ mV is applied to the sample. The inset shows the first seconds of the trace. b) Traces measured at bias voltages from $+20$ mV up to $+90$ mV

observe a systematic decrease of the induction time with bias. At $G > 1G_0$, the presence of a metallic Ag filament connecting the bottom electrode with the STM tip is expected. In the traces presented in Fig.5.4a, the final conductances (not shown in the plot) reach values as high as hundreds G_0 . In order to test for metallic conductance, we switch the sample to the high conductance state with $+110$ mV and measure an IV curve (Fig.5.4b). The resulting curve is linear, with a slope indicating a resistance of 124Ω , in this example. This confirms the metallic behavior of the sample which we attribute to the formation of a Ag

filament inside the Ag₂S film.

To verify that the filament formation does not occur in the low voltage regime (from 0 to +60mV) we measured traces for times much longer than the 300s typically used. Figure 5.4c shows one of the traces measured by applying a bias voltage of +50mV for 1000s. The trace is plotted as the conductance (G/G_0) vs time. It is clear from the figure, that there is no sudden increase in the current and that the sample, even after 1000s, has a conductance lower than $1G_0$, although it is not much smaller. At this point, we performed IV measurements to probe the current-voltage behavior at this stage. Figure 5.4d presents the resulting non-linear IV curve, which confirms that the conductance is dominated by the dynamic doping behavior of the Ag₂S semiconductor.

Two processes are clearly observed from the behavior of the traces of current vs time: Ag surface nucleation, and Ag filament formation inside the Ag₂S film. At room temperature we demonstrate that this transition occurs at 70mV. It is important to mention that this threshold voltage varies with temperature and with the electrode material used. We have used Ag as the bottom electrode, which fixes the chemical potential at the Ag/Ag₂S interface [24] and therefore all changes occur near the Pt tip. In previous studies, we observed that if we use Pt as the bottom as well as for the top contact the threshold voltage to full conductance switching increases up to 200mV [47].

In the current versus time traces the increase of the current is linked to the growth of a Ag cluster on the sample surface, giving rise to an increasing contact size to the Ag₂S film. Because the feedback of the STM is turned off when the positive bias voltage is applied, the tip does not change its position and the growth of a cluster will occur between the STM tip and the sample surface. As the gap between tip and surface is only of the order 1nm, the cluster will make contact with the STM tip at the very start of the process. As long as the positive bias is applied the cluster will continue growing. The growth is expected to be in the radial direction increasing the contact area with the Ag₂S surface and filling the volume between the tip and the surface. These two points are tested further in the following.

In order to confirm that the tip is indeed in contact with the cluster and that the cluster is metallic, we perform the measurement illustrated in Fig. 5.5a.

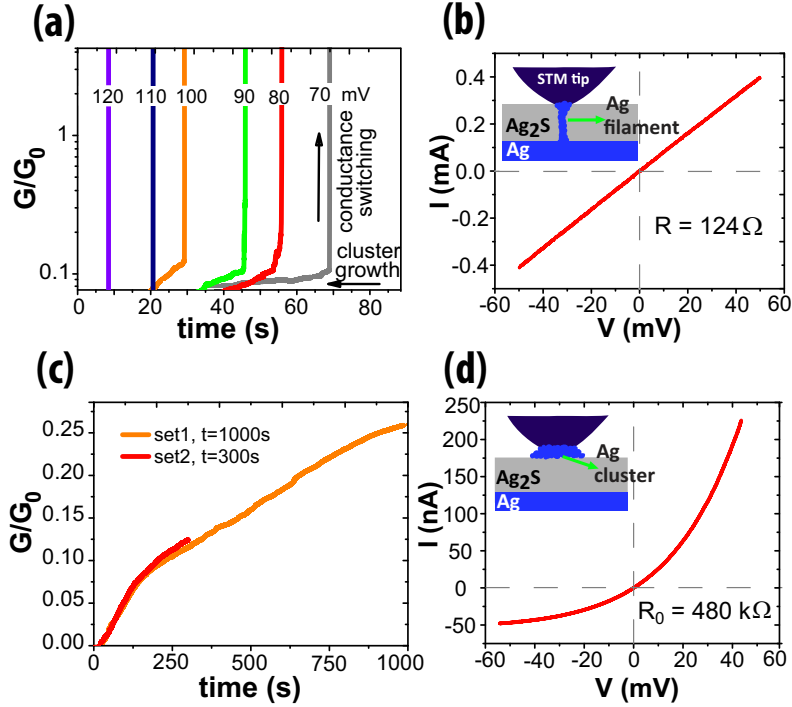


Figure 5.4: a) Conductance switching induced at bias voltages $\geq +70$ mV. The plot shows the increase of the conductance above $1G_0$ and a systematic decrease in the induction time with bias. b) IV curve measured in the high conductance state of the sample, indicating metallic behavior. c) Conductance trace measured for 1000s, applying a bias voltage of +50 mV. The trace in red presents another trace measured at +50 mV for 300s. The trace does not show a sudden increase of the conductance for full switching. d) IV curve measured at $t = 60$ s of a trace measured with +50 mV, demonstrating semi-conducting behavior dominated by the bias induced changes in ion concentration in the Ag₂S film [74].

For the measurement presented in Fig.5.5a, we formed a cluster by applying +20 mV sample bias. The current was allowed to increase to 1 nA, and then the tip was retracted at a speed of 4 nm/s. It takes approximately 16 s for the current to completely drop to the initial value. We observed that the drop of the current starts immediately upon tip retraction from the surface (See line at $t \approx 82$ s in Fig.5.5a). When the cluster is metallic, the drop of the current should be related with a decrease of the cross section area at the Ag₂S/Ag-cluster interface. This occurs if the tip is dragging up a large part of the cluster when it is moving away

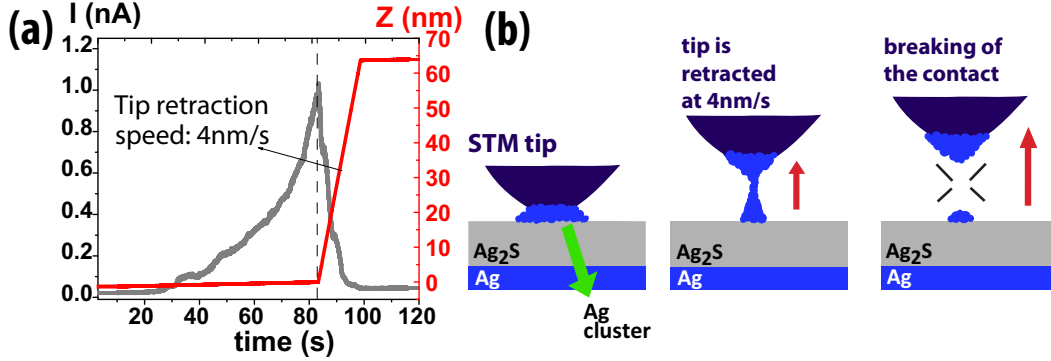


Figure 5.5: a) Ag cluster formation induced at +20mV. When the tip current reaches 1 nA, the tip is retracted at a speed of 4nm/s. As a consequence, the tip loses contact with the cluster and the current drops. b) Schematic diagram of the cluster growth and neck formation when the tip is retracted.

from the surface, as illustrated by the cartoon in Fig.5.5b. Figure 5.5a shows that in 16 seconds the tip is retracted as much as 64 nm from the sample surface in the Z direction. At much faster retraction rates, the time to break the contact with the cluster is considerably shorter. This experiment clearly shows that the cluster is in contact with the tip and that we can mechanically break this contact by retracting the tip over tens of nanometers.

5.5 Topography scans

We scanned the surface of the Ag_2S film before and after the growth of a cluster (Fig.5.6). For the scanning we used the tunneling parameters -600mV and 1 nA. The sample was cooled down to $T \approx 240$ K in order to reduce ion diffusion and prevent complete dissolution of the cluster before the scanning was performed.

We scanned an area of 250 x 250 nm (in Fig.5.6 we show only an area of 142 x 142 nm) and in the topography image we selected a flat spot on the sample to grow the cluster. The tip was placed above the selected position, and with the feedback on we applied a sample bias of +300mV. This large bias voltage will induce the growth of a large cluster, observed by the large displacement of the Z piezo. This positive bias voltage was applied for 100s. After the 100 s, the

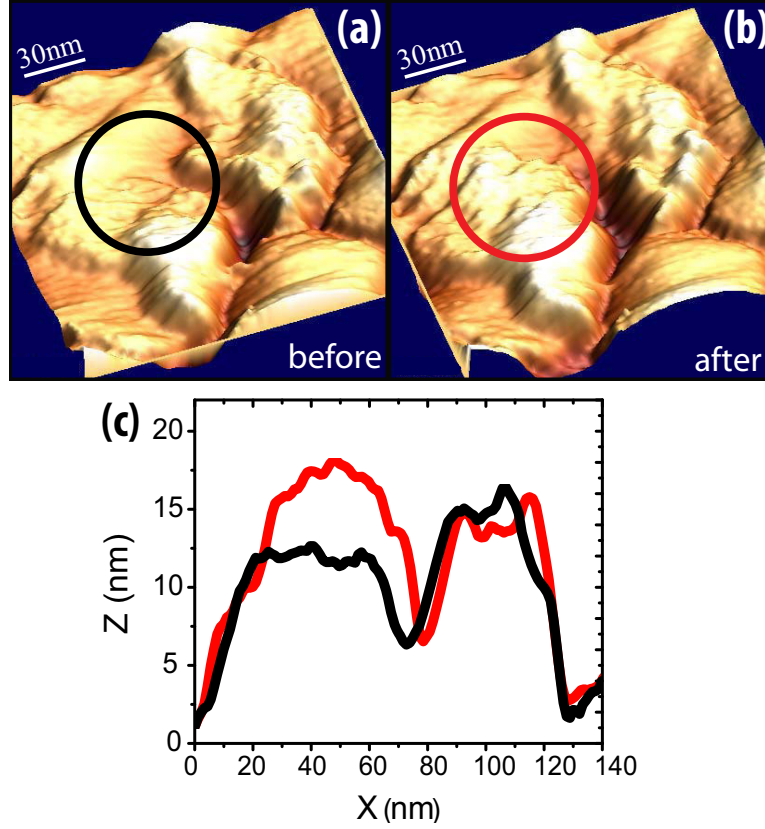


Figure 5.6: Topography scan (a) before and (b) after the growth of a cluster. c) Line scan through the remnant of the grown cluster

tunneling bias was set back (-600mV) and the tip restarted scanning the same area as before cluster growth.

Due to the large roughness of the surface of approximately 30nm a slow scan speed needed to be used. The time taken from the moment the cluster was grown to the moment when the area of the cluster was scanned was more than 100s. At room temperature and with -600 mV sample bias the cluster is expected to be fully dissolved back in the Ag_2S , as confirmed by our experiments. At 240 K, we observed that after 100 s, a small part of the cluster is still visible when the surface is imaged. A line scan through the remnants of the cluster (Fig.5.6c), shows a height difference of 5nm, which is significantly smaller than the expected cluster height just after the switch (the measured displacement of the Z piezo while performing the measurement was approximately 100nm). Nevertheless, the two

distinct surface morphologies before and after the growth are clearly observed.

5.6 Discussion

To understand the nucleation and the evolution of the cluster with time, we performed the following analysis. When a voltage V is applied to the Ag₂S sample, between the Ag bottom contact and the Pt tip, the voltage drop over the sample V_s imposes an electrochemical potential difference for the electrons at the two sample boundaries,

$$-e V_s = \tilde{\mu}_e'' - \tilde{\mu}_e' \quad (5.1)$$

with $-e$ the electron charge. Note that the total voltage applied drops partially over the tunneling gap and partially over the sample. Due to the large resistance of the sample, $V \approx V_s$.

The electrochemical potential gradients of Ag⁺-ions and electrons are related to the chemical potential gradient of atoms by, $\nabla\mu_{\text{Ag}} = \nabla\tilde{\mu}_{\text{Ag}^+} + \nabla\tilde{\mu}_e$.

Initially, the Ag⁺-ions and electrons are distributed uniformly in the sample, thus $\nabla\mu_{\text{Ag}} = 0$. When the voltage is switched on, the gradients of the electrochemical potentials of electrons and Ag⁺-ions, will be identical in magnitude but opposite in sign. Opposing currents of ions (j_{Ag^+}) and electrons (j_e) are therefore set up in the sample.

When the top contact is an ion blocking contact (e.g. a Pt tip in contact with the Ag₂S sample), the silver ion current (j_{Ag^+}) builds a concentration gradient at the Ag₂S/Pt-tip interface, until an equilibrium with the electrical potential gradient $\nabla\tilde{\mu}_e$ is reached, resulting in a steady state and a vanishing current of ions. Increasing the voltage further, increases the Ag concentration gradient, until the supersaturation reaches a critical value and metallic Ag is nucleated inside the Ag₂S. This will occur at $V_s > 70\text{mV}$ as demonstrated previously [73, 74].

Contrary to a blocking contact, in the present experiment there is initially a tunneling gap between the tip and the sample surface. Therefore ions are not fully blocked at the Ag₂S/vacuum interface, and surface nucleation is allowed.

Anticipating that the surface nucleation energy is lower than the bulk nucleation energy, a Ag nucleus can be formed at the surface of the Ag₂S film at lower Ag saturation. The nucleus is produced by Ag⁺-ions that are reduced at the surface of the Ag₂S film. Initially the nucleus contacts the STM tip without causing a noticeable change in the current due to the large resistance of the sample.

The further evolution of the cluster radius with time, $r(t)$, is modeled as follows. We define the flux of Ag⁺-ions, which cross the Ag₂S/Ag-cluster interface, that are subsequently reduced to metal atoms and added to the nucleus, as J_{Ω_t} . The flux J_{Ω_t} into the nucleus, therefore, corresponds to a volume change ($d\Omega_t(r)/dt$) of the nucleus according to,

$$J_{\Omega_t} A(r) \Omega_a = \frac{d\Omega_t(r)}{dt} \quad (5.2)$$

where J_{Ω_t} is in units of atoms/m²s, $A(r)$ is the cross section area of the Ag₂S/Ag-cluster interface, and Ω_a is the volume per atom. The parameter r is the radius of the cluster, which we assume for simplicity to be cylindrically symmetric.

We first solve the equations above for the case of a simplified model of tip and surface geometry. We assume an STM tip with an apex radius R_0 and smooth sample surface. We furthermore assume that the cluster grows such that it fills the space between the STM tip and the sample surface. A schematic diagram of this model system is shown in Fig.5.7.

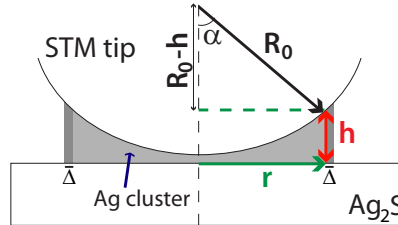


Figure 5.7: Schematic diagram of the tip and sample geometry, used to model the growth of the cluster with time. R_0 is the tip radius, r is the cluster radius and h is the cluster height. Δ is the width of the edge ring where the Ag atoms are incorporated into the nucleus.

Using the parameters defined in Fig.5.7, and assuming that $R_0 \gg r$, the height of the cluster can be expressed as $h \approx \frac{r^2}{2R_0}$ and the volume of the cluster as:

$$\Omega_t(r) = \frac{\pi r^4}{4 R_0} \quad (5.3)$$

To solve Eq.5.2, let us first analyze J_{Ω_t} . From the measurements presented in Fig.5.3, we estimate that the flux of atoms into the cluster is much less than 1% of the full ion current density in Ag₂S (here, the full ion current is obtained from the electronic current using $j_{Ag^+} = 0.1j_e$ [25]). Therefore, when the cluster is growing, the deviation from steady state is very small, and at fixed bias voltage, after allowing for some settling, we can assume that J_{Ω_t} is constant over time.

Because the flux of atoms into the cluster is much smaller than the full ionic current density, we know that the atoms are restricted at the Ag₂S/Ag-cluster interface. This restriction is the cluster itself. The addition of extra atoms at the cross section area just under the cluster is not likely, since the new atoms would have to work against the atoms in the cluster, to displace them and accumulate in the cluster. At the edge there is no restriction. Thus, we propose that the addition of Ag to the cluster occurs only at the edge of the cluster, this edge having width Δ . This forms an effective surface defined by the edge of the cluster ($2\pi r(t)$) and a width Δ of atomic dimensions. The parameter $A(r)$ in Eq.5.2 is then given by $A(r) = 2\pi r(t)\Delta$ with $r(t)$ the radius of the cluster and Δ constant.

We fill in $\Omega_t(r, t)$ and $A(r, t)$ into Eq.5.2, and now we only need to integrate over time. Eq.5.2 then results in,

$$J_{\Omega_t} \Omega_a t = \frac{r(t)^3}{6R_0\Delta} \quad (5.4)$$

or

$$r(t) = (6R_0\Delta J_{\Omega_t} \Omega_a t)^{1/3} \quad (5.5)$$

an expression which describes the evolution of the radius r of the cluster with time.

The flux of atoms into the cluster J_{Ω_t} is proportional to the difference of the chemical potential gradients of Ag atoms and ions in the Ag_2S , $J_{\Omega_t} \propto \nabla\mu_{\text{Ag}} - \nabla\tilde{\mu}_{\text{Ag}^+}$ which is expected to be small. To lowest order this flux will be linear in the bias voltage V_s . Then Eq. 5.5 becomes

$$r(V_s, t) \propto (R_0\Delta\Omega_a V_s t)^{1/3} \quad (5.6)$$

As we will see below, this relation describes the data in some cases very well, but not in general. We note that the power $n = 1/3$ in Eq.5.6 comes from the specific geometry for the STM tip and cluster presented in Fig.5.7. In fact, Eq.5.6 can be written as a general function f of the time t and bias voltage V_s , where f generalizes the power n of $r(V_s, t)$ defined by the specific shape of the tip and cluster. Then, in general terms,

$$r(V_s, t) = f(\Psi V_s t) \quad (5.7)$$

with $\Psi = R_0\Delta\Omega_a$.

Using the expression above and the dependence of the electronic current with the top contact size, we can write a scaling relation for the traces of current I vs time t measured at different bias voltages.

As mentioned above, the nucleus formation and growth occur at near-equilibrium conditions, i.e., near steady state, in which case the electronic current is expressed as, [74]

$$I(V_s) = K\sigma_0 \frac{k_B T}{e} (e^{(eV_s/k_B T)} - 1) \quad (5.8)$$

where k_B is Boltzmann's constant, the temperature $T = 295\text{K}$ and $K = \alpha r$ describes the contact geometry, where α is a constant of order unity and depends on the size and shape of the top contact. In our case, the top contact is the Ag cluster that is growing at the surface, therefore, $r = r(V_s, t)$.

From Eq.5.7 and Eq.5.8, we obtain the final form,

$$I(V_s, t) = \Gamma f(\Psi V_s t) (e^{(eV_s/k_B T)} - 1) \quad (5.9)$$

5. BULK AND SURFACE NUCLEATION PROCESSES IN Ag₂S CONDUCTANCE SWITCHES

with $\Gamma = \alpha \sigma_0 \frac{k_B T}{e}$.

Equation 5.9 predicts that if we plot $I(V_s, t) / (e^{(eV_s/k_B T)} - 1)$ versus $V_s t$, for one set of data of current versus time traces, for example the set presented in Fig.5.3b, the data should collapse onto a single curve. This is confirmed in Fig.5.8 for three different sets of data. Each set of data contains traces of current versus time, measured at voltages from +20mV to +60mV. Each set of data was measured with a different tip and at a different position on the sample, resulting in a different function f and/or proportionality constant Γ . For example, the data set 1 was measured with an etched STM tip with a well defined shape, and the data of sets 2 and 3 were measured with a manually cut tip of which the geometry is not well defined. This can explain variations in the power law and the fact that the best scaling with a power law given by Eq.5.6 is obtained for the etched tip (set 1).

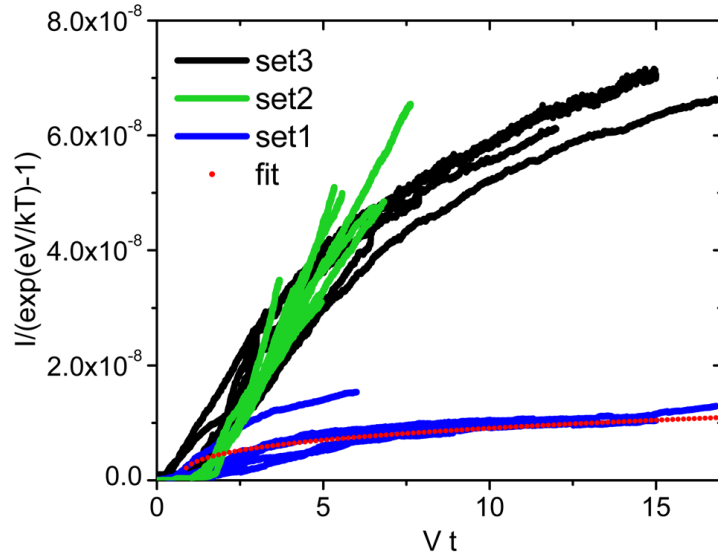


Figure 5.8: Scaling of three sets of data, measured at different positions on the sample and with different STM tips. The red dotted curve is a fit to one of the traces from set 1 with a power law of $V_s t$ of $1/3$, as the result obtained with our simplified model (Eq.5.6)

5.7 Conclusion

We have observed the occurrence of two physical processes in Ag_2S under the influence of the applied bias voltage: nucleation of a Ag cluster on the surface and, at higher bias, nucleation of a wire inside the Ag_2S film. We have found that surface nucleation is possible at very low bias voltages, below 20mV. Nucleation of a nanowire inside the film occurs at bias voltages higher than 70mV at room temperature. At this point it is not possible to decide whether the nucleation is governed strictly by the bias voltage alone, or by the electric field that it causes, as was recently demonstrated for amorphous-crystalline phase change materials [76, 77, 78]. A note on this topic is presented in the Appendix A.

Ag_2S forms an interesting model system for the understanding of memristive nano-ionic devices. In nanoionic devices, the ion transport properties plays a significant role in the determination of retention times, cycling endurance and writing and reading voltages. The type of measurements presented here are important to screen and select future candidate materials and processes for memory resistive devices.

5. BULK AND SURFACE NUCLEATION PROCESSES IN Ag₂S CONDUCTANCE SWITCHES

6

Observing “Quantized” Conductance Steps in Silver Sulfide: Two Parallel Resistive Switching Mechanisms

We demonstrate that it is possible to distinguish two conductance switching mechanisms in silver sulfide devices at room temperature. Previously we show that in a metal/Ag₂S/metal device, the switch to a high conductance state is related with the formation of a conductive path between the electrodes. We argue this conductive path to be composed of a metallic silver nanowire accompanied by a modification of the surrounding lattice structure. Metallic silver nanowires decaying after applying a negative voltage allow observing conductance steps in the breaking traces characteristic for atomic-scale contacts, while the lattice structure deformation is revealed by gradual and continuously decreasing conductance traces.

J.J.T. Wagenaar, M. Morales-Masis and J. M. van Ruitenbeek, accepted for publication in *J. Appl. Phys.*

6.1 Introduction

Part of the interest in solid electrolyte memories, lies in the prospects to scale the devices down to few nanometers, and if possible to the atomic scale. Terabe et al. [23] reported atomic switching behavior by electrochemical reactions taking place in a vacuum gap between microfabricated Pt and Ag₂S electrodes. They showed switching between integer values of the unit of conductance, $G_0 = (12.9 \text{ k}\Omega)^{-1}$, at room temperature and attributed this to the formation of a contact made up of few atoms. In a later report the decay with time of the high-conductance state was explored for implementing artificial synapses [61].

In the references above ([23, 61]), however, the presence of a vacuum gap is not supported by evidence, and one may argue that the assumption of the formation of a vacuum gap prior to the switching operation is unlikely. For the functioning of the device, the vacuum gap it is not needed because switching occurs inside the Ag₂S film, as commented in Chapter 3. Furthermore, in the previous chapter we demonstrated that control of the tip-sample distance requires biasing well below or well above the band gap when working with Ag₂S, therefore, the initial conductance of $1\mu\text{S}$ of the measurement in Ref.[61] is most likely for the STM tip in contact with the Ag₂S.

In this chapter we report on the conditions for observing such atomic switching behavior without a vacuum gap. We used a device composed of a thin film of Ag₂S deposited on top of a wide Ag layer, and the Ag₂S film is contacted with the Pt tip of a scanning tunneling microscope (STM). Applying a voltage between the electrodes leads to the reversible formation of a conductive path, defining the ‘on’ and ‘off’ states of the device. We analyzed the ‘on’ to ‘off’ conductance traces and found evidence for the coexistence of two parallel breaking mechanisms.

6.2 Experimental details

The samples are prepared as described in Chapter 2 Section 2.7. As the top electrode, we use an STM tip which is manually cut from a Pt wire. The measurements are performed in the JEOL UHV STM/AFM system. In this STM setup, the tunneling voltage is applied to the sample while the tip is connected to ground. The FEMTO (DLPCA-200) current amplifier is used to replace the

standard JEOL current amplifier in order to cover a larger current amplification range. The measurements are performed at room temperature and at a pressure of 10^{-9} mbar.

6.3 Results

6.3.1 IV characteristics

Before starting the measurements we need to confirm that the tip is in contact with our sample. This can be decided based upon the measured current-voltage relation. When a large tunneling gap is formed the resistance is dominated by vacuum tunneling and the IV curve is nearly linear, for sufficiently low bias. On the other hand, when in contact an exponential current-voltage curve described by the expression derived in Chapter 4 is observed. The expression given by,

$$I(V) = K\sigma_0 \frac{k_B T}{e} (e^{(eV/k_B T)} - 1) \quad (6.1)$$

with $\sigma_0 = 7.8 \cdot 10^{-2} \Omega^{-1}m^{-1}$ the electronic conductivity of Ag_2S at zero bias [25], $T = 295$ K is the temperature, k_B is Boltzmann's constant, and K is a geometrical factor with dimensions of length representing the contact size.

We measured IV curves by ramping the bias voltage and measuring the current with a sampling rate of 10000 samples per second. In fitting the data with Eq. (6.1) K is the only fitting parameter, from which we determine the size of the Pt STM tip contact. Figure 6.1b presents the IV curve for the low-conductance state (off-state) and the fit of the curve to Eq. (6.1). From the quality of the fit we conclude that the sample is in its pristine, semiconducting, state and that the Pt tip is in contact with the sample. Increasing the voltage further causes switching to the on-state (Fig. 6.1a) due to the formation of a conductive path. Figure 6.1c shows an IV curve for the on-state, and the linear fit indicates metallic behavior. Subsequently, returning to a sufficiently large negative voltage the sample switches back to the off-state.

After switching the device several times the off-state conductance of the sample becomes strongly modified. The evolution of the off-state IV curves with the number of switching cycles is presented in Fig. 6.2. The switching cycles were

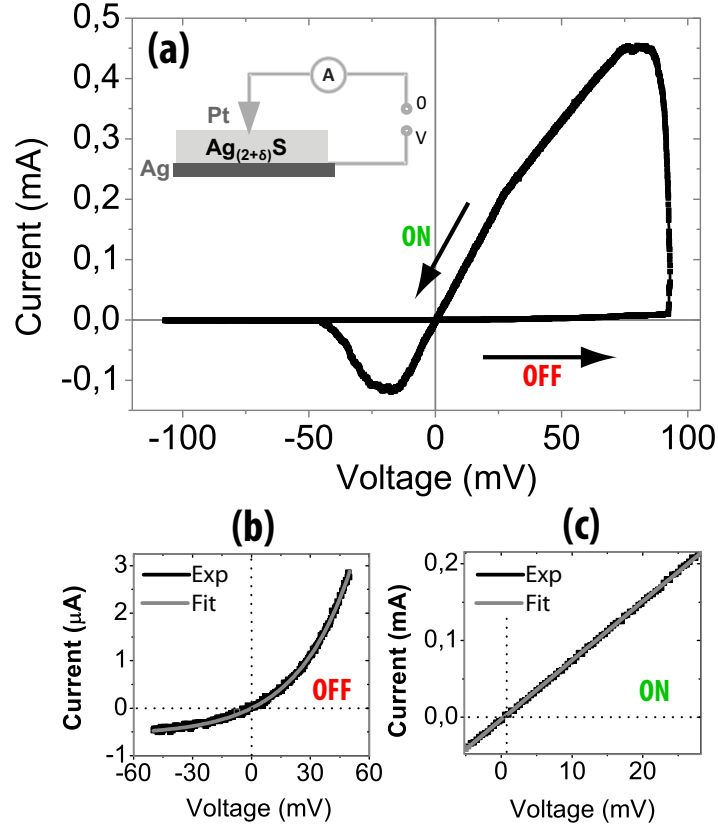


Figure 6.1: a) Current-voltage characteristics of a Ag/Ag₂S/Pt device (see inset) measured for a cycle duration of 1s. The ramp started at 0V and follows the arrows. In this IV curve full conductance switching is observed. The inset illustrates the contact geometry. b) Expanded scale view of the section of the IV curve in the ‘off’ state in (a). This part of the IV curve is fit very well by Eq. (6.1) (gray curve), indicating that the Pt tip is in contact with the Ag₂S film, and that the film is in its equilibrium (semiconducting) state. The zero-bias conductance of the off-state is approximately $0.2G_0$ for this contact size. c) On-state section of the IV curve in (a). At this stage the sample has a conductance of $100G_0$, and the linear fit (gray line) indicates metallic behavior.

similar to the one shown in Fig. 6.1 and the IV curves were recorded a few seconds after every cycle. Starting from the IV characteristics of the pristine sample (green curve) we observed the conductance increasing from $0.1G_0$ to $1G_0$ after the sixth cycle.

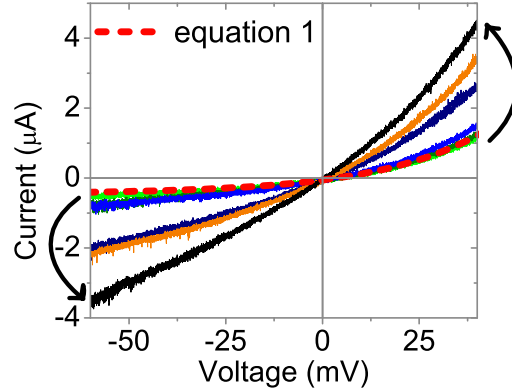


Figure 6.2: Evolution of the off-state conductance curve for a Ag_2S film with an increasing number of switching cycles. Each of the IV curves in the plot is measured after a full switching cycle, such as the one shown in Fig. 6.1a. The first curve (green) is measured after the first switching cycle, and the fit to Eq. (6.1) indicates that it remains close to the initial state of the pristine sample. The arrows give the direction of evolution for consecutive cycles. The zero-bias conductance of the junction changes from $0.1 G_0$ (green curve) to approximately $1 G_0$ (black curve).

Initially, the IV curves are described well by Eq. (6.1) (the red dashed curve). After several switching cycles the IV characteristic can only be fit by adding a significant linear term to Eq. (6.1). This changing sample conductance characteristics after switching has been reported previously and is referred to as the learning behavior of the switching mechanism [79], and is being explored for realizing artificial synapses [61].

6.3.2 Breaking

We measured traces of conductance as a function of time by control of the bias voltage in the following way: when the conductance was seen to fall below $0.5G_0$ a positive bias voltage was applied to the sample. To achieve rapid switching we used a voltage of $+100\text{mV}$. A high-conductance path was formed and the conductance was seen to rise to values above $100G_0$. Once G was detected to pass above $100G_0$ a negative bias voltage of -100mV was applied to the sample in order to break the conductive path, until the conductance approached the initial state of $G < 0.5G_0$. In this way the formation and breaking process is more controllable than by applying fixed pulses to the sample.

We measured many breaking traces at different spots on the sample and we recognized two types of traces: traces having a step-like pattern, and traces showing only a slow and continuous decay of the conductance. The observed patterns in the traces indicate the coexistence of two switching mechanisms.

The first mechanism is the dissolution of a metallic silver conductance path showing, at the final stages of the breaking, atomic conductance steps. When a metallic silver filament dominates the conductance, upon applying a negative voltage the filament at its weakest point will become reduced to only a few bridging atoms. In this way quantum properties of the conductance of the silver filament will show up [19]. Figure 6.3 shows some examples of atomic conductance steps observed in conductance traces recorded as a function of the breaking time. In Fig. 6.3a one observes that the conductance decays almost linearly until arriving at about $5G_0$, when steps of close to $1G_0$ in height start to be visible. Very pronounced plateaus and steps of approximately $1G_0$ can also be seen in the plots of Fig. 6.3(b), with a very long plateau of 0.4s in the middle trace. The upper trace also shows two level fluctuations with an amplitude close to $1G_0$ that is typical for atomic-scale contacts [19].

In an earlier series of measurements using a wire top-contact, we also observed steps in the breaking traces of conductance in a Ag/Ag₂S device cooled down to 220K. Two examples are presented in Fig. 6.4. The well defined step pattern, with the steps height close to $1 G_0$, supports the assumption that, when the Ag filament is at the last stage of breaking and the weakest point is reduced to few atoms, atomic conductance steps are visible. The plateaus are longer than the ones observed in the traces measured at room temperature, which is expected due to the sample temperature of 220K.

However, there appears to be a second mechanism active. We conclude this from the observation of a slower and nearly continuous decrease of the conductance. Traces with atomic conductance steps at room temperature appeared only when the conductance rapidly dropped below $0.5G_0$ in approximately one second. When the decrease in the conductance was slower, we observed behavior as illustrated by the upper trace in Fig. 6.5. This is accompanied by a change in the IV characteristics similar to Fig. 6.2. We attribute this behavior to a second mechanism, most likely due to a modification of the local lattice structure giving rise to a region of increased conductance. This modification is probably induced

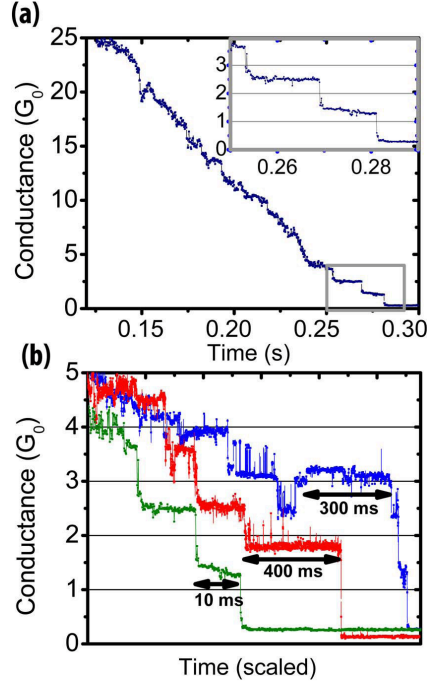


Figure 6.3: Steps in the conductance become visible when breaking the conductive path at a bias of -100mV . The conductive path was formed by applying a voltage of $+100\text{mV}$, allowing the conductance to reach $100G_0$ within a second. a) Breaking trace with three clear conductance steps of approximately $1G_0$ observed at the last stages of breaking. The inset shows a zoom of the steps. b) Three breaking traces with atomic conductance steps having different lengths in time. The measurements were performed on different spots of the sample and using different Pt-tips. The upper trace shows two-level fluctuations that are typical for atomic size contacts, and are attributed to single atoms oscillating near the contact.

by the electric field and the increased concentration of silver in the region of switching. It has been previously shown that the electric field can induced phase transitions, or decrease the phase transition temperature in materials like vanadium dioxide [80] and complex perovskites [81]. After applying a negative voltage silver diffuses back to the Ag bottom reservoir and the lattice slowly relaxes to its equilibrium structure.

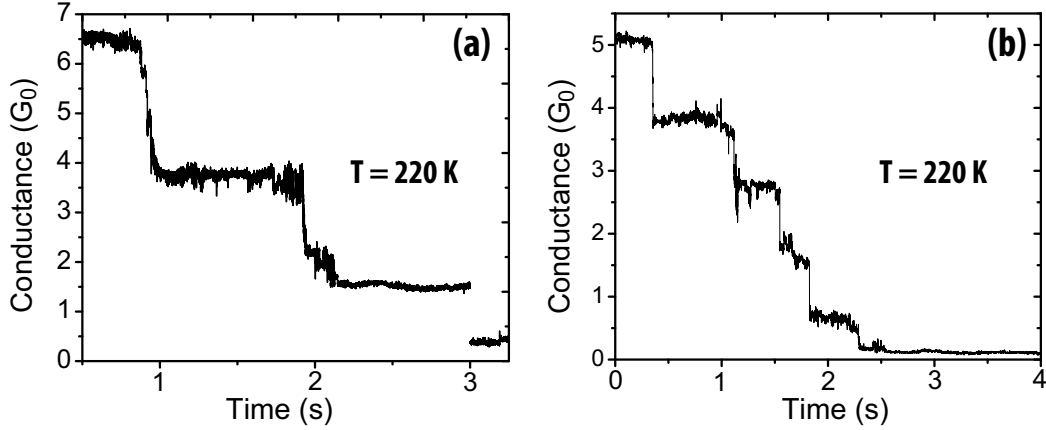


Figure 6.4: Steps in the conductance observed at 220K when breaking the conductive path at a bias of -100mV . The breaking traces show clear conductance steps of approximately $1G_0$ at the last stages of breaking.

Occasionally the two processes can be observed together, as illustrated in the middle trace in Fig.6.5: around $6G_0$ atomic conductance steps are visible, while somewhat later there is a continuous decrease over five seconds from 2 to $1G_0$. In terms of the two mechanisms described above this may be explained as being due to two parallel conductance paths.

6.3.3 Controllable switching

The continuous evolution of the IV characteristics in Fig. 6.2 and the continuous ‘on’ to ‘off’ conductance traces suggest that the local structure of the Ag_2S film has been modified. The conductance in this state can be controlled by applying positive bias voltages smaller than the threshold voltage. The voltages can be chosen to obtain specific values of conductance as illustrated in Fig. 6.6. In this example the conductance of the contact at a bias of -110mV was $0.3 G_0$, slightly higher than the conductance of the contact in the pristine state of $0.1 G_0$.

This nanoscale resistive switch in the regime of the quantum of conductance should not be confused with an atomic scale switch. The steps that we attribute to intrinsic atomic scale structure (‘quantization’) are only short lived (Fig. 6.3), and the IV curves in this state are linear, so that the conductance does not depend on the bias voltage. By controlling the second mechanism of conductance

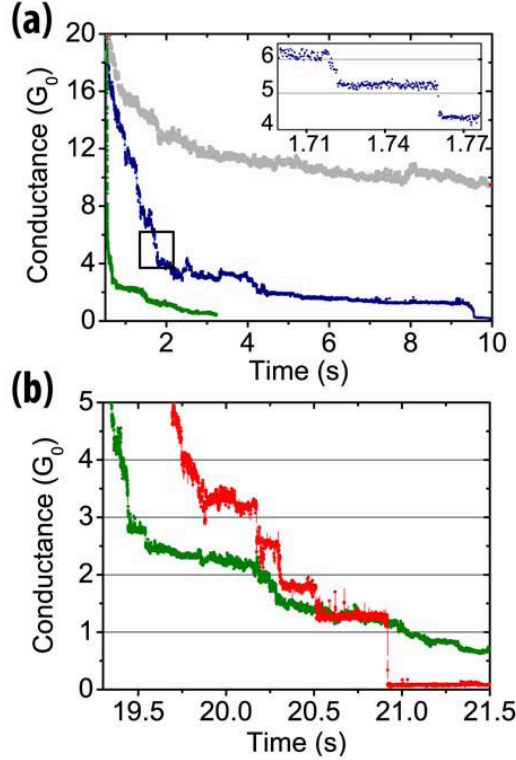


Figure 6.5: a) Continuous conductance changes observed when breaking a preformed conductive path at a bias voltage of -100mV . Mixed behavior is seen in the middle trace. The inset shows a magnification of the steps of approximately $1G_0$. The upper trace shows only continuous behavior and illustrates the high-conductance that is visible in some measurements after switching several times. The lower trace also shows only continuous behavior but the high-conductance state decays in few seconds to a conductance around $0.1G_0$. b) Comparison between a continuous trace (lower trace presented in (a)) and a trace with atomic conductance steps (red trace in Fig.6.3b)

switching any conductance, including ‘quantized’ values, can be set and maintained. The time scale for this process is much longer, and it allows manipulating the conductance over a wide range (Fig. 6.6).

6.4 Discussion

We have observed two types of conductance breaking traces, which we associate to the occurrence of two switching mechanisms in Ag_2S . From previously performed experiments [19] we can state that a Ag atomic scale point contact presents steps

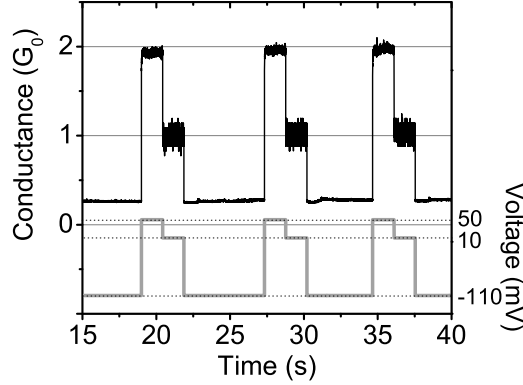


Figure 6.6: Switching between targeted values of conductance by applying specific low-bias voltages to the Ag_2S device. In this experiment the voltages were chosen such as to obtain approximately the first two integer conductance values, in analogy to the experiments by Terabe et al.[23]. Here we use fixed bias voltages instead of short pulses. This controllable switching can only be achieved after preparing the sample by several switching cycles. This example is chosen for illustration of the ambiguity that may arise when deciding whether a device is a true atomic scale switch.

in the conductance at the last stage before it breaks. However, the controllable switching, the continuously changing IV characteristics, and the gradually decreasing conductance traces cannot be explained by the formation of a metallic filament alone. The fact that the gradually decreasing conductance traces can take several seconds to return to the ‘off’ conductance (Fig.6.5), and decay of concentrations gradients in Ag_2S occurs much faster than a second [74] points towards the view that a modification of the lattice structure is induced, which we refer to as the second mechanism of conductance switching. Figure 6.7 shows a cartoon of the three different structures that may contribute in parallel to the total conductance: the pristine semiconducting sample (Ag_2S), metallic silver filaments (Ag), and the as yet undefined modified structure (X).

Our interpretation is consistent with the observations by Xu et al.[75] from *in situ* switching measurements of a $\text{Ag}/\text{Ag}_2\text{S}/\text{W}$ device. From real time measurements inside a high resolution transmission electron microscope (HRTEM), Xu et al. determined that the conductive path formed when applying a positive voltage to the Ag electrode, is composed of a mixture of metallic Ag and argentite Ag_2S .

At room temperature, the equilibrium lattice structure of silver sulfide is the

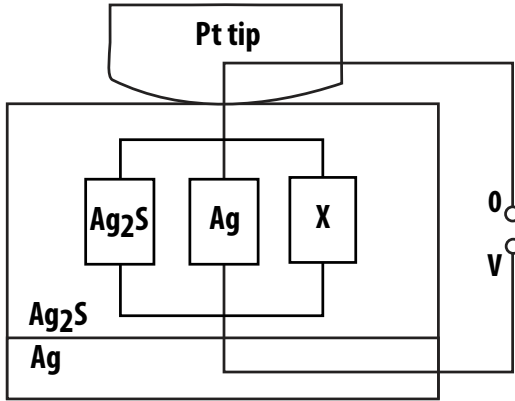


Figure 6.7: The measurements suggest that three structures are involved in the conductance after full resistive switching. Before switching we have our pristine sample which obeys the IV relation of Eq. (6.1). During switching a high-conductive path is formed by metallic silver and, in parallel, by a modified structure of the silver sulfide (X). An interpretation of this modified structure comes from comparison of our results with Xu et al.[75], who identified it in HRTEM studies as the argentite phase of silver sulfide.

so called acanthite phase. Above 450 K, the lattice undergoes a phase transition to the argentite structure. Argentite has an electronic conductivity that is three orders of magnitude higher, and behaves like a metal [29]. The argentite structure has previously been stabilized at room temperature by rapidly cooling of silver sulfide from high temperatures [46]. According to Xu’s interpretation this phase transition to the argentite phase is not caused by Joule heating because the currents are quite low at the off state, but is believed to be driven by the increased silver ion concentration and the applied field.

Adhering to this interpretation of the phase transition we explain the observed continuous traces and mixed traces shown in Fig.6.5 as follows. The bias voltage drives both switching mechanisms: metallic filament formation and the local partial phase transition. When a silver filament is formed that stretches fully across the thickness of the film its high conductance dominates the observed electron transport. Break down of the filament at the last stages produces a connection formed by just a few atoms, and when these disconnect one by one this becomes visible as near-quantized steps in the conductance. When the metallic silver of a filament dissolves very rapidly or an incomplete filament is formed, atomic conductance steps will be absent and the conductance will drop continuously, as a result of the gradual decay of the locally modified structure. When the breaking of the silver filament occurs on the same time scale as the decay of the modified structure back to the initial room temperature phase, mixed behavior as seen in the middle curve in Fig. 6.5 can be observed. The conditions for the formation

of a metallic silver filament and the observation of atomic conductance steps are not yet fully understood, since the two processes are controlled by the same bias voltage.

6.5 Conclusion

In summary, we identify two mechanisms of conductive path formation inside a thin film of silver sulfide. The first mechanism is the formation of a metallic silver filament which we associate with the observation of atomic conductance steps. Second, there is a modification of the silver sulfide structure to a higher-conductance phase. The conductance of this modified structure is continuously tunable, and allows setting the conductance to any target value by applying appropriate positive voltages. Contrary to previous reports [23, 61], we argue that this controllable switching cannot be attributed to an intrinsic atomic scale structure. The memory functions explored by Ohno et al.[61] cannot be explained by a metallic filament formation alone. Our results point towards the role of the two switching mechanisms in deciding whether the information is maintained for shorter or longer times.

7

Discussion and Outlook

In this chapter, we present a summary and discussion of the research in Ag_2S . Furthermore, the scientific and technical challenges for the future of the conductive bridge memories are discussed.

7.1 Introduction

In this chapter we present a conclusive summary of the research performed with Ag_2S as a model system. In the first two sections we comment on the application of Ag_2S as a model system to study conductance switching, and as a prototype material for fabrication of conductive bridge memories (CB-RAM). In the third section, a brief description of the future challenges and approaches reported in literature for development of the CB-RAM's is presented.

7.2 Ag_2S as a model material to study conductance switching

In our research, we have used Ag_2S as a model system to study resistance switching in mixed conductors. Ag_2S has been studied previously and can be fabricated by relatively straightforward techniques (See Chapter 2).

Most processes described in this thesis are also valid for many other mixed conductor materials. For example this applies to the Hebb-Wagner formalism for transport under steady state, the requirement of a supersaturation of the cations before nucleation of the metal phase, and the presence of two parallel conductance switching mechanisms. All this makes Ag_2S a good model system.

The property that sets Ag_2S apart is the fact that, the formation of a space charge layer at the electrode-electrolyte interface is negligible in the case of Ag_2S , which is not necessarily the case in other mixed conductor materials. This is due to the high ionic defect concentration in Ag_2S . In general, the formation of a space charge layer occurs in solid electrolyte/metal interfaces, and this effect has a larger influence when working at the nanoscale. When reducing the solid electrolyte film thickness to a few tens of nanometers, the film could reach the dimensions of the space charge layer, and even an overlap of the depletion layers of both electrolyte/electrode interfaces can occur. In such a case, the bulk properties of the electrolyte are expected to change [83]. This is, therefore, an important distinction to consider when working with other mixed conductor materials, where the ion defect concentrations are much lower than in Ag_2S .

7.3 Ag₂S as a material for resistive memories

Although Ag₂S forms an appropriate model system to study the physics of switching, it presents disadvantages as a prototype material for memory devices. First, the fast diffusion of ions at room temperature in Ag₂S is a disadvantage in view of the short memory retention time associated with it. Second, the low writing voltage (threshold for switching), although an advantage in terms of low energy operation, is a disadvantage in the definition of the read voltage. The read voltage has to be significantly lower than the writing voltage, such that, when reading it does not change the state (resistance) of the device. However, as seen in the experiments presented in Chapter 6 Section 6.3.3, even very low voltages (10mV) can modify the resistance of the ‘off’ state of the device. Third, the modification of the sample after several switching cycles is a disadvantage in terms of endurance, i.e. the amount of switching cycles before failure. On a non-optimized sample the maximum number of switching cycles achieved with our Ag₂S devices was approximately 500. To compete with contemporary flash memories, the number of switching cycles should be larger than 10⁷ [2].

7.4 Challenges for the future of conductive bridge memories

Several ideas have appeared in literature for the development of nanoionic memory devices that fulfill the requirements of retention, endurance and performance of typical memories. Most of the approaches are in the direction of materials innovation, not only for the resistive layer, but also for the active layer (supplying the metal ions) and counter electrode (the inert metal). The list of materials that can be used as the ion conducting layer has been rapidly growing in the last few years, to the point that it includes not only solid electrolytes but all kind of semiconducting and insulating oxide materials. A summary of reported material combinations used for the fabrication of CB-RAM’s is given in Ref.[82].

A further requirement for the development of CB-RAM memories, is the potential for scalability of the memory cells. This is actually a great motivation for the research in CB-RAM. The high scalability is due to the possibilities to reduced the metal filament dimensions to only a few atoms in cross section, bridging across the resistive thin film. The vertical scalability then requires the

electrodes and the resistive film to be only few nanometers thick, i.e. 5nm or less each. The lateral scalability will require the memory cell to be less than 20 nm in diameter, and that the memory cell will have a well defined switching area, where the metallic nanowire grows and shrinks. Advances in this direction have been reported in literature. One example is GeSe devices showing scalability to below 20nm, and no device degradation when scaling to those dimensions [84]. As mentioned in Chapter 1 of this thesis, the ultimate scaling will be that in which the metallic filament is composed on only a few atoms. If possible even down to a single atom. So far, only Terabe et al. [23] reported the fabrication of an atomic switch. However, we have shown that the operation mechanism differs from their interpretation and the reproducibility of the switch needs to be further investigated.

Finally, to create a working memory with high density storage, the individual memory cells must be integrated into cross-bar arrays. The cross bar arrays are sets of parallel bottom electrodes, and perpendicular top electrodes, with a resistive material between the electrodes at each cross point. Because many of the memory cells can be connected in a line by either of the electrodes, crosstalk can occur through neighboring cells. The integration of the memories into cross-bar arrays, requires the addition of components or adjustments in the design of the memories cells, this mainly to prevent crosstalk (also called sneak path currents [85]) and misreading of the memories. One approach to solve the sneak path problem would be to use a rectifier element in series with each of the cells. Thin film diodes have been proposed in the literature for use as rectifying elements in cross bar circuits [86]. Another interesting approach, reported by Linn et al.[85] consists of a complementary resistive switch (CRS) composed of two memory cells connected antiseriially. The CRS prevents the occurrence of sneak path currents and opens the possibility for building large passive cross bar arrays.

The investigations of resistive switching devices and implementation into cross bar arrays, have also led to new emerging ideas. For example, the synthesis of inorganic artificial synapses, with the prospect to build artificial neural networks. Two recent papers have shown the possibility to use the resistive switching memory cells as individual synapses. The first report uses a phase change memory cell as the synapse element [87], and the second report, uses a Ag₂S memory switch [61]. The short and long term memory of the synapses (also called plasticity) are determined by the conductances changes in the memory switch induced by

voltage pulses. If the conductance decreases rapidly just after a weak voltage signal, it is called short term plasticity (STP). If the conductance remains for a long period of time after repeated strong voltage signals, it is called long-term plasticity (LTP). So far, the principle of artificial synapse has been shown only for individual memory cells, therefore, being no more than a concept implemented to the changes in conductance induced by voltage signals. However, the principle of artificial synapses is very attractive, and one can predict that several of the materials tested for resistive memories, will probably be tested for the fabrication of artificial synapses. Nonetheless, for a ‘real’ artificial neural network, reproducibility of the response to the voltage pulses, and to the operation of several synapses in a network is required. Finally, to match the complexity of the human brain, artificial neural networks need to contain around 10^{15} synapses [88].

7.5 Conclusion

Although several materials and memory cells are proposed in literature, the combination of all factors: performance, endurance, retention, scalability and integration into cross bar arrays, still need to be demonstrated for these memories. This leaves a wide set of open questions, materials and design issues to explore. Collaboration with several fields (chemistry, physics, electronics, materials science) is necessary for further investigations. Understanding the fundamental mechanism of switching is an important part of the research that will lead to a better design of the memory devices.

7. DISCUSSION AND OUTLOOK

Appendix A

In Chapters 3, 4 and 5 we mention the presence of a threshold voltage above which nucleation and growth of a metallic phase inside the Ag_2S film occurs, leading up to conductance switching. Although it has been called a threshold voltage, it has not yet been clarified whether the switching is governed strictly by the bias voltage alone, or by the electric field that it causes. Specifically, it remains unclear what the rate determining process for conductance switching is.

The main observations from the chapters regarding the threshold voltage for conductance switching are as follows:

In Chapter 3, we find a threshold voltage of 225 mV in a device with the configuration Pt (bottom electrode)/ Ag_2S /Pt (micro-wire), where the Ag_2S is at the stoichiometric composition. In Fig.3.5 of the same chapter, we also show that after multiple cycles, the voltage at which the switching occurs is reduced to approximately 100 mV.

In Chapter 4, we find a threshold voltage for switching above 70mV, in a device with the configuration Ag (bottom electrode)/ Ag_2S /Pt (micro-wire and nano-contact). Here the Ag_2S is at the maximum stoichiometry in equilibrium with Ag. This threshold voltage did not show a significant change after several switching cycles.

Next, in Chapter 5, we confirm the 70 mV threshold voltage for Ag nucleation inside the Ag_2S film in the same device as Chapter 4. Additionally, we find that nucleation of Ag outside the Ag_2S film requires less than 20 mV.

The observation that for Ag_2S with lower Ag concentration ($\delta \approx 0$) the threshold voltage is larger than for the case of Ag_2S with maximum Ag concentration ($\delta = \delta_{max}$), indicates that the 225mV found for the first case, is related to the fact that initially, a local Ag ion accumulation is needed to reach supersaturation, at which the metal phase nucleates. This first step, involving ion migration is electric field driven. Once the Ag_2S film is locally modified, the threshold voltage is reduced to values close to the 70mV found in the case with $\text{Ag}_{2+\delta_{max}}\text{S}$.

The difference of the threshold voltage found for Ag_2S and $\text{Ag}_{2+\delta_{max}}\text{S}$, is comparable with values reported by Bonnecaze et al.[25]. Bonnecaze determined a potential larger than 105 mV to change the stoichiometry of $\text{Ag}_{2+\delta}\text{S}$ from $\delta = \delta_{max}$ to $\delta = 0$.

On the other hand, if the rate determining step is the charge transfer, the threshold voltage must be independent of concentration gradients, and the same threshold voltage for switching must be observed for both devices (with Ag or Pt bottom electrodes), which is not the case at least at the first switching cycles. Moreover, the fact that nucleation on the surface is possible at much lower voltages, below 20mV, points towards the conclusion that the rate determining step for conductance switching inside the Ag_2S is the nucleation of the new metal phase. Although, from the experiments performed we cannot fully exclude a field driven process, in view of the arguments above, we will rather tend to favor a voltage driven process, related with the nucleation of metallic Ag inside the Ag_2S .

Finally, it is important to mention that, whether the charge transfer, nucleation of the metal phase or slow diffusion under the influence of an electric field is the rate determining step, strongly depends on the memory resistive device, i.e. on the electrodes and the electrolyte material used [82].

Bibliography

- [1] T. Mikolajick, M. Salinga, M. Kund, and T. Kever, *Adv. Eng. Mater.* **11** 235-240 (2009).
- [2] R. Waser, R. Dittmann, G. Staikov and K. Szot, *Adv. Mater.* **21** 2632 (2009).
- [3] Y. V. Pershin and M. Di Ventra, *Advances in Physics* **60** 145-227 (2011).
- [4] R. Waser, R. Dittmann, M. Salinga and M. Wuttig, *Solid-State Electron.* **54** 830-840 (2010).
- [5] M. N. Kozicki and M. Mitkova, *Nanotechnology* (Wiley-VCH Verlag GmbH & Co. KGaA, 2010)
- [6] S. R. Ovshinsky, *Phys. Rev. Lett.* **21** 1450 (1968).
- [7] M. Wuttig and N. Yamada, *Nat. Mater.* **6** 824-832 (2007).
- [8] Y. Hirose and H. Hirose, *J. Appl. Phys.* **47** 2767-2772 (1976).
- [9] M. N. Kozicki, M. Yun, L. Hilt and A. Singh, *Pennington NJ USA: Electrochem. Soc.* (1999).
- [10] G. I. Meijer, *Science* **319** 1625-1626 (2008).
- [11] T. Siegrist, P. Jost, H. Volker, M. Woda, P. Merkelbach, C. Schlockermann and M. Wuttig, *Nat. Mater.* **10** 202-208 (2011).
- [12] D. Lencer, M. Salinga, B. Grabowski, T. Hickel, J. Neugebauer and M. Wuttig, *Nat. Mater.* **7** 972-977 (2008).
- [13] G. W. Burr, M. J. Breitwisch, M. Franceschini, D. Garetto, K. Gopalakrishnan, B. Jackson, B. Kurdi, C. Lam, L. A. Lastras, A. Padilla, B. Rajendran, S. Raoux and R. S. Shenoy, *J. Vac. Sci. Technol. B* **28** 223-262 (2010).
- [14] R. Waser and M. Aono, *Nat. Mater.* **6** 833-840 (2007).
- [15] Y. C. Yang, F. Pan, Q. Liu, M. Liu and F. Zeng, *Nano Lett.* **9** 1636-1643 (2009).
- [16] S. S. Hong, J. J. Cha and Y. Cui, *Nano Lett.* **11** 231-235 (2011).

BIBLIOGRAPHY

- [17] K. Szot, W. Speier, G. Bihlmayer and R. Waser, *Nat. Mater.* **5** 312-320 (2006).
- [18] D. H. Kwon, K. M. Kim, J. H. Jang, J. M. Jeon, M. H. Lee, G. H. Kim, X. S. Li, G. S. Park, B. Lee, S. Han, M. Kim and C. S. Hwang, *Nature Nanotechnology* **5** 148-153 (2010).
- [19] N. Agrait, A.L. Yeyati and J.M. van Ruitenbeek, *Physics Reports-Review Section Of Physics Letters* **377** 81-279 (2003).
- [20] F. Q. Xie, L. Nittler, Ch. Obermair and Th. Schimmel, *Phys. Rev. Lett.* **93** 128303 (2004).
- [21] F. Q. Xie, R. Maul, A. Augenstein, Ch. Obermair, E. B. Starikov, G. Schon, Th. Schimmel and W. Wenzel, *Nano Lett.* **8** 4493-4497 (2008).
- [22] C. A. Martin, R. H. M. Smit, H. S. J. van der Zant and J.M. van Ruitenbeek, *Nano Lett.* **9** 2940-2945 (2009).
- [23] K. Terabe, T. Hasegawa, T. Nakayama and M. Aono, *Nature* **433** 47-50 (2005).
- [24] H. Schmalzried, *Prog. Solid State Chem.* **13** 119-157 (1980).
- [25] U. Bonnecaze, A. Lichanot and S. Gromb, *J. Phys. Chem. Solids* **39** 299-310 (1978).
- [26] S. R. Barman, N. Shanti, A.K. Shukla and D.D. Sarma, *Phys. Rev. B.* **53** 3746-3751 (1996).
- [27] C. Wagner, *Z.physik. Chem.* **25** B21 (1933).
- [28] R. J. Cava, F. Reidinger and B. J. Wuensch, *J. Solid State Chem.* **31** 69-80 (1980).
- [29] S. Kashida, N. Watanabe, T. Hasegawa, H. Iida, M. Mori and S. Savrasov, *Solid State Ionics* **158** 167-175 (2003).
- [30] M. H. Hebb, *J. Chem. Phys.* **20** 185-190 (1952).
- [31] Z. C. Wang, T. K. Gu, T. Kadohira, T. Tada and S. Watanabe, *J. Chem. Phys.* **128** 014704 (2008).
- [32] I. C. Lekshmi, G. Berera, Y. Afsar, G. X. Miao, T. Nagahama, T. Santos and J. S. Moodera, *J. Appl. Phys.* **103** 093719 (2008).
- [33] K.D. Becker, H. Schmalzried and V. Vonwurm, *Solid State Ionics* **11** 213-219 (1983).
- [34] R. L. Allen and W. J. Moore, *J. Phys. Chem.* **63** 223-226 (1959).
- [35] C. Wagner, *J. Chem. Phys.* **21** 1819-1827 (1953).
- [36] T. Kudo and K. Fueki, *Solid State Ionics* (VCH Weinheim, 2010).
- [37] J. Frenkel, *Z. Physik* **35** 652-669 (1926).

-
- [38] D. M. Smyth, *The Defect Chemistry of Metal Oxides* (Oxford University Press, Inc., 2000).
- [39] L. Onsager, Phys. Rev. **38** 2265 (1931).
- [40] D. Grientschnig and W. Sitte, J. Phys. Chem. Solids **52** 805-820 (1991).
- [41] I. Yokota and S. Miyatani, Solid State Ionics **3-4** 17-21 (1981).
- [42] I. Bartkowicz and A. Stoklosa, Solid State Ionics **24** 45-49 (1987).
- [43] A. Panneerselvam, M.A. Malik, P. O'Brien and J. Raftery, J. Mater. Chem. **18** 3264-3269 (2008).
- [44] H. Meherzi-Maghraoui, M. Dachraoui, S. Belgacem, K.D. Buhre, R. Kunst, P. Cowache and D. Lincot, Thin Solid Films **288** 217 - 223 (1996).
- [45] A. Nuñez Rodríguez, M. T. S. Nair and P. K. Nair, Semicond. Sci. Technol. **20** 576 (2005).
- [46] M. Kundu, K. Terabe, T. Hasegawa and M. Aono, J. Appl. Phys. **99** 103501 (2006).
- [47] M. Morales-Masis, S. J. van der Molen, W. T. Fu, M. B. Hesselberth and J.M. van Ruitenbeek, Nanotechnology **20** 095710 (2009).
- [48] K. Terabe, T. Nakayama, T. Hasegawa and M. Aono, J. Appl. Phys. **91** 10110 (2002).
- [49] A. Nayak, T. Tamura, T. Tsuruoka, K. Terabe, S. Hosaka, T. Hasegawa and M. Aono, J. Phys. Chem. Lett. **1** 604-608 (2010).
- [50] G. A. Armantrout, D. E. Miller, K. E. Vindelov, T. G. Brown, J. Vac. Sci. Technol. **16** 212-215 (1979).
- [51] M. Kundu, T. Hasegawa, K. Terabe, and M. Aono, J. Appl. Phys. **103** 073523 (2008).
- [52] D. Bräuhäus, C. Schindler, U. Böttger and R. Waser, Thin Solid Films **516** 1223-1226 (2008).
- [53] E. Vanhoecke, M. Burgelman and L. Anaf, Thin Solid Films **144** 223-228 (1986).
- [54] T. Ben Nasrallah, H. Dlala, M. Amlouk, S. Belgacem and J.C. Bernède, Synthetic Metals **151** 225-230 (2005).
- [55] T. Okabe and M. Nakagawa, J. Crystal Growth **46** 504-510 (1979).
- [56] S. Kasukabe, J. Crystal Growth **65** 384-390 (1983).
- [57] R. S. Wagner and W. C. Ellis, Appl. Phys. Lett. **4** 89-90 (1964).
- [58] S. Miyatani, J. Phys. Soc. Jpn. **10** 786-793 (1955).
- [59] D. Karashanova and N. Starbov, Appl. Surf. Sci. **252** 3011-3022 (2006).

BIBLIOGRAPHY

- [60] C. H. Liang, K. Terabe, T. Hasegawa and M. Aono, *Nanotechnology* **18** 485202 (2007).
- [61] T. Ohno, T. Hasegawa, T. Tsuruoka, K. Terabe, J. K. Gimzewski and M. Aono, *Nat. Mater.* **10** 591-595 (2011).
- [62] T. Hino, T. Hasegawa, K. Terabe, T. Tsuruoka, A. Nayak, T. Ohno and M. Aono, *Sci. Technol. Adv. Mater.* **12** 013003 (2011).
- [63] V. Lehmann and H. Rickert, *J. Appl. Electrochem.* **9** 209-217 (1979).
- [64] D. Strukov, G. S. Snider, D. R. Stewart and R. S. Williams, *Nature* **453** 80-83 (2008).
- [65] S. H. Jo, K. H. Kim and W. Lu, *Nano Lett.* **9** 496-500 (2009).
- [66] Q. Liu, C. M. Dou, Y. Wang, S. B. Long, W. Wang, M. Liu, M. H. Zhang and J. N. Chen, *Appl. Phys. Lett.* **95** 023501 (2009).
- [67] C. Wagner, Proc. 7th Meeting Intern. Committee on Electrochemical Thermodynamics and Kinetics, Lindau 1955, Butterworth Scientific Publ., London. **361** (1957).
- [68] A. J. Bard, L. R. Faulkner, *Electrochemical Methods: Fundamentals and Applications / 2nd ed.* (John Wiley & Sons, Inc., 2001).
- [69] J. Mizusaki, K. Fueki and T. Mukaibo, *Bull. Chem. Soc. Jpn.* **48** 428-431 (1975).
- [70] H. Rickert and H.-D. Wiemhöfer, *Solid State Ionics* **11** 257-268 (1983).
- [71] N.F. Mott, R.W. Gurney, *Electronic Processes in Ionic Crystals / 2nd ed.* (Oxford University Press, 1950).
- [72] E. Budevski, G. Staikov and W. J. Lorenz, *Electrochim. Acta* **45** 2559-2574 (2000).
- [73] H. Rickert and H.-D. Wiemhöfer, *Ber. Bunsenges. Physikal. Chem.* **87** 236-239 (1983).
- [74] M. Morales-Masis, H. D. Wiemhofer and J. M. van Ruitenbeek, *Nanoscale* **2** 2275 (2010).
- [75] Z. Xu, Y. Bando, W. L. Wang, X. D. Bai and D. Golberg, *Acs Nano* **4** 2515 (2010).
- [76] V. G. Karpov, Y. A. Kryukov, I. V. Karpov and M. Mitra, *Phys. Rev. B* **78** 052201 (2008).
- [77] I. V. Karpov, M. Mitra, D. Kau, G. Spadini, Y. A. Kryukov and V. G. Karpov, *Appl. Phys. Lett.* **92** 173501 (2008).
- [78] D. Krebs, S. Raoux, C. T. Rettner, G. W. Burr, M. Salanga and M. Wuttig, *Appl. Phys. Lett.* **95** 082101 (2009).
- [79] T. Hasegawa, T. Ohno, K. Terabe, T. Tsuruoka, T. Nakayama, J. K. Gimzewski and M. Aono, *Adv. Mater.* **22** 1831-1834 (2010).

-
- [80] A. Pergament, P. Boriskov, A. Velichko and N. Kuldin, *J. Phys. Chem. Solids* **71**, 874 (2010).
- [81] X. Zhao, W. Qu, X. Tan, A. A. Bokov and Z. G. Ye, *Phys. Rev. B* **75**, 104106 (2007).
- [82] I. Valov, R. Waser, J. R. Jameson and M. N. Kozicki, *Nanotechnology* **22** 254003 (2011).
- [83] J. Maier, *Phys. Chem. Chem. Phys.* **11** 3011-3022 (2009).
- [84] M. Kund, G. Beitel, C.-U. Pinnow, T. Röhr, J. Schumann, R. Symanczyk, K.-D. Ufert and G. Müller, *IEDM Tech. Digest* 754757 (2005).
- [85] E. Linn, R. Rosezin, C. Kugeler and R. Waser, *Nat. Mater.* **9** 403-406 (2010).
- [86] B. S. Kang, S.-E. Ahn, M.-J. Lee, G. Stefanovich, K. H. Kim, W. X. Xianyu, C. B. Lee, Y. Park, I. G. Baek and B. H. Park, *Adv. Mater.* **20** 3066-3069 (2008).
- [87] D. Kuzum, R. G. D. Jeyasingh, B. Lee and H.-S. P. Wong, *Nano Lett.* <http://dx.doi.org/10.1021/nl201040y> (2011).
- [88] D. B. Strukov, *Nature* **476** 403-405 (2011).

BIBLIOGRAPHY

Summary

Non-volatile memories, computer memories that store information even when the power is off, are becoming increasingly important in information technology. The most common non-volatile memories used nowadays are flash memories, present in the memory cards of our cellphones, cameras and USB flash drives for example. With the appearance of new technologies there is a large demand for small, light and high capacity storage non-volatile memories. However, these memories are now reaching the miniaturization limits. The reason why there is a miniaturization limit, is because these memories store information by accumulating charge in memory cells^{*}. The smaller these memory cells become the less charge can be accumulated and the less reliably the data storage. Because of this, new memory concepts are being investigated nowadays.

One proposed new memory concept is based on resistance switching, where data is stored as well defined resistance states on a material and not by accumulating charges. The resistance of a material determines how easy a material allows the passage of electrical current. Resistance switching is the change of the electrical properties of a material between two states, one state that allows the passage of current (low resistance state) and one state that prevents the passage of current (high resistance state). In terms of the memory concept, the low resistance state is called ‘on’ state (or 1) and the high resistance state is called ‘off’ state (or 0).

There are different mechanisms by which a material can change its resistance state. For example, a transformation of the crystal structure of the material, or the movement of atoms inside the material forming conducting paths. In this thesis I focus on the study of resistance switching due to movements of atoms inside a material and the reversible formation of a conductive path. These ‘proof-of-concept’ memories are also called ‘Conductive-Bridge Memories’.

The Conductive Bridge memories are composed of two metal electrodes and a resistive material between them. Applying a voltage between the electrodes, induces a

^{*}A memory cell is where one bit (a 0 or 1 in a binary language) of data can be stored

change in resistance, caused by the reversible formation of a conductive bridge. The formation or dissolution of the conductive bridge depends on the polarity of the voltage applied. The presence or absence of the conductive path forms the low and high resistance states respectively. Figure 7.1 presents a schematic diagram of the conductive bridge resistance switching concept.

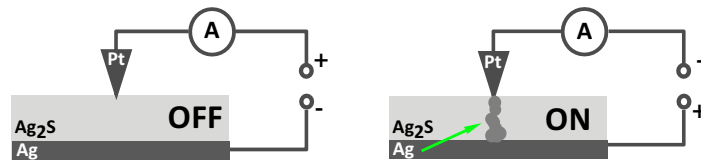


Figure 7.1: Schematic diagram of resistance switching in Ag₂S

The schematic diagram also represents the system studied in this thesis. In our experiments a silver (Ag) thin film is the bottom electrode, the middle layer is silver sulfide (Ag₂S), and the top electrode is a platinum (Pt) micro (10⁻⁶) or nano(10⁻⁹)-scale contact. To create such a small top contact we used an atomic force microscope tip coated with platinum (Pt) or a scanning electron microscope (STM) Pt tip.

Silver Sulfide, Ag₂S, is a mixed conductor material, which means that its total conductivity is due to the motion of both Ag⁺-ions and electrons. Mixed conductors are special materials because of their dual conductivity (ionic and electronic). In comparison, the conductivity of metals is only due to electron transport. The ion transport property of mixed conductors is the key ingredient for the conductive bridge memory presented in this thesis. Ions can easily move due to the applied electric field created by the voltage, and can form a conductive bridge between the top to bottom electrode. Once the bridge reaches from top to bottom electrode, the mixed conductor is short circuited, and the resistance drops. When the electric field is reversed (change in polarity of the voltage), the ions can move back to their 'original' position, the bridge breaks and the resistance increases again.

As with the Ag/Ag₂S/Pt switching device, several other material combinations have been tested and demonstrated in literature as resistance switches, that work under the conductive bridge concept. The large interest in this research subject comes with the possibility to create a switch where only few atoms need to be moved to connect and disconnect the electrodes. This would mean scalability of the memory cell to a few nanometers (10⁻⁹m) in size. In 2005, the research group led by Prof. M. Aono at

NIMS-Japan, reported the creation of an ‘atomic switch’ with a Ag₂S device. In their publication they claimed that the ‘on’ and ‘off’ states of conductance were due to the formation of a metallic filament composed of only a few atoms.

Although many of the points above sound fascinating, little has been explained in literature about the physical processes that drive resistance switching. Many details about the microscopic processes occurring before, during and after switching are unknown. For our research we aimed at understanding the mechanisms that drive resistance switching, and we focused less on device development. Understanding the fundamentals of the switching, helps for future development of the field, to make material choices when designing the memories, as well as to evaluate the true possibilities for future development of this type of memories.

The study of resistive switching in Ag₂S is presented in this thesis as follows. In Chapter 1 we describe the physical properties of Ag₂S. The semiconductor properties, crystal structure and the main phases at which Ag₂S can exist. In Chapter 2 we present the two fabrication methods we used to grow our samples, the advantages and disadvantages of each method and the characterization of the Ag₂S devices.

In Chapter 3 we present measurements of resistance switching in Ag₂S devices. We apply a voltage ramp to the device in the direction from 0V to V_{max} , then from V_{max} to $-V_{max}$ and then back to 0V, and measure the response of the current. We present this in so-called IV-curves. We performed IV-curve measurements with different voltage amplitudes (V_{max}) and we observed a change in the shape of the IV curves with increasing V_{max} . The most notable change is that above a certain voltage, the IV-curves show an open loop (also called hysteresis), indicating that the voltage induces changes in the sample, and therefore, the current response is different in the forward and backward direction of the voltage ramp. At the largest voltage tested, the IV-curve clearly shows semiconductor behavior and high resistance up until a certain voltage. At a certain voltage the behavior changes and the sample switches to metallic behavior and low resistance. This state remains like this until V_{max} . Then, upon lowering the voltage towards $-V_{max}$ the metallic behavior remains until a certain negative voltage. There the sample switches back to a high resistance and semiconductor behavior. This demonstrates the so-called ‘resistance switching’.

In Chapter 4 we study the processes before switching, i.e. the IV curves at very low voltages, where no hysteresis is observed. This type of IV curves represents the steady state, and defines the pre-switching state. An important result from this chapter is that not only the reduction of the Ag⁺-ions ($\text{Ag}^+ + e^- \rightarrow \text{Ag}_{metal}$) at the Pt electrode is

important to start the switching, but that a supersaturation (increased concentration) of Ag at the region close to the Pt tip is necessary to nucleate the metallic Ag. This metallic Ag is what later forms the conductive bridge. We describe the switching in our Ag₂S devices as follows. The formation of the conductive path is induced by applying a voltage between the electrodes. The applied voltage creates an electric field across the Ag₂S, that causes a flux of Ag⁺-ions and electrons. If the negative voltage is at the Pt electrode, the Ag⁺-ions move towards the Pt tip and accumulate in the region near to the tip. When the accumulation of ions is large enough, metallic Ag starts to nucleate. Because of the strong field created near the nucleated Ag, a Ag filament grows towards the Ag electrode, finally connecting the electrodes. This is the switching ‘on’ process, when the Ag₂S changes from the ‘high’ resistance state to the ‘low’ resistance state.

The prerequisite of supersaturation for the nucleation of metallic Ag and further resistance switching is confirmed in Chapter 5. We also find in this chapter that the nucleation of Ag on the surface of the Ag₂S can occur at voltages much lower than the voltage require for switching inside the Ag₂S.

In Chapter 6 we study the switching off process. We find that the low resistance state in Ag₂S is not only due to the formation of a metallic filament (as commonly assumed in literature), but that there is also a modification (possibly a phase transition) of the Ag₂S lattice. This leads to two important conclusions. First, using a mixed conductor like Ag₂S, the formation of a single atom switch is very unlikely to be achievable. This is because it is not only the movement and positioning of Ag atoms forming a bridge which defines the low resistance state, but also the surrounding Ag₂S lattice which is modified. The local modification of the Ag₂S lattice contributes to the low resistance. It then becomes difficult to determine if the low resistance state is due to the metallic Ag wire or to the modified structure of the Ag₂S. Following this, the second conclusion is that we can measure the same values of resistance characteristic of an atomic switch. However, those values of resistance are not due to the presence of a metallic contact of a few atoms, but results from a local modification of the Ag₂S lattice. Comparing our results with the results published in 2005 of the ‘atomic’ switch, we believe that those results should be explained in a different way than just a few atoms switching.

Although we made a large step forward in understanding the resistance switching process, there are still many open questions about the possibilities for scalability and performance of the conductive bridge switches before they can be used in real memory devices.

Samenvatting voor de leek

Niet-vluchtig geheugen (NVG), computergeheugen dat informatie bewaart zelfs als er geen spanning op de chip staat, wordt steeds belangrijker in elektronische apparatuur. De meest gangbare vorm van NVG is tegenwoordig ‘flash’ geheugen. Flash geheugen vinden we in geheugenkaarten van mobiele telefoons, cameras en in USB sticks. Met de ontwikkeling van nieuwe elektronica neemt de vraag naar kleiner, lichter geheugen met een steeds grotere opslagcapaciteit enorm toe. De huidige generatie geheugen is echter aan haar limiet van miniaturisatie aanbeland. De reden dat er een ondergrens zit aan de miniaturisatie is dat deze generatie geheugen de informatie opslaat in de vorm van lading. Hoe kleiner deze geheugens worden, des te minder lading ze opslaan, waardoor ze minder betrouwbaar worden. Om nog kleinere geheugens te kunnen maken, zullen nieuwe NVG concepten moeten worden ontwikkeld.

Eén van de concepten voor een nieuwe generatie NVG is gebaseerd op het schakelen van de elektrische weerstand. Data wordt dan opgeslagen als een bepaalde weerstandswaarde, in plaats van als lading. De weerstand van een materiaal wordt bepaald door hoe goed een materiaal elektrische stroom geleidt. Het schakelen van de weerstand is het veranderen van de elektrische geleiding van een materiaal tussen twee mogelijke toestanden: in de ene toestand heeft het materiaal een lage weerstand en laat het de elektrische stroom door, in de andere toestand heeft het een hoge weerstand en laat het de stroom niet of nauwelijks door. In termen van binaire computergeheugen is de lage weerstand gelijk aan een ‘1’ oftewel aan en de hoge weerstand gelijk aan een ‘0’ of ‘uit’.

Er zijn verschillende mechanismen waardoor de weerstand van een materiaal kan veranderen. Zo kan de kristalstructuur veranderen, of kunnen er atomen in het kristal van plek veranderen, en zo een geleidend pad vormen door het kristal. In dit proefschrift heb ik gekeken naar het veranderen van de weerstand als gevolg van het bewegen van atomen, en het reversibele vormen en afbreken van een geleidend pad door het kristal. Deze nieuwe generatie geheugens heet dan ook ‘conductive bridge memories of afgekort: CBM.

Een CBM bestaat uit een weerstandsschakelbaar materiaal met aan weerszijden twee elektrodes. Wanneer er een spanningsverschil over de elektrodes wordt aangelegd, verandert de weerstand van het tussenliggende materiaal doordat er een geleidende brug wordt gevormd tussen de elektrodes. Het maken dan wel verbreken van de geleidende brug wordt bepaald door de polariteit van het aangelegde spanningsverschil. Het aan- dan wel afwezig zijn van de geleidende brug komt overeen met respectievelijk de lage en hoge weerstandstoestand. Figuur 7.2 toont een schematische weergave van het concept van een CBM.

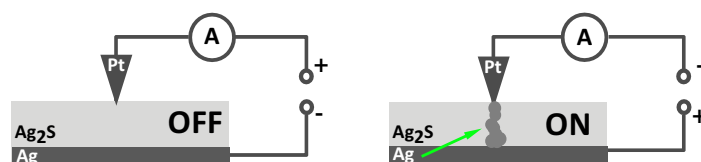


Figure 7.2: Schematische weergave van het schakelen van de weerstand in Ag_2S

Deze schematische weergave laat meteen het systeem zien dat ik in dit proefschrift bestudeerd heb. In onze experimenten wordt de onderste elektrode gevormd door een dunne laag zilver (Ag). De middelste laag is zilver sulfide (Ag_2S). De bovenste elektrode is een platina micro- (10^{-6}) of nanocontact (10^{-9}). Om zo een klein contact te maken hebben wij het tast puntje van een ‘atomic force microscope (AFM) gebruikt, dat gecoat was met platina (Pt), of het platina puntje van een scanning tunneling microscope (STM). Zilver sulfide, Ag_2S , is een zogenaamde ‘mixed conductor’, wat betekent dat de geleiding van het materiaal bepaald wordt door de stroom van zowel de elektronen als de Ag^+ -ionen. Mixed conductors zijn bijzonder vanwege deze duale vorm van elektrische geleiding (ionisch en elektronisch). Daartegenover staan bijvoorbeeld metalen, waarbij de geleiding alleen gedragen wordt door de elektronen.

De beweging van de Ag^+ -ionen in het materiaal levert de belangrijkste bijdrage aan het ontstaan van de geleidende brug in Ag_2S . Deze ionen kunnen relatief makkelijk bewegen in het materiaal, en onder invloed van het aangelegde elektrische veld, vormen ze een brug van dat bovenste naar de onderste elektrode. Als de brug eenmaal reikt van de bovenste totaan de onderste elektrode, is de ‘mixed conductor’ kortgesloten, en daalt de weerstand scherp. Als het elektrische veld wordt omgekeerd (andere polariteit), bewegen de ionen terug naar hun oorspronkelijke positie, en breekt de brug waardoor de weerstand weer omhoog gaat.

Naast de combinatie Ag/Ag₂S/Pt, zijn er vele andere materialen en materiaalcombinaties onderzocht als kandidaten voor geheugens op basis van schakelende weerstand volgens het CBM principe. De grote belangstelling voor dit onderwerp komt door de mogelijkheid om een schakelaar of geheugen te maken waar slechts een paar atomen hoeven te bewegen om het aan of uit te schakelen. Dit zou betekenen dat de minimale afmeting van een geheugen teruggebracht zou kunnen worden tot slechts een paar nanometers (10^{-9} m). In 2005 heeft de onderzoeksgroep van Prof. Aono bij het NIMS in Japan de ontwikkeling van een atomaire schakelaar van Ag₂S gepubliceerd. In deze publicatie worden de aan en uit standen van de geleiding toegeschreven aan de vorming van een metallische draadje van slechts een paar atomen.

Ondanks dit fascinerend perspectief, is er in de literatuur maar weinig bekend over de fysische processen die het schakelen van de weerstand bepalen. Veel details over de microscopische processen die plaatsvinden vóór, tijdens en na het schakelen zijn nog onbekend. Wij hebben ons onderzoek gericht op het begrijpen van de mechanismen die het schakelen van de weerstand bepalen, en minder op het ontwikkelen van een echte geheugencel. Het doorgronden van de fundamentele fysica van het schakelen zal de ontwikkeling van dit vakgebied stimuleren, enerzijds bij de keuze van de materialen en ontwerp, en anderzijds om de daadwerkelijke mogelijkheden van dit soort geheugen te evalueren.

Het onderzoek naar het schakelen in Ag₂S wordt in dit proefschrift als volgt uitgewerkt. In hoofdstuk 1 beschrijven we de fysische eigenschappen van Ag₂S. De halfgeleider eigenschappen, de kristal structuur en de verschillende toestanden waarin Ag₂S kan bestaan. In hoofdstuk 2 presenteren wij de twee methodes die wij gebruikt hebben om onze samples te maken, de voordelen en nadelen van elke methode, en de karakterisering van de Ag₂S samples.

In hoofdstuk 3 presenteren wij metingen van het schakelen van de weerstand in onze Ag₂S samples. We leggen een spanning aan over het sample, en verhogen die geleidelijk van 0V tot V_{max} , van V_{max} naar $-V_{max}$ en dan van $-V_{max}$ terug naar 0V. We meten dan de stroom door het sample en presenteren dit in een zogenaamde IV-curve. Deze IV-curves zijn gemeten met verschillende maximale voltages (V_{max}) en we zien een duidelijke verandering in de vorm van de IV-curve met toenemende V_{max} . Het duidelijkst meetbare verschil is dat boven een bepaald voltage de IV-curve hysteresis begint te vertonen (de curve opent zich). Dit toont aan dat het aangelegde voltage een verandering in het sample teweeg brengt, en dat daardoor het gedrag van het sample is bij het verhogen van 0V naar V_{max} anders is dan bij het verlagen naar 0V. Bij het

hoogste geteste voltage laat de IV curve duidelijk halfgeleider gedrag zien bij het opgaan van het voltage. Bij een gegeven voltage verandert echter het gedrag, en schakelt het sample naar metallisch gedrag en een lage weerstand. Dit blijft zo totaan V_{max} . Daarna, bij het neergaan van het voltage richting $-V_{max}$ blijft het metallische gedrag totaan een bepaald negatief voltage. Daar schakelt het sample weer terug naar een hoge weerstand en halfgeleider gedrag. Dit is het schakelen van de weerstand.

In hoofdstuk 4 bestuderen we de processen in het sample nog voordat het schakelt, oftewel de IV-curves bij laag voltage, waar er nog geen hysteresis te zien is. Dit type IV-curves is de zogenaamde ‘steady state’ en is de toestand vóór het schakelen. Een belangrijk resultaat uit dit hoofdstuk is dat niet alleen de reductie van de zilver ionen bij de platina elektrode belangrijk is voor het schakelen, maar dat een zogenaamde supersaturatie (toegenomen concentratie) van zilver nodig is om metallisch zilver te maken in de buurt van de Pt tip. Dit metallisch zilver zal later de geleidende brug vormen naar de andere elektrode. Wij beschrijven het schakelen in onze Ag_2S samples als volgt: De vorming van het geleidende pad wordt veroorzaakt door het aanleggen van het spanningsverschil over de elektrodes. Dit voltage legt een elektrisch veld over het Ag_2S wat zorgt voor een flux van Ag^+ -ionen en elektronen. Als de platina elektrode een negatieve spanning heeft, zullen de Ag^+ ionen daarheen bewegen, en zich ophopen bij deze elektrode. Als de accumulatie een bepaald niveau heeft bereikt, begint er metallisch Ag te vormen bij de elektrode. Vanwege het sterke elektrisch veld dat zich vormt bij deze nucleus van Ag atomen, begint er een filament te groeien in de richting van de andere (Ag) elektrode, totdat het daar contact maakt. Dit is het moment dat de weerstand plotseling zakt, en het element schakelt van de hoge naar de lage weerstand.

Het belang van de supersaturatie voor het vormen van een nucleus van metallisch zilver en latere schakelen van de weerstand, wordt verder uitgewerkt in hoofdstuk 5. In dit hoofdstuk laten wij ook zien dat de nucleatie van Ag aan het oppervlak van het Ag_2S reeds kan beginnen bij lagere voltages dan benodigd zijn voor nucleatie binnen in het Ag_2S kristal.

In hoofdstuk 6 bestuderen we het proces van het uitschakelen. Hierin laten we zien dat de lage weerstand niet alleen wordt veroorzaakt door het metallische filament, zoals algemeen wordt verkondigd in de literatuur, maar dat er ook een verandering plaatsvindt in de structuur van het Ag_2S . Dit brengt ons tot twee belangrijke conclusies. Ten eerste, dat het zeer waarschijnlijk niet mogelijk is om een atomaire schakelaar te maken met met een ‘mixed conductor’ zoals Ag_2S . Dit omdat niet alleen de beweging en positie van de zilver atomen bepalend is voor de lage weerstand, maar ook het om-

liggende kristal. De locale veranderingen in de kristalstructuur dragen daarmee bij aan de lage weerstand. Het is daarom moeilijk te bepalen of de lage weerstand veroorzaakt wordt door het Ag filament, of door het omgevende kristal. De tweede interessante conclusie is dat we zeer specifieke weerstandswaardes meten die we verwachten voor filamenten van enkele atomen, maar dat deze níet veroorzaakt worden door een metallisch filament, maar door het omgevende Ag_2S kristal.

Als we deze resultaten vergelijken met de in 2005 gepubliceerde data van het atomaire contact, geloven wij dat de resultaten uit 2005 anders zouden moeten worden geïnterpreteerd dan enkel met het ontstaan van een atomaire contact.

Hoewel wij een grote stap gezet hebben in het begrijpen van het proces van weerstandsschakelen, zijn er nog steeds veel onbeantwoorde vragen over de schaalbaarheid en het functioneren van dit soort geheugens voordat zij daadwerkelijk hun weg kunnen vinden naar commerciële producten.

Acknowledgments

Four years and six months in The Netherlands, and exactly the same amount of time at Leiden University doing the research that is now written in this PhD thesis. The work presented in this book would not have been possible without the help, advice and support from many colleagues and friends.

I am very thankful to my supervisor Jan van Ruitenbeek, for his guidance, his encouragement and focus on high-quality research and for his time for discussions even while serving as institute director during most of my PhD. To Sense Jan van der Molen, for his excellent advice, guidance, critical comments and interest in my work. To Prof. Dr. Hans-Dieter Wiemhofer, for his very important input from which we gained understanding of mixed conducting materials. Our collaboration resulted in a joint paper and is presented in Chapter 4. For the fabrication of the lithographic samples at the clean room facilities in Groningen (presented in Chapter 2) I want to thank Bram Slachter. For the X-ray measurements I thank Prof. W.T. Fu at the Chemistry Department in Leiden. I want to thank Dr. Tsuyoshi Hasegawa for his invitation to spend three months in his group at the National Institute of Materials Science in Tsukuba, Japan. To Marcel Hesselberth, for the support with the setups on the sixth and seventh floor. To Federica Galli, for the technical support with the AFM and STM. Marcel and Federica, thank you both for fruitful discussions. To Bert Crama for his support in solving the issues related to electronics. Ruud van Egmond and the FMD in general for their technical support in the development of various parts of equipment. Ellie and Danielle, for the administrative help.

I want to thank my paranympths, Annette and Manohar, both great friends and colleagues. For your advice, good scientific discussions, support and unforgettable times in and outside the lab.

From the AMC group I want to thank Constant for our great collaboration in the lab and the office, Marius for his scientific input and help with complicated Labview programs, Christian, Sebastian, Jaap, Edwin, Tim, Elena and Mo for helpful discussions and fun times. During my first PhD years, Roel Smit, Christian Martin and Sander Otte for helpful discussions and scientific input. I am grateful to Jelmer Wagenaar, for his enthusiasm and good work during his bachelor project which resulted in an article (presented in Chapter 6). To the MSM group, for all the nice discussions at

ACKNOWLEDGMENTS

the group meetings and coffee breaks. Vio, gracias por tu amistad, consejos y apoyo.

During this long PhD journey there were many ups and downs. The support and motivation from many friends outside the lab has been extremely important. Marco, gracias por todo!. Pum, thanks for being here all this time!. Marta, gracias por los buenos consejos y apoyo.

De familie in Netherland, Heleen, bedankt voor alles. U bent mijn voorbeeld van een sterke vrouw.

A mi familia, mis padres, Moises y Patricia, porque de ustedes he aprendido los valores que me hacen la persona que soy. Ericka y Rebecca, por el apoyo que siempre me han dado. A Jose Pablo, todo lo que haces es un gran orgullo para mi, siempre vas a tener mi apoyo y seguí tus sueños. A todos gracias!

Y Marcelo, esta página no es suficiente para agradecerte por todo lo que he recibido y aprendido a la par tuya. Ahora solo puedo decir, gracias mi vida!

Curriculum vitae

Monica Morales Masis was born on August 6th 1982 in Cartago, Costa Rica. There, she attended primary and secondary school from 1987 to 1999. In 2000 she started her Bachelor studies in Physics at the University of Costa Rica. She obtained her Bachelor degree in December 2004. During her Bachelor years and later in 2005, she worked as a research assistant at the Center for Materials Science (CICIMA) at the University of Costa Rica. Her main research was on porous silicon.

In December 2005, Monica started her Master's studies in Physics at Wright State University in Dayton, Ohio, USA. There she was working as a research assistant at the Semiconductor Research Center, and worked on the fabrication of ZnO nanostructures. In May 2007 she was awarded the Graduate Student Excellence Award. In June 2007 she received her MSc. degree in Physics.

In July 2007, Monica started working as a PhD student at Leiden University, The Netherlands, under supervision of Prof. dr. J. M. van Ruitenbeek on the subject of resistance switching in mixed conductor materials, using Ag₂S as a model system. During this period she also taught undergraduate physics students in experimental lab courses. Starting April 2010 she spent three months as a visiting scientist at the National Institute of Materials Science (NIMS), in Tsukuba, Japan. There she worked in the group of Dr. T. Hasegawa in STM studies on Ag₂S switches.

List of Publications

- **Bulk and surface nucleation processes in Ag₂S conductance switches**, M. Morales-Masis, S. J. van der Molen, T. Hasegawa and J.M. van Ruitenbeek, Phys. Rev. B **84** 115310 (2011)
- **Observing “Quantized” Conductance Steps in Silver Sulfide: Two Parallel Resistive Switching Mechanisms**, J.J.T. Wagenaar, M. Morales-Masis and J.M. van Ruitenbeek, Accepted for publication in J. Appl.Phys.
- **Towards a Quantitative Description of Solid Electrolyte Switches**, M. Morales-Masis, H.D. Wiemhofer, and J.M. van Ruitenbeek, Nanoscale **2** 2275 (2010)
- **Conductance Switching in Ag₂S devices fabricated by in-situ sulphurization**, M. Morales-Masis, S.J. van der Molen, W.T. Fu, M.B. Hesselberth, and J.M. van Ruitenbeek, Nanotechnology **20** 095710 (2009)